CHAPTER ONE

INTRODUCTION

1.1 Background of the Study

The importance of energy in our lives and in nation building cannot be over emphasized. This cuts across the socio-economic and political lives of the citizenry both in rural and urban areas. In spite of the fact that energy lies around us in vast quantities within the dynamic forces of nature - the sun, winds, tides, and waves; there must be a technological approach of harnessing them from a low grade form to a high one in order to achieve a desired purpose. Several studies have been made that indicate that the peak year of oil production has gone already (Asif and Muneer, 2007). The depletion and problems caused by the existing energy source (i.e. fossil fuel) have encouraged researchers to continue to search for most efficient and economic mode and device for tapping the huge solar energy available on earth. The standard of living of a nation currently depends on the energy consumption. Any reduction in its supply may lead to abrupt change in the lifestyle of the people and equally affect national security.

A good policy by the interested countries brings about an enhanced economic and technological achievement. The United States of American Government, established the National Renewable Energy Laboratory in 1977 through the adoption of the Solar Energy Research Development and Demonstration Act of 1974 by the Congress. In the same vein, Nigerian government enacted Decree 62 of 1979, establishing the Energy Commission of Nigeria ECN., charged with the responsibility of strategic planning and co-ordination of national policies in the field of energy led to the establishment of Solar Energy Society of Nigeria, in 1980.

In this development, four energy centres at Ife, Zaria, Nsukka and Sokoto were established for the development of nuclear energy (Ife and Zaria) renewable energy technologies (Nsukka and Sokoto).Emerging economies including China and India, account for almost two-third of the increase in world energy use and are expected to double their energy demand by 2025 on the 2002 baseline. In China, the renewable energy shows an annual growth rate of 25% in wind power, solar, wave, tidal and biomass power (Asif and Muneer, 2007).

The main advantages of the renewable energy technologies are that they are devoid of environmental damage e.g. air pollution and global warming. In relative terms for example, solar energy is a viable alternative energy source since solar radiation from the sun reaches all parts of the earth thereby, making the existence of a global village possible where energy availability is no longer a function of geological change.As Africa is blessed with enough solar radiation and its conducive environment for the development of solar technology, new and better technologies are therefore required to harness this energy and this will encourage more scientific activities and collaboration on a wide spectrum of solar science and technology such as photo-thermal, photochemical, photovoltaic processes, etc. The direct and most efficient mode of conversion to electrical power is with the help of photovoltaic (PV) or solar cell devices. Photovoltaic systems are the alternative to fossil or nuclear fuels for the generation of electricity due to the fact that sunlight does not use up the irreplaceable resources.

In the past, the available solar cells were those made of silicon (Si) or gallium arsenide (GaAs) but their disadvantages were that they are expensive and have very low efficiency (about 16%). Also the difficulty in the deposition techniques for the materials made the availability difficult.
Most recent researches on solar energy focus on finding conversion systems that have the simultaneous promise of efficiency, durability, and low cost aswell as solar devices whose

absorption of solar radiation are wavelength dependent. To achieve this goal, photovoltaic cells made of polycrystalline thin films such as ZnO, CdO, PbO, In_2O_3, and Cu_2O as well as non-silicon materials that are relatively inexpensive and readily available are used.

The usefulness of thin films and their applications cut across microelectronics, magnetic and gas sensors, optics, corrosion protection, wear resistance, and solar control devices among others.The special types of these films are the transparent conducting oxides (TCOs) which playimportant roles in many large and small scale applications in selective window coatings, solar cells andflat panel displays (FPDs).

1.2 The Transparent Conducting Oxides (TCOs)

Most of the photovoltaic cells in the market today, made of wafers of high-grade silicon, operate at an efficiency of less than 16%. This is in spite of the fact that the maximum theoretical efficiency for such cells is 32.3% and some scientific advancements have created an efficiency of about 28.2% in the laboratory which is yet to be tested in the uncontrolled environment. Since silicon wafers are costly as well as labour and energy intensive to manufacture, recent researches therefore focus on photovoltaic systems that are made of polycrystalline thin films as well as non-silicon materials that are relatively inexpensive and readily available.

These films though less efficient are usually ultra-thin layers of compounds with thickness in the range 50Å to 5000Å (Chandra *et al*., 1979) created ab initio by the gradual condensation of atoms/molecules/ions or their species on a substrate.The metal elements are capable to form a variety of oxide compounds which can adopt a vast number of structural geometries with an electronic structure that can exhibit various interesting properties.

In the chemical and petrochemical industries, products worth billions of dollars are generated every year through processes that use metal oxide catalysts. For the control of environmental pollution, catalysts or sorbents that contain oxides are employed to remove the CO, NO_x, and SO_x species formed during the combustion of fossil-derived fuels. Furthermore, the most active areas of the semiconductor industry involve the use of oxides. Thus, most of the chips used in computers contain an oxide component.

The wide variety of electronic and chemical properties of metal oxides make them exciting materials for basic research and technological applications. Oxides span a broad range of electrical properties from wide band-gap insulators to metallic and superconducting (Chandrasekaran, 2013) . The oxides of transition metals are an important class of semiconductors, which have applications in magnetic storage media, solar energy transformation, electronics and catalysis (Eslamian, 2017). .

Oxides such as tin oxide and zinc oxide are examples of transparent conducting oxides (TCOs). Others are the oxides of cadmium, indium and gallium .These oxides play important roles in many large and small scale applications, some of them are passive (e.g. cold/heat mirrors and selective window coating) and others are active (e.g. solar cells and flat panel displays). The FPDs have wide variety of applications ranging from instrument panels for airplanes and automobiles, video phones, consumer electronics as well as special requirements for medical and military establishments. These diverse applications of FPDs have varying display requirements that have met with optical enhancement (Lewis and Paine, 2000).

The first published work on TCOs was by Badeker (Badeker, 1907) when he reported that thin films of cadmium metal deposited in a glow discharge chamber could be oxidized to become transparent while remaining electrically conductive. Since then, transparent conducting films have been prepared from a wide variety of materials. They are characterized by the simultaneous occurrence of high optical transparency (> 80%) in the visible region, low effective mass, high carrier mobility and high electrical conductivity (> $10^5\Omega^{-1}m^{-1}$). This is usually achieved by creating an electron degeneracy in a wide band gap (>3eV) semiconductor through the controlled introduction of non-stoichiometry or appropriate dopant (Chopra *et al.,* 1983) while others have band gaps less than 3eV.

The primary n-type TCOs have remained virtually unchanged in the last two decades of simple oxides such as ZnO, CdO, SnO_2, and InO_3 (Wu *et al*., 1999, Bowden and Cardile, 1999). There exists considerable interest in developing p-type TCOs which are expected to open theway not only to a new generation of transparent electrical contacts of semiconductors but also produce transparent oxide electronics in combination with n-type materials. This perception will open the door for the production of improved devices.

These p-type materials exhibit their properties in $CuAIO_2$ and $CuSnO_2$ (Yamamoto and Katayama-Yoshida, 1999) TCOs in which the Seebeck coefficient gave positive values indicating that the majority carriers are holes. It has also been observed in copper-based high T_c superconductors, the existence of CuO planes is critical for many of the electronic properties of these compounds. Also reports show that an n-type ZnO became p-type TCO when doped with nitrogen and gallium (Yamamoto and Katayama-Yoshida, 1999, Lanje,*et al*., 2010). This

improved materials allow the fabrication of all oxide devices with the potential advantages of transparency, high temperature performance, and radiation hardness.

It is now clear that some of the transition elements (those that share similar orbital structure and chemical properties) such as cadmium, copper, and zinc are important constituents for n or p-type TCOs. Since it is usually difficult to obtain simultaneously a high transmission coefficient in the visible region and good conductivity qualities, it follows that the combination matrices of these elements will likely produce properties that suit many TCO uses. This is based on the recognition that a given application affects the choice of compound and the method used for its deposition.

It is clear that the sustenance of transparent conducting coatings revolve on the oxide-based compounds which could be improved upon using a two solution based methods; SILAR and solution growth technique, which are the choice for this work.

1.3 Desired Material Properties for PV Applications

For an effective and efficient energy conversion, several requirements have to be fulfilled. Efficient light absorption, efficient charge separation, transport and collection are the essential requirements.The material needs to have band gap which separates the usually occupied electronic states from the usually unoccupied states. In indirect band gap materials, the maximum of the valence band is found at different k-vectors relative to minimum of conduction band. The smallest distance for band transition from valence to conduction band is hence shifted away from location of valence band maximum.

Therefore, a band transition must involve absorption of phonon, which makes the process much difficult to occur, and the overall absorption of light is inefficient. Hence, the effective absorption is only possible in direct band gap materials (Chopra *et al.*, 2004).

The material must be a good light absorber with solar optical absorption of about 10^5/cm.

The optical depth of a semiconductor is increased with increasing thickness of the film. Semiconductors with almost perfect absorption can be obtained for material thicknesses in μm range, which is of the order of the inverse of the optical absorption coefficient. For good absorption, the optical depth must be high for energies above the band gap and reflectivity should be small.The material should be a good conductor in order to deliver the charge carriers to the external circuit without considerable losses. Defects and impurities act as recombination site and their number has to be kept as low as possible to achieve long diffusion length, which corresponds to long minority carrier life time, and low recombination velocity.

1.4 Alloys

An alloy is a mixture of metals or a mixture of a metal and another element. Alloys are defined by a metallic bonding character. An alloy may be a solid solution of metal elements (a single phase) or a mixture of metallic phases (two or more solutions). An alloy is distinct from an impure metal in that, with an alloy, the added elements are well controlled to produce desirable properties, while impure metals such as wrought iron, are less controlled, but are often considered useful. Alloys are made by mixing two or more elements, at least one of which is a metal. This is usually called the primary metal or the base metal, and the name of this metal may also be the name of the alloy.

The other constituents may or may not be metals but, when mixed with the molten base, they will be soluble and dissolve into the mixture. The mechanical properties of alloys will often be quite different from those of its individual constituents. Although the elements of an alloy usually must be soluble in the liquid state, they may not always be soluble in the solid state(Callister , 2007). If the metals remain soluble when solid, the alloy forms a solid solution, becoming a homogeneous structure consisting of identical crystals, called a phase. As the mixture cools the constituents become solids, they may separate to form two or more different types of crystals, creating a heterogeneous microstructure of different phases, some with more of one constituent than the other phase has.

However, in other alloys, the insoluble elements may not separate until after crystallization occurs. If cooled very quickly, they first crystallize as a homogeneous phase, but they are supersaturated with the secondary constituents. As time passes, the atoms of these supersaturated alloys can separate from the crystal lattice, becoming more stable, and form a second phase that serve to reinforce the crystals internally. Some alloys, such as electrum which is an alloy consisting of silver and gold, occur naturally.

The primary metal is called the base, the matrix, or the solvent. The secondary constituents are often called solutes. If there is a mixture of only two types of atoms (not counting impurities) such as a copper-nickel alloy, it is called a binary alloy. If there are three types of atoms forming the mixture, such as iron, nickel and chromium, then it is called a ternary alloy. An alloy with four constituents is a quaternary alloy, while a five-part alloy is termed a quinary alloy. In this respect, all the various forms of an alloy containing only two constituents, like iron and carbon,

is called a binary system, while all of the alloy combinations possible with a ternary alloy, such as alloy of iron, carbon and chromium is called a ternary system (Verhoeven, 2007).

1.5 Statement of Problems

Energy is essential to economic growth of the world and healthy life of the citizenry. Traditional energy resources such as fossil fuel, fire wood and coal are the major sources of global warming and air pollution. As a result of the negative effect on the world climate, research is ongoing to find sustainable energy alternatives which are environmental friendly. The energy from the sun is renewable energy and is considered to be the promising solution to world energy problem. Photovoltaic materials are capable of converting solar radiation into electricity.

In this study, transparent metal oxide alloyed materials with simultaneous combination of properties capable of converting solar radiation into solar energy will be studied, and also be a solution towards solving problems in the areas of optoelectronics, sensor applications and other passive applications.

1.6 Aim and Objectives of the Study

The aim of the study is to deposit and characterize $ZnO:SnO_2$, $PbO:SnO_2$, $CuO:SnO_2$, $CdO:SnO_2$ alloyed thin films using dual solution synthesis; SILAR and SGT and also deduce their possible device applications.

The objectives are:

1. To deposit the oxide alloyed samples,
2. Tocharacterize the deposited samples in order to determine the effect of annealing on ,

the deposited samples.

3.To deduce the possible applications within the spectrum of solar energy technology,

4. To deduce the possibleactive and passive applications,

1.7 The Significance of the Study

The need and the desire to produce high quality transparent oxide semiconductor thin films with combinational qualities in the areas of applications led to the choice of the study on dual solution synthesis and characterization of $ZnO:SnO_2$, $PbO:SnO_2$, $CuO:SnO_2$, $CdO:SnO_2$ alloyed thin films for possible device applications.

The outcome of the study will provide a good platform for large scale production of high quality alloyed thin films.

1.8 Scope of Study

This research will be centered on alloyed thin films using two solution base methods: SILAR and solutiongrowth technique to prepare $ZnO:SnO_2$, $CdO:SnO_2$, $PbO:SnO_2$, and $CuO:SnO_2$ alloyed thin films. Reagents required include: zinc chloride, lead nitrate ($Pb(NO_3)_2$, cadmium chloride ($CdCl_2$), zinc chloride ($ZnCl_2$), tin chloride ($SnCl_2$), ammonia (NH_3), and sodium hydroxide (NaOH). The deposited samples will be annealed using Master Chef annealing machine at varying temperatures.

X-ray diffractometer (XRD) and scanning electron microscope(SEM) will be used to determine the structural properties of the samples, Rutherford Backscattering Spectroscope (RBS) will be used to determine the composition and thickness of the deposited samples and UV-1800 double beam spectrophotometer will be used to determine the optical properties of the samples.

CHAPTER TWO
LITERATURE REVIEW

2.1Thin Films

Thin films are materials whose fabrications are formed by atoms/molecules/ions/clusters of species condensation process. It is also described as a form of crystalline or non-crystalline material developed two dimensionally on a substrate surface by physical or chemical methodranging from fractions of a nanometer to several micrometers.The phenomenal rise in thin film researches is, no doubt, due to their extensive applications in the diverse field of electronics, optics, space science, aircrafts, defense and other industries. These investigations have led to numerous invention in the forms of active devices and passive components, piezo-electric devices, micro-miniaturization of power supply, rectification and amplification, sensor element, storage of solar energy and its conversation to other forms, magnetic memories, superconducting films, interference filters, reflecting and antireflection coating and many others (Kuanr, *et al.*, 2008 ,Rao, 2013, Eom and Susan McKinstry, 2012) .

Thin solid films may be divided into two categories of passive and active films. Passive thin films including coatings are used for aesthetic and decoration purposes, or protection of the underlying surfaces, against moisture, oxygen, high temperature, and mechanical forces to avoid corrosion, surface damage, etc. On the other hand, active thin films can in fact respond to specific triggering effects, such as light, heat, and contact with gases and biological analysis and generate a response for energy conversion, sensing, mechanical actuators, etc.

Therefore, the combination of one or more active thin films, and perhaps some passive thin films, can make a thin film device, such as thin film solar cells (SCs), transistors, thermoelectric

devices, sensors, and actuators, to name a few. Various types of thin film devices may share similar principles of operation or fabrication processes, and therefore advances in one device may provide new windows of opportunity for the development of other devices. As an example, molecular semiconductors, such as perovskites developed for perovskite SCs, may be used in other devices, such as thin film transistors.

Most of the thin film devices employ graphene and carbon nanotubes in their structures, and advances in one field may be utilized in other fields, as well (Morteza, 2016).

Thin films can be applied in such areasas thin film transistors, organic light-emitting diodes (OLED), thin film thermoelectric devices, thin film gas and biosensors, thin film smart materials and actuators etc.

Thin films of large deposition structures are as a result of:

1.High substrate temperature ,

2.Low activation energy for the surface diffusion,

3.Low boiling point of film materials,

4.Low rate of deposition,

5.Low energy of absorption between the film and substrate.

However, once the critical nuclei have been formed, growth occurs by captures of mobile absorbed atoms. Coalescence occurs between growing nuclei resulting in sufficient films occurring. The film structure is influenced by such deposition parameters as: substrate composition and surface structure, source and substrate temperature, deposition rate and pressure

of the ambient atmosphere (Thun, 1985). The thickness, method of formation and growth determine the nature of thin film (Amuh, 1991).

Thin films could be grown either by:

1. Layer – by – Layer: This model comes into play either when the ad-atoms have little mobility (as in amorphous deposition) or under extreme conditions of very low supersaturation, single crystal substrate and ultra high vacuum deposition.
2. Stranski-Krastanov: Under this mode, the films grow just as layer-by layer mode and then convert itself into three dimensional nuclei.
3. Three-Dimensional Growth: This model occurs when the ad-atoms mobility is larger and the size of the nucleation center is small. This model commonly results in oriented thin film.

2.2 Deposition Techniques in Thin Film Technology

The deposition techniques and their various parameters play important roles in the nucleation and growth of thin films thereby altering their physical properties. In spite of the expected efficiency, a cost effective as well as large area deposition, uniform and controlled deposition is necessary if the films are to be economically viable for terrestrial applications. Those with well defined structures and opto-electric properties are expensive to deposit. In view of the effort to minimize costs and improve efficiency, these techniques are constantly being modified to develop variants.

A recent example is the high rate vapour transport deposition (HRVTD) technique which takes seconds to deposit films on a large scale for photovoltaic modules.

All the thin film deposition processes involve the following three steps: creation of atomic/molecular/ionic species, transport of these species through a medium and condensation of these species on a substrate.

Thin film deposition techniques can be classified under the following headings depending on the mode of creation of vapour species:physical vapour deposition (PVD),chemical vapour deposition (CVD),chemical solution deposition (CSD),electrochemical deposition (ECD) and hybrid technique resulting from the combination of PVD with CVD.

Regardless of whichever technique adopted, it must be able to satisfy the criteria of simplicity, cost effectiveness, large uniform area and controlled deposition, metallurgical and electro-optical properties.

Here, the various techniques are briefly reviewed below:

2.2.1 PhysicalVapour Deposition (PVD)

Physicalvapour deposition uses mechanical, electromechanical or thermodynamic means to produce a thin film of solid. Evaporation source can be categorized by the method of energy supply. One has to consider also that not each material can be evaporated from each source. Chemical reactions between crucible and evaporation material are possible which can lead to impurities in the film or destroy the evaporation source (Savale, 2016). Physical vapour deposition includes the following:

(a) Vacuum Evaporation

In this technique, a material heated at a sufficiently high temperature produces the desired vapour pressure that enables the vapour atoms to condense on a substrate (kept at low temperature) to yield the thin films.A variant of vacuum evaporation uses an electron beam evaporator to melt materials on a substrate. Because of the added precision, materials of lower

vapor pressure can be melted than in standard thermal evaporation *(*Pankove, 1971*).* The process is characterized by the decomposition or dissociation in alloys and other compounds due to the thermal instability of their various constituents and evaporation of elements as natural atoms only (Roitan, 1994), and the relationship in which the rate of free evaporation of vapour atoms from a clean surface of unit area in vacuum is given by the Langmuir-Dushman kinetic theory equation given by

$$N_e=3.513 \times 10^{22} P_e(1/MT)^{½} mol/cm^2 s \qquad (2.1)$$

where N_e, P_e, T and M are the number of molecules evaporated per second, the equilibrium vapour pressure (torr) evaporant under saturated conditions, is the temperature at saturation and is the molecular weight of vapour species respectively.

(b) Sputtering

Sputtering is the mechanical ejection of atoms from the surface of the target material by energetic non-reactive ions to create vapour species which condenses on the substrate in form of a thin film (Chopra and Das, 1983).The characteristics of this technique include energy intensive which is best for thin film of multi-component compounds of different kinds as well as alloys (Callister, 2007) and the sputtering yield S which is defined by the equation

S = (no. of atoms ejected)/(no. of incident ions) (2.2)

The underlying principle of the technique is the impact theory in which momentum is transferred from impinging ions to the target atoms being bombarded. The maximum energy transferred to the largest atom in hard sphere collision is therefore given by

$$E_{Tmax} = \frac{4M_{ion}\, M_{target}\, E_{ion}}{(M_{ion} + M_{target})^2} \qquad (2.3)$$

whereM_{ion} and $M_{tanget,}$ are the masses of the sputtering ion and target atoms respectively. At maximum sputtering, this energy is equal to or greater than 50keV with about 5% of the sputtering energy being carried off by the ejected atoms.

DC (Diode) Sputtering

In this technique, sputtering is achieved when the anode (substrate) and the cathode (target) are separated by a few centimeters with a sputter at the middle.

Rf Sputtering

An rf field when applied directly to the anode through a high frequency coil (or capacitor for metals) placed inside or outside the discharge region produces sputtering at low pressure (~ 10^{-3}torr).

Ion Plating

This process involves the bombardment of a substrate with some other particles from a thermal source in addition to the required vapour species (Wiley, 2007). This results in well compactness and strong adherence of films. Sputter etching of the films during growth and trapping of energetic gas ions are the major set-back in this technique. A better and meaningful ion plating technique involves ionization of vapour by bombardment with accelerated electrons from the thermal source and depositing the ions onto a substrate with or without post ionization acceleration.

Other sputtering deposition techniques include: glow discharge sputtering, magnetron sputtering, reactive sputtering, plasma ionization for producing thin oxide films, plasma polymerization of organic films, plasma etching, and plasma deposition of inorganic films at low substrate temperature.

(c) Molecular Beam Epitaxy

Epitaxial growth is the process by which a crystal receives its crystallographic orientation from the substrate. This may be homoepitaxy, autoepitaxy or, isoepitaxy in which the crystal and its substrate are of the same material (e.g., silicon on silicon or germanium or germanium). It may also be heteroepitaxy – growth in which the crystal and its substrate are of different materials (germanium on silicon or gallium arsenide on germanium). The term epitaxy, is more loosely used to describe any growth process in which both the substrate and the crystal are monocrystalline regardless of the crystallographic orientation of the crystal with respect to the substrate (Aeger, 2002).

Molecular beam epitaxy, is an expitaxial growth in which the crystal is grown by the condensation of one or more direct beams of atoms or molecules from Knudsen effusion source under ultra-violet vacuum condition.

The principle of the technique is based on the fact that in surface crystallography, the thin film surface is not always the same as in the bulk structure.

However, the only limitation of the method is that it is used primarily for epitaxial studies of the growth II – VI and III – V compound semiconductors.The technique had been in use since 1970s for the deposition of II – VI and III – V compound semiconductors.

2.2.2 Chemical Vapour Deposition (CVD)

In the chemical vapour deposition (or vapour phase epitaxy) technique, deposition takes place by volatizing the compound containing the required material on the substrate through a pressure differential or by using heat, light, X-rays, an rf field, an electric arc, electron bombardment or catalytic action of the substrate surface.

This technique does not require vacuum, but requires temperature or concentration gradient between the substrate and its surrounding for the transportation of the vapour species.

In spite of the complex processes involved and the corrosive gases used, they have been used for the deposition of multi-component alloys (Dorval-Dion and Tavares, 2013).

The examples of the technique are thermal decomposition, reduction reactions and disproportionate reaction.

(a) Thermal Decomposition

Thermal decomposition takes place when a compound in the gaseous state is made to undergo pyrolytic dissociation (pyrolysis) on hot substrate in air or inert gas or atmosphere to yield pure elemental deposits as given in the relation.

$$AB_{(g)} + \text{heat} \rightarrow A_{(s)} + B_{(g)} \qquad .(2.4)$$

where g and s denote gaseous and solid states respectively.

Some of these reactions require low pressure and a higher substrate temperature to improve the adhesion and other properties such as purity and crystallinity (Cointea*et al.*, 2010). Examples of this technique includes,the decomposition of silane at a temperature (>750^{0}C) and pressure (< 8 torr) with reaction equation of the form

$$S_i H_4 \xrightarrow{800^oC\text{-}1300^oC} Si_{(s)} + 2H_{2(g)} \quad (2.5)$$

the decomposition of the metal borohydrides and hydrides at temperature (<600^{0}C and metal halides at temperature (>600^{0}C).

the other materials obtained with this technique also include Fe, Ni, Ge, SiO_2, MnO_2 and Al_2O_3.

(b) Reduction Reactions

Reduction reaction occurs when a compound in the gaseous state is reduced by hydrogen (Seshan, 2002) (hydrogen aided decomposition at a lower temperature) with an equation of the form.

$$2CD_{(g)} + H_{2(g)} \rightarrow 2C_s + 2HD_{(g} \quad (2.6)$$

The examples of this technique is found in the reduction of silicon tetrachloride in the presence of hydrogen,

$$SiCl_{4(g)} + 2H_{2(g)} \xrightarrow{>300^oC} Si_{(s)} + 4HCl_{(g)} \quad (2.7)$$

Also it can be found in the reduction of tungsten hexafluoride in the presence of hydrogen

$$WF_{6(g)} + 3H_{2(g)} \xrightarrow{>600^oC} W_{(s)} + 6HF_{(g)} \quad (2.8)$$

The other depositions obtained with this technique also include Sn, Cr, Fe, Ge, and SiO_2 as well as chlorides of Ni, Fe and Co which are reduced at intermediate temperatures.

(c) Disproportionation Reaction

Disproportionation reaction is the process in which a compound in a gaseous state is transported from a higher temperature to a lower temperature to obtain deposition on a substrate as given by the relation for compounds involving elements of multiple valence states.

$$2X\ Y_{(g)} \rightarrow X_{(s)} + XY_{2(g)} \quad (2.9)$$

The technique is essentially a chemical transport reaction in which non-volatile compounds are transported to the substrate by means of a relatively high volatile chemical vapour and

subsequently thecompound is deposited on the substrate, which is dependent on the temperature and pressure (Chen *et al*., 2011).

An example is the halide disproportionation of tetraiodide at temperature

($<1000^0$C) with an equation of the form

$$2GeI_2 > 1000^{\circ}C \longrightarrow Ge_{(S)} + GeI_{4(g)} \quad (2.10)$$

The other depositions obtained with the technique are Al, Si, III – V compound alloys as well as metal, doped and mixed oxides.

2.2.3 Chemical Solution Deposition Technique

In the chemical deposition technique, the reaction between the ions may take place either of these processes:

1. Dipping of the substrates into the mixture of the reactants for a particular period of time depending on the required thin film thickness or

2. Spraying of an aqueous solution of the soluble salts of constituent atoms of the desired compound on the substrate maintained at an elevated temperature.

The technique is useful for the deposition of films uniformly on insulators as well as complex and inaccessible parts without any excessive build-up since no contacts of power supply is required. Examples of the technique are: sol-gel, chemical bath deposition and spray pyrolysis and successive ionic layer adsorption and reaction (SILAR).

(a) Sol-Gel Technique

The sol-gel coating technique is a dip method in which the substrate is inserted into a solution containing hydrolysable organo-metallic compounds and then pulled out at constant speed into the atmosphere (Aldona*et al*., 2003).

The principle of the technique is based on the reaction equations of the form

$$M(OR)_x + xH_2O \rightarrow M(OH)_x + xROH$$

$$M(OH)_x \rightarrow MO_x + xH_2O \qquad (2.11)$$

where M is the metal cation, R is the alkyl group and x is the number of moles. Subsequently, annealing at a moderate temperature of about 500^0C removes the water and the carbon compounds present to yield good quality films of transparent oxides.

The technique has been in vogue since 1953 to produce heat/cold mirrors and in the middle and late 1960s, it was used to produce antireflective and architectural coatings. Other coatings produced with this technique include fluorescent lamp envelop, grounding films in cathode ray tubes, flat panel displays (FPDs), and solar energy devices (Manea*et al*., 2007).

(b) Successive Ionic Layer Adsorption and Reaction (SILAR) Method

SILAR method is one of the newest solution method for the deposition of thin films.It has a number of advantages :it offers extremely easy way to dope films with virtually any element in any proportion by merely adding it in some form of cationic solution, unlike closed vapour deposition method.

SILAR does not require high quality target or substrates or does it require vacuum at any stage, which is great advantage if it is applied in industries, the deposition rate and the thickness of the films can easily be controlled over a wide range by changing the deposition cycles, operating at room temperature can produce films on less robust materials, unlike high power methods, such as radio frequency magnetron sputtering (RFMS).

It does not cause local overheating that can be detrimental for materials to be deposited, there are virtually no restrictions on substrate material dimensions or its surface profile, it is relatively inexpensive, simple and convenient for long area deposition.

In this solution modification, thin films are obtained by immersing substrates into separately placed cationic and anionic precursors and rinsing takes place between every immersion with ion-exchanged water. The rinsing time in the ion-exchange water is critical for ionic layer formation. Thus precipitation formation is avoided in SILAR method.

SILAR method is a new and less investigated method first reported in 1985. The name SILAR was ascribed to it by Nicolau (Nicolau and Minnard, 1988), which was used to deposit ZnS, CdZnS and CdS thin films.It is useful for the deposition of chalcogenide group of, I-VI, II-VI, III-VI, V-VI,VII-VI binary films and I-III-VI, I-II-VI, II-III-VI, II-V-VI and II-VI-V ternary chalcogerides and composite films.

The SILAR method is mainly based on the adsorption and reaction of the ions from solution and rising between every immersion with de-ionized water to avoid homogeneous precipitation in the solution(Pathan and Lokhande, 2004).The collection of a substance on the surface of another substance is known as adsorption which is the fundamental building block of the SILAR method.

Adsorption can be defined as the interfacial layer between two phases of a system.Adsorption may be expected when two heterogeneous phases are brought together . Hence, gas-solid, liquid-solid, and gas-liquid are three possible adsorption system. Here, we are only concerned with liquid-solid system.

Adsorption is an exothermic process. Adsorption is a surface phenomenon between ions and surface of substrate and it is possible due to attraction force between ions in the solution and surface of the substrate. These forces may be cohesive forces or Van-der Waals forces or chemical attraction forces. Atoms or molecules of substrate surface are not surrounded by atoms or molecules of their kinds. Therefore, they possess imbalance or residual force and hold the substrate particles. This ad-atoms can be holding on the surface of the substrate.

The factors affecting adsorption process include: temperature of solution, pressure, nature of the substrate, concentration of the solution, area of the substrate etc. The reaction in pre-adsorbed (cations) and newly adsorbed (anions) forms the thin films of desired materials.

The chemical reaction involving two heterogeneous solid phase and solvated ions in solution is given in equation (2.12),

$$(pK_{aq}^{a+} + q\ X^{b-}_{aq}) + (b'\gamma^{q'-}_{aq} + aA^{p-}_{aq}) \longrightarrow Kp'Aa_s\downarrow + q\ X^{b-}_{aq} + b'\gamma_{aq}^{q'+} \quad (2.12)$$

Such that $ap = bq = b'q'$

where K is the cation (Cd^{2+}, Zu^{2+}, Fe^{2+}, Cu^{2+}, Pb^{2+}etc), P is the number of cations a is the numerical value of the charge on cation, X is an ion in cationic precursors having negative charge (X= SO_4^{2-}, Cl^-, NO_3^-etc), q is the number of X in cationic precursor, b is the numerical value of changes on X, b' is the number of Y in the anionic solution, q' is the numerical value of change on Y, Y is the ion which is attached to chalcogen ion, A is the anion (O,S, Se, Teetc).

Therefore, in the presence of complexing agent, the above reaction can be written as

$$P[CK)^{a+}]_{aq} + qX^{b-} + b'Y^{q+}{}_{aq} + Aa^{p-}K_pA_a\downarrow + C + qX^{b-}{}_{aq} + b'Y^{q+}{}_{aq} \quad (2.13)$$

where C is the complexing agent.

SILAR method, involves four stages: adsorption, rinsing, reaction and rinsing.

At the adsorption stage, the cations in the precursor solution are adsorbed on the surface of the substrate and hence form the Helmholtz electric double layer. This layer is composed of two layers: the inner (positively charged) and outer (negatively charged layer). The positive layer consists of the cations and the negative form, the counter ions of the cations (Pathan and Lokhande, 2004).

In the rinsing stage, excess adsorption PK^{a+} and aA^{p-} are rinsed away from the diffusion layer. This results into saturated electrical double layer.

Reaction occurs when anions from anionic precursor solution are introduced to the system. The solid substance K_pA_a is formed on the interface, which is as a result of the reaction between PK^{a+} surface species and anionic precursor aA^{p-}.

In the last stage of SILAR cycle, the excess and unreacted species aA^{p-}, X, Y and the reaction product form the diffusion layer are removed. SILAR method can either be manual based, computer based or microprocessor based.

These stages of SILAR cycle are shown in Figure 2.2. By repeating these cycles, a thin layer of material K_pA_a can be grown: following the above mentioned steps, the maximum increase in film thickness per one reaction cycle is theoretically one monolayer. This results into a solid layer of the compound K_pA_a. Dividing the measured overall film thickness by number of reaction cycles,

growth rate may be determined. This gives a numerical value for growth rate under certain conditions. If the measured growth rate exceeds the lattice constant of the material, a homogenous precipitation in the solution would take place. The process involves alternate immersion of the substrate in a solution containing a soluble salt of the cation of the compound to be grown.

The substrate supporting the growing films is rinsed in highly purified de-ionized water after each immersion. Some factors such as the nature of precursor solutions, pH values, concentration, counter ions, individual rising and dipping time, complexing agent and the pre-treatment of the substrates etc. Figure 2.1, shows pattern of SILAR growth on substrates.

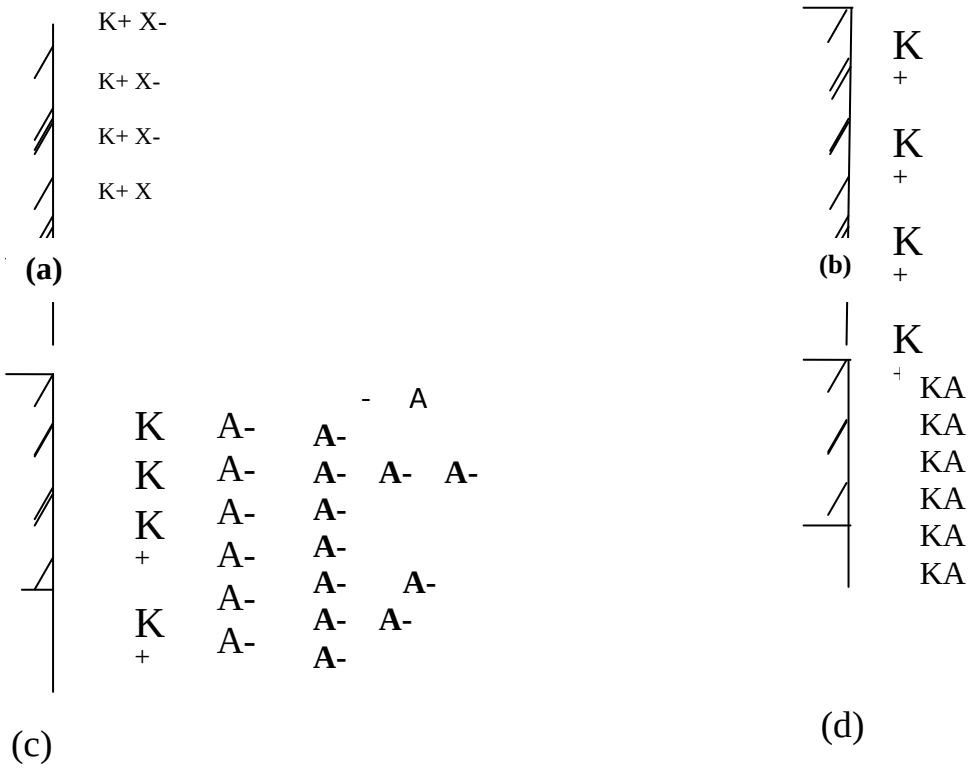

Figure 2.1 Pattern of SILAR growth (Pathan and Lakhande, 2004)

(a) Adsorption of KX and formation of electrical double layer.

(b) Rising (1) removes excess unabsorbed K^+ and X^-

(c)Reaction of A^- with pre-adsorbed K^+ ions to form KA and

(d) Rising (2) to remove excess and unreacted species to form the solid phase KA on the surface of the substance.

(a) Manually operated SILAR method

This system does not require any power supply for operations, hence it is economical. In this system, four or more glass beakers of typically 50 ml capacity containing precursor solutions and de-ionized water are placed separately in the tray.

The beakers containing precursor solutions and de-ionized water are alternately placed.

The beaker containing de-ionized water is placed in between the beakers containing cationic and anionic precursor solutions. The immersion and rinsing of substrates are done manually as shown in Figure 2.2.

The growth mechanism involves three most important steps:

i. specific adsorption of the most strongly adsorbed ions of the compound to be grown, by the substrate immersed in the solution of the cationic precursor.
ii. rinsing of the excess solution adhering to the substrate and
iii. chemical reaction between the most strongly specific adsorbed cations and the less strongly adsorbed anions by the subsequent substrate immersed in the solution.

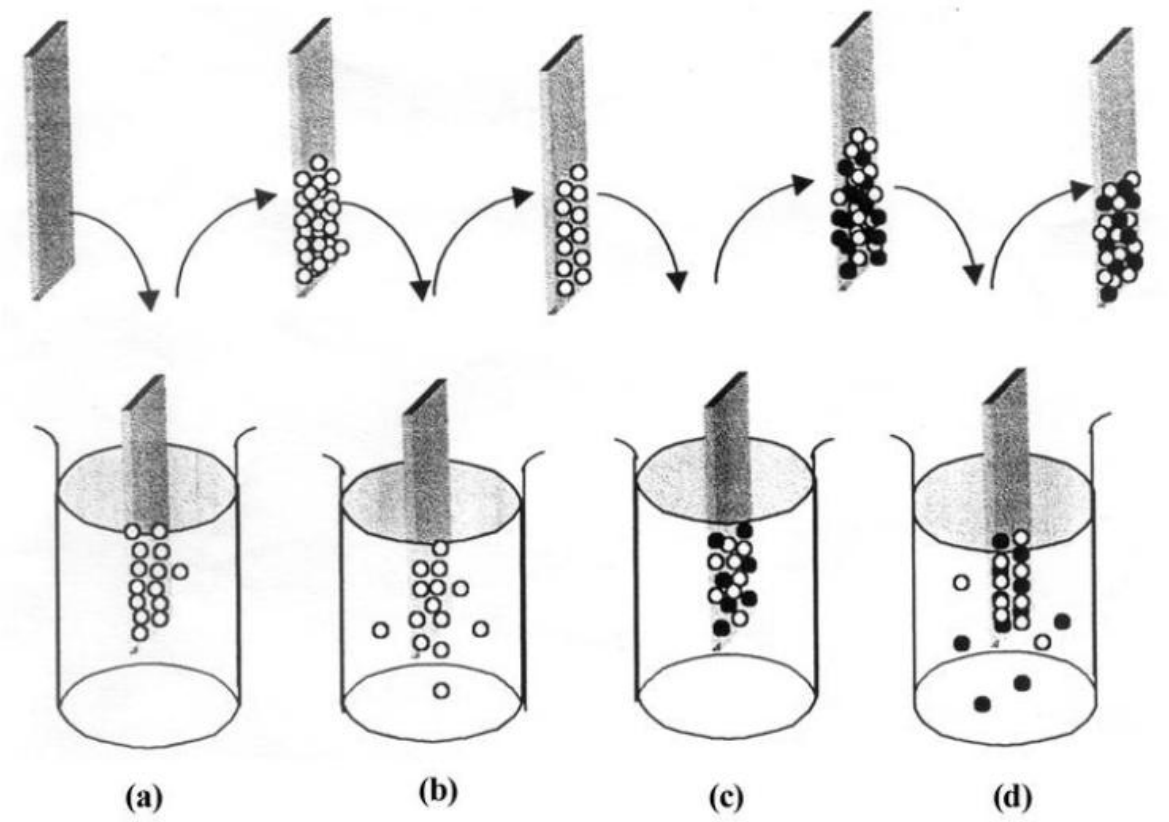

Figure 2.2 The stages of SILAR deposition process (Pathan and Lokhande, 2004)

a. Cationic precursor
b. Ion exchange water
c. Anionic precursor
d. Ion exchange water

(b) Computer based SILAR Method

The schematic diagram of computer-based operating system is shown in Figure 2.3. The equipment consists of two beakers of 50 ml each containing the precursor solution and two rinsing vessels, lying in a circle on the circular tray. Each rinsing vessel being placed in between beakers containing cationic and anionic precursor solutions. The substrates are attached vertically by means of four arms. The arms are set out in line or a right angle and supported on the spindle. The spindle can turn and slide tightly in a bearing. Two steeping motors drive it. The

computer program governs the vertical and translation movement of the spindle (Pathan and Lokhande, 2004).

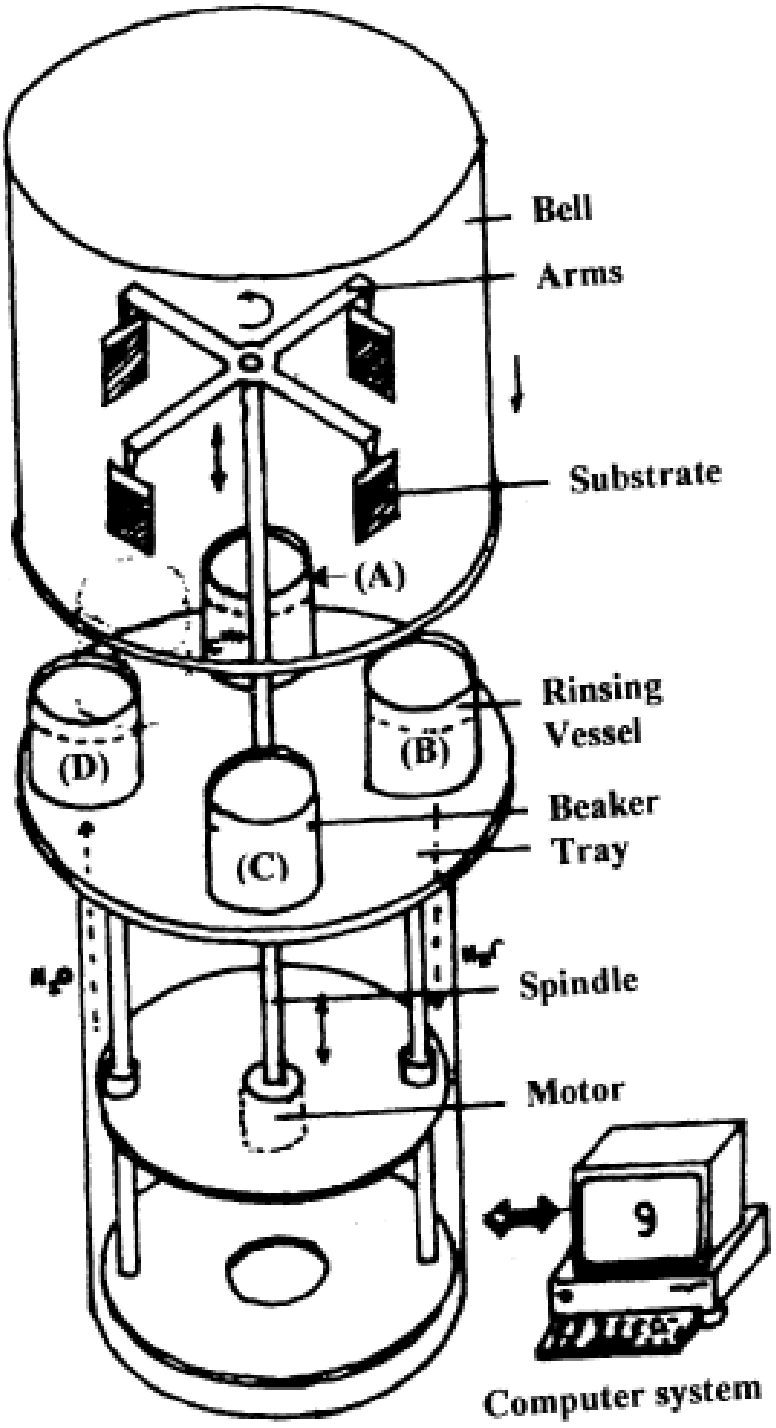

Figure 2. 3Computer based SILAR method(Pathan and Lokhande, 2004).

(c) Microprocessor Based SILAR Method

The schematic diagram of microprocessor-based operating system is shown in Figure 2.4. The equipment is feasible for elemental, binary, ternary, composite etc materials. Each rinsing vessel being placed in between beakers containing cationic and anionic precursor solutions. The substrates are attached vertically by means of robotic arms. The microprocessor governs the vertical and translational movement of the robotic arms (Pathan and Lokhande, 2004).

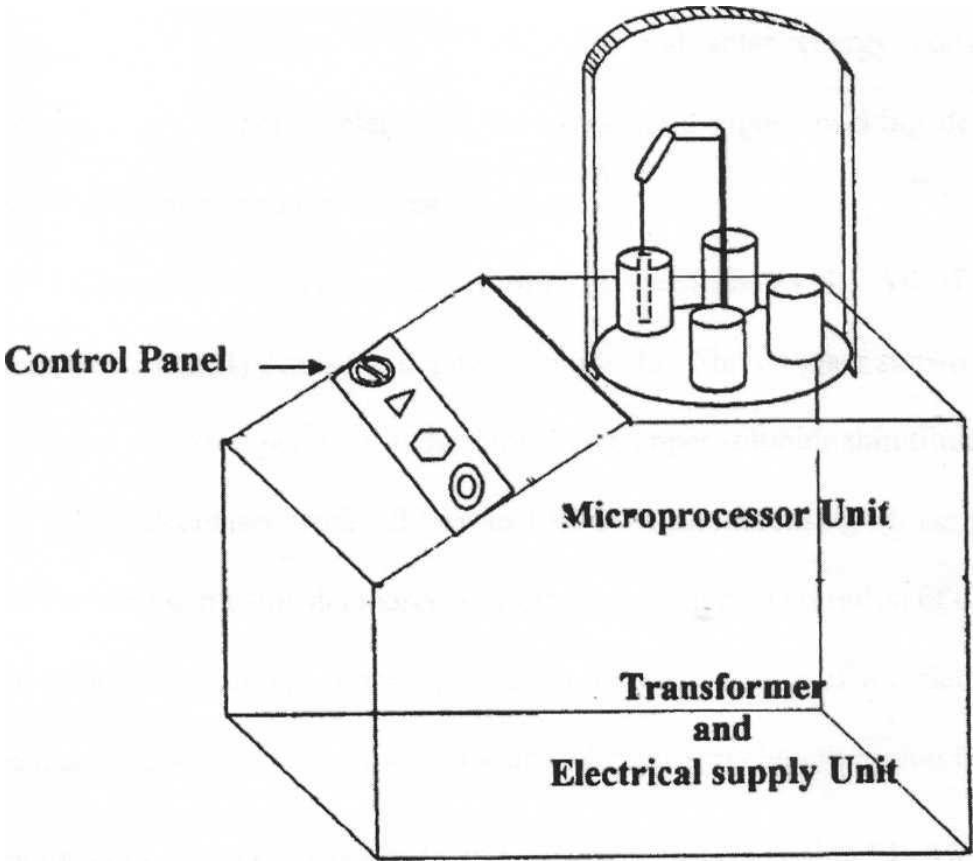

Figure 2.4 Microprocessor Based SILAR method (Pathan and Lokhande, 2004).

(c) Solution Growth Technique

The solution growth technique (chemical bath deposition technique or electroless deposition) is the process in which substrates (metallic or non-metallic) are dipped into solution baths containing the reactants to obtain depositions in the absence of external electric fields. It was first used to prepare PbS films in 1940s for infra-red applications.

The unique features of solution growth technique include:

1.Low deposition temperature, thereby allowing the use of substrates of different types and shapes,

2. Simplicity and inexpensive nature of apparatus required,

3. Reduced environmental impact on the deposited films,

4. Homogeneous precipitation which ensures uniform thickness at various deposition durations.
The chosen parameters (i.e concentration, volume, temperature, pH and time of deposition) were found largely by trial and error and there are no means of guaranteeing that they lead to the best possible optical and electrical properties (Eze, 1998).
The ions present are far apart that they are free from mutual interference and therefore are completely dissociated. The dissociation relation is of the form

$$A_mB_n(s) \leftrightarrow mA^{n+} + nB^{m-} \quad (2.14)$$

where m and n are the number of ions of each molecule. If the concentrations of the reactants and products are in equilibrium at a given temperature,

$$K_{eq} = \frac{[A^{n+}]^m[B^{m-}]^n}{[A_nB_m]} \quad (2.15)$$

where K_{eq} is the equilibrium constant. The denominator is constant since the concentration of a pure substance in itself cannot change at constant temperature. Hence the product

$$[A^{n+}]^m [B^{m-}]^n \text{ is constant (IP)} = K_{sp}$$

is known as the ionic product, which is equal to the concentration of ions in a saturated solution of sparingly soluble salts and$K_{sp}$is known assolubility product constant.

When reactants and products are in equilibrium at a given temperature, we obtain

$$IP = K_{sp} \quad (2.16)$$

However, some salts do not have solubility product because of their relatively high solubility in water in which case, the law of mass action (concentration of reactants and product are in equilibrium at a particular temperature) does not hold.

In terms of rate, the solubility product relationship can be found also on the assumption that

rate of reaction = rate of deposition

$$K_r = K_d [A^{n+}]^m [B^{m-}]^n \quad (2.17)$$

Hence equation (2.17) becomes,

$$K_{sp} = \frac{K_r}{K_d} = [A^{n+}]^m [B^{m-}]^n \quad (2.18)$$

where K_r and K_d are the proportionality constants, for the reaction and deposition. Thus if ionic product, IP exceeds the solubility product SP (IP > SP), then precipitation occurs otherwise there will be continuous dissolution of the solid phase in the solvent.

The elimination of spontaneous precipitation (in order to obtain controlled, ion – by – ion, interaction) can be achieved by the use of a complexing agent, which forms a stable ligand with the metal cation but does not react or form complex with the anion.

The complexing agent inhibits the reaction and provides the controlled number of free cations according to the relation,

$$M(A)_n^{2+} = M^{2+} + nA \quad (2.19)$$

Hence the concentration of the free metal ions at a particular temperature becomes

$$K_i = \frac{M^{2+}][nA]}{[M(A)_n^{2+}} \quad (2.20)$$

where K_i is the instability constant of the complexing ion in depositing thin films. Recently, Nair and his colleagues have been consistent in using the technique to obtain deposition of binary compounds, sequential deposition of binary multilayer materials as well as post deposition on coated substrates. A stable and appropriate complexing agent is usually chosen so that the concentration will make the medium conducive for thin film deposition. The choice of the complexing agent depends on the reactants, since various metals form stable complexes with different complex compounds. The typical examples of complexing agents are NH_3, EDTA, TEA, etc.

This technique was first used by Cashman 1946 when he deposited PbS (Cashman, 1946). Subsequent use of the method has been intensified in our laboratories through the work of However, the major setback of the technique is the difficulty of controlling the stoichiometry of the deposited thin films for sophisticated application in research and in industry.

The chemical bath deposition technique has been extended to the growth of oxide films in our laboratories. Basically, this is possible because some cations in an alkaline medium are precipitated during hydrolysis as hydrous oxides, instead of hydroxides. If a substrate is immersed in the solution, a film of hydrous oxide is obtained by ion-by-ion interaction process. On subsequent heating in a well controlled oxygen environment, dissociation takes place resulting in pure oxide films. (Kaur, 1980).

The growth behavior of solution-grown oxides is similar to those of suphides and selenides. Under certain growth conditions of metal-ion concentration, nature and concentration of complexing agent, pH and temperature of solutions, the films acquire terminal thickness. With proper choice of reactants and complexing agents, the technique can be useful for the preparation of oxides of Cr, Fe, Mo, Ti, V, Zn, Cu, etc .

(d) Spray Pyrolysis

The spray pyrolysis is a thermally stimulated process in which aqueous solution of the soluble salts containing the atoms of the desired compound are sprayed on a heated substrate in form of tiny droplets (liquid / vapour atoms) using a carrier gas.

The substrate provides the thermal energy for the thermal decomposition and subsequent recombination of the constituent species followed by sintering and recrystallization of the clusters of crystallites giving rise to a coherent film (Chopra and Das, 1983).

The technique is based on the principle that a metallic compound dissolved in a liquid mixture undergoes pyrolytic decomposition when sprayed on a pre-heated substrate in air or inert gas atmosphere according to the equation

$$ZY_g \rightarrow Z_s + Y_{(g)} \qquad .(2.21)$$

whereZ is the single crystal or cluster of crystallites of the desired compound while Y is the excess solvent and volatile by- product which escapes in the form of vapour.

The technique was first used in 1970s to deposit the transparent oxide thin films and it is still preferred technique at present.

The main problem associated with spray pyrolysis is that the film may be contaminated if a metal is used as a reactant of the compound (eg. HCl) formed during the reaction process may react with the walls of the deposition character.

2.2.4 Electrochemical Deposition

In the electrochemical deposition technique, the electrolyte may be aqueous, non-aqueous or fused salts. The processes involved are the:

1. Attraction of unlike charges at the electrodes to establish dynamic equilibrium when an electric field is applied. The electrolyte decomposes, thereby making the ions to migrate to the cathode substrate for decomposition

2. Chemical changes that occur which are based on Faraday's laws of electrolysis;

$$m \alpha It$$

$$m=Zlt \quad (2.22)$$

where m is the mass of the element, I is the current, t is the time and Z is the electrochemical equivalent.

Faraday's law, states that if the same quantity of electricity passes through different electrolytes the masses of the elements deposited are proportional to their electrochemical equivalents.

The technique makes possible the deposition of various thin films whose structure depend on bath composition, temperature, electrode shape, current density and pH of the electrolyte (Li *et al*., 2005). Examples of this technique are anodization and electrophoresis technique.

(a)Anodization

Anodization is the field assisted form of thermal-assisted growth in which a metal is converted to its oxide or the preferential formation of a protective layer of oxide (Perrillo and Rodriguez, 2014).

The principle is based on electrolysis in which the electrolyte provides the required oxygen during decomposition while hydrogen evolution takes place at the cathode. With the constant voltage mode, the increase in thickness depends on the increase in voltage (but small current) with the limiting value occurring when there is a break-down (stoppage) in the growth of the oxide film. This is due to the fact that as the oxide film thickness increases, the voltage across the film increases while the field strength decreases, which eventually becomes weak in forcing the ions through the metal oxide film (Ottone*et al*., 2014).

Hence, the thin film thickness, t of the layer growth per unit voltage, V defines the anodization constant k_a given by

$$K_a = \frac{t}{V} \quad (.2.23)$$

which is about 20Å/V.

The main disadvantage at the constant voltage mode is that very high current densities are required in the initial stages of growth.

The technique has been used in the preparation of oxide films for MOS devices and other stable surface semiconductor devices

(b) Electrophoresis

Electrophoresis or electrophoretic deposition is the process in which electrically charged particles suspended in a liquid medium are deposited on an electrode.

Deposition of both conductors and non-conductors such as metal, alloys, oxides, polymers refractory compounds, salts and the combinations of all these.

The as-deposited thin films in the technique are loosely adherent coatings. This consists of pressurized compaction powder. In order to obtain an adherent compact and mechanically strong surface coating a post-deposition treatment is required (Ferrari *et al*., 1998). This consists of pressurized compaction and a heat treatment to dry out traces of the suspension medium and sinter the particle within the film. Figure 2.6 represents a broad view of different deposition techniques adopted in various depositions (Ohring, 2002).

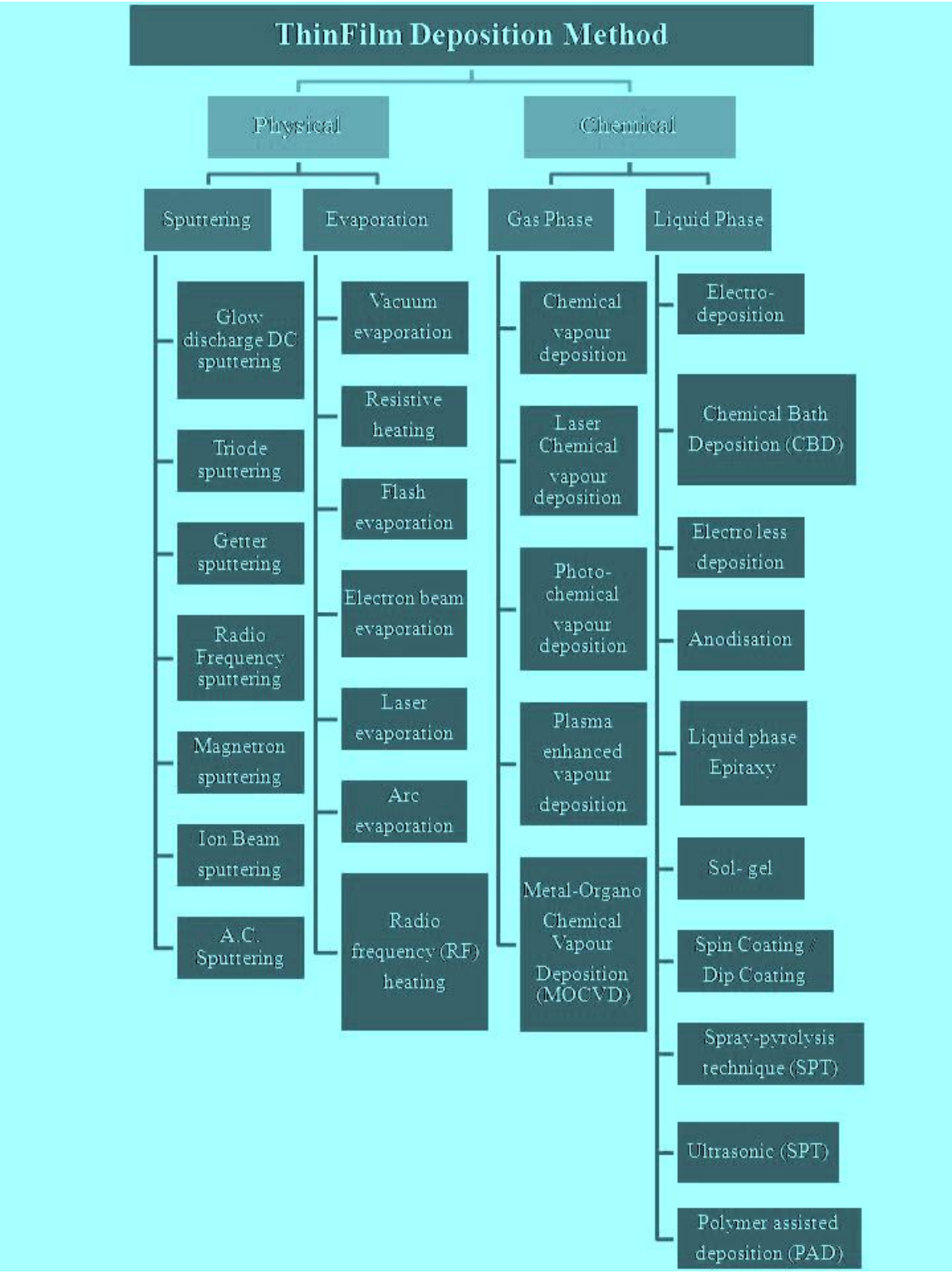

Figure 2.5 Classification of thin films deposition techniques (Ohring, 2002)

2.3 Single Crystal Growth

The subject of crystal growth has held a high level of interest, both scientifically and technologically, for a very long period. Nearly all basic solid materials of modern technology are made up of crystals. Hence an understanding of how crystals are grown is an important aspect of the science of materials. The need of better quality crystals in industries and technology cannot be met from the diminishing natural sources (Girase, 2013).Crystals are the most important constituent in the modern technology. Without materials in the crystal forms, electronic industry, photonic industry and fibre optic communication would have been not possible. The crystals used in these sectors are semiconductor, metal, insulator, superconductor, non-linear, magnetic, etc. materials.

Crystal growth is an interdisciplinary topic covering physics, chemistry, materials science, chemical engineering, metallurgy, crystallography, mineralogy, etc. In the past few decades, most of the focus is on crystal growth processes due to increasing demand of materials for technology application. It is very difficult to grow single crystal materials compare to the polycrystalline materials because single crystals are regular and repeated periodic arrangement of atom in three dimensions. The effects of grain boundaries in single crystals are responsible for the important changes in physical, optical and electrical properties.

The main significance is the anisotropy, uniformity of composition and the absence of boundaries between individual grains, which are certainly present in polycrystalline materials. Single crystals play important role in the optoelectronic devices but to achieve high performance from the optoelectronic devices, good quality single crystals are needed.

Growth of single crystals and their characterization towards device fabrication have assumed great movement due to their importance for both academic as well as applied research field (Cabric and Pavlovic,2000).They find application as high pressure, high temperature lubricants, catalysts, as electrode material for solar energy conversion purposes and in the development of primary and secondary batteries.

Growth of crystal ranges from a low cost technique to a complex sophisticated expensive

Growth from melts | Growth from vapour | Growth from solution | Gel Growth

crystals may be produced by the transport of crystal constituents in the solid, liquid or vapourphase. On the basis of this, crystal growth may be classified into following categories given below. The techniques for crystal growth are given in Figure 2.6. Small changes in the growth parameters, variation in the procedure etc., gives rise to different growth techniques(Srivastava and Palit, 2005).

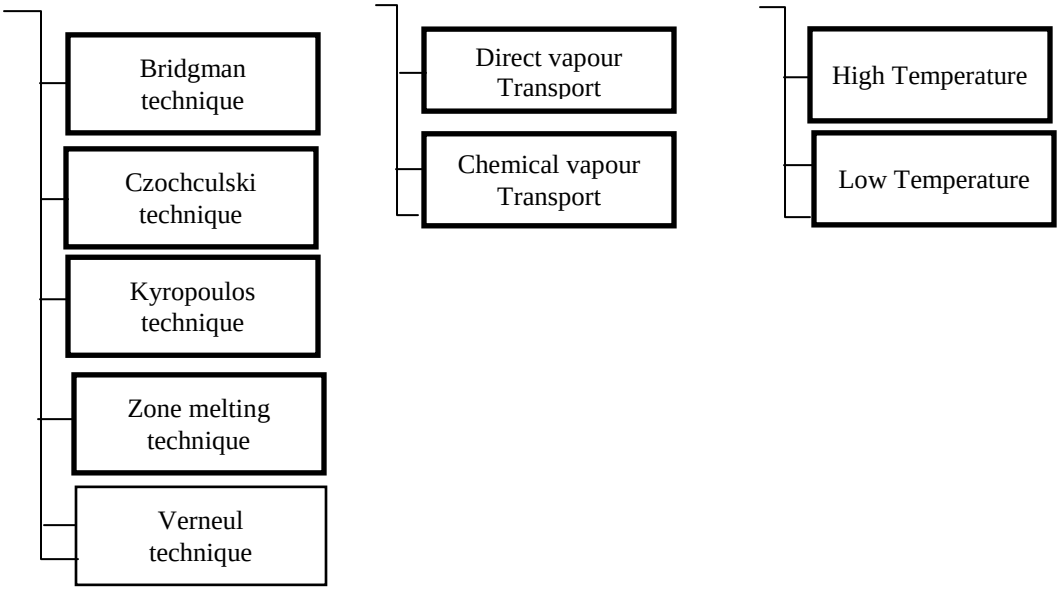

Figure 2.6 The Technique for Single Crystal Growth (Srivastava and Palit, 2005).

2.4Semiconductor Concept

Solids are primarily classified as insulators, metals and semiconductors. Semiconductors are materials that have conductivities between conductors (high conductivity) and insulators (no conductivity), conductivity roughly in the range of 103 to 108 siemens per centimeter.

The concept of energy bands is very useful in classifying materials as insulators, semiconductors and conductors.

The energy band diagram is a representation of the different allowed and available energy levels which an electron can occupy. The most important concept in the energy band diagram is the shape of the bands and their mutual energy separation. When similar atoms are brought close enough to each other to form a solid, the independent degenerate wave functions of their electrons overlap and as a way to satisfy the Pauli‘s exclusion principle (no two electrons can occupy the same quantum state), this degeneracy splits and the corresponding energy levels spread into a continuous range of energy levels instead of discrete levels in an isolated atom called the energy band.

There may (as in insulators and semiconductors) or may not (as in metals) exist an energy gap(forbidden band) between bands. This is given in Fig. 2.7, depending on a number of factors, including the type of atom(s) in the solid, lattice structure and temperature. The band gap in insulators may be as wide as 6 eV. In semiconductors, the conduction band is separated from the valence band usually by a narrow band gap of about. In metals, the conduction band overlaps the valence band (Yram, 2015).

2.5 Conductivity in Semiconductors.

The band structure of semiconductors is such that at absolute zero, the valence band is completely filled (all atoms are in the ground state) and the conduction band is completely empty. In order for conduction to occur, electrons must be excited to the next higher band, known as the conduction band. In semiconductors, the conduction band is normally empty at absolute zero but is separated from the valence band by only a small amount of energy gap of about 0.1 to 1eV (Yram, 2015). Valence electrons can overcome this barrier by absorbing a small amount of energy from thermal or optical sources. This then creates a free electron in the conduction band and a hole (missing electron) in the valence band.

Conductivity in semiconductors is also affected by temperature, as temperature is increased, some electrons gain sufficient amount of energy and move across the gap into the conduction band where they can move freely and conduct when a field is applied. Thus conductivity of semiconductors is said to be greatly dependent on the band gap and temperature. Within certain limits, higher temperatures gives rise to high electron concentration in the conduction band resulting in higher conductivity and an equal number of unoccupied states called holes in the valence band as depicts in Figure 2.7.

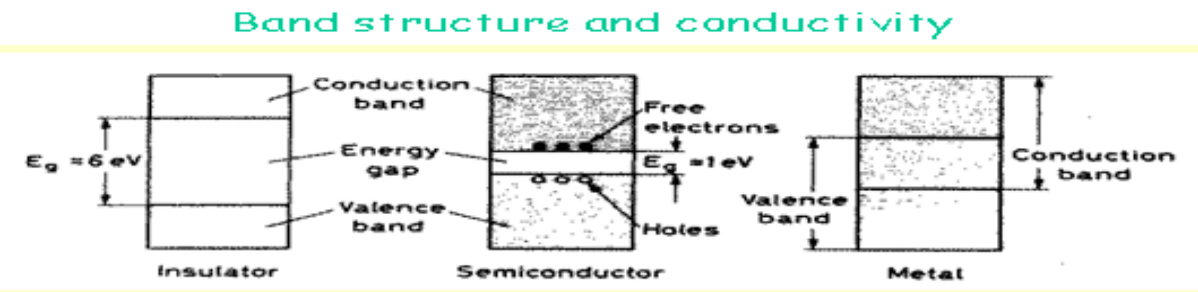

Figure 2.7 Energy band structures of conductors, semiconductors and insulators(Yram, 2015).

2.6 Classification of Solids

There are several ways of classifying solids and one important division is into crystalline, polycrystalline and amorphous. Each type is characterized by the size of an ordered region within the material. An ordered region is spatial volume in which atoms or molecules have a regular geometric arrangement or periodicity (Neamen, 2003).

2.6.1 Crystalline Solids

A crystalline material consists of atoms that are arranged in a periodic, regularly repeated three dimensional pattern as depicts in Fig. 2.8(a). In crystalline materials, a radial distribution function exhibits series of sharp peaks indicative of the long-range order. The electronic band structure in these materials have periodicity of the atomic structure, and the presence of long-range order results in a band structure with allowed and forbidden electronic levels, with sharp band edges and a fundamental energy gap separating valence band from conduction band. (Yacobi, 2003)

2.6.2 Polycrystalline Solids

A polycrystalline material consists of crystal grains that are randomly oriented with respect to each other as depicts in Fig. 2.8(b). Between two grains, a grain boundary exists. An important parameter is the grain size and its distribution. Polycrystalline solids are used in cheap, large – area applications such as solar cells or thin- film transistors. Polycrystalline material can be fabricated from an amorphous material using annealing procedures (Yram, 2015).

2.6.3 Amorphous Solids

An amorphous solid is any non-crystalline solid in which the atoms and molecules are not organized in a definite lattice pattern or a solid whose atomic structure is random such that long range atomic order is absent as shown in Figure 2.8(c). Amorphous solids, nevertheless, retain the short range order due to valence bonding of atoms, which is also characteristic of crystalline solids. The short-range order is responsible for the observation of semiconductor properties such as an optical absorption edge and also thermally activated conductivity. Amorphous materials can be re-crystallized into polycrystalline materials upon annealing. The number of nearest neighbors to any atom is not much different from the corresponding number in the crystalline material (Yacobi, 2003).

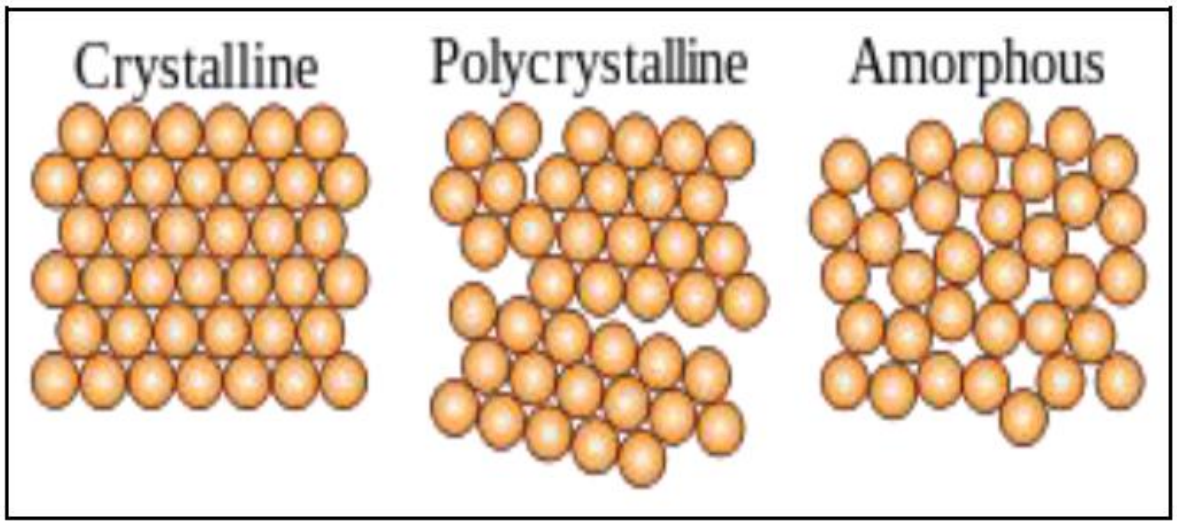

Figure 2.8 Types of semiconductor solid materials (Yram, 2015).

2.7 Applications of Thin Films

(a) Optical Coatings

The high reflection from most dielectrics semiconductors and metal surfaces can be reduced considerably by anti-reflection coating (Rosenberg *et al*., 1980). Thin films have been in use as ati- reflection coatings on window glasses, video screens, camera lenses and other optical devices. The thicknesses of the films, usually made from transparent materials, are always less than 100nm. The refractive indices are of the order of the square root of those of the substrate. This anti reflective property is particularly important for solar cell applications.

(b) Solar Control Coating

Thin films with high absorbance and low emittance are employed as coatings on roofing panels for the conversion of sunlight to useful heat. This is more than ordinary black paint which was earlier in use. The best known selective coating is electroplated blade chrome; it consists of chromium particles embedded in an amorphous Cr_2O_3 host (Rosenberge*et al*., 1980). Heat loss by conduction and convection are minimized by proper insulation of the panel. By using focusing devices to concentrate sunlight onto collecting devices, one can obtain temperature high enough to produce steam and electricity (250^0C – 500^0C).

The ideal material is the black chrome but it gives good and stable result only up to 250^0C. However, alternatives are still being developed under single materials, heat mirrors semi conductor – metal stacks and interference stacks.

(c) Thin Film Solar Cell

The active semiconductor layers in thin film solar cells are polycrystalline or disordered films of CdS, Si, GaAs, CdSe, CdTe, etc, that have been deposited on electrically active or passive substrate such as glass, plastic ceramics, metal, graphite or metallurgical silicon. The device has

its best performance if the thickness of the semiconductor is larger than the reciprocal of the absorption coefficient which enables most of the incident light to be absorbed. Similarly, if the diffusion length is larger than the film thickness, most photo-generated carriers can be collected.

The low cost advantage due to low processing cost and the relatively low cost materials has shifted the interest of researchers towards fabricating highly efficient thin film solar cell. However, because of grain boundary effects, poor quality semiconductor materials grown on foreign substrate and the chemical reactions of the semiconductors with ambient, the efficiency achieved has remained low accompanied by long-term instability. The highest efficiency achieved so far is 10% with Cu_2S- CdS cells.

The useful solar cells can be made in semiconductors containing very high defect density if the semiconductor films are sufficiently thin and have high absorption coefficient near the band edge complete with requisite nobilities (Sze, 1981).

(d) Thin Film Transistor (TFT)

A thin film transistor is a metal-oxide-semiconductor field effect transistor (MOSFET) fabricated on an insulating substrate by employing all thin film constituents (Migliorato, 1992). It has thickness of less than 1μm. It is mainly fabricated from either amorphous or polycrystalline materials. The pioneering work on TFT was carried out by Brody and co-workers at Westinghouse using cadmium selenide. However, at the level of TFT development today, only amorphous and polycrystalline silicon have industrial interest.

Pocket television sets with screen measuring up to 5 inches have been produced at commercial level using a Si- TFT. It is also being applied as switching devices in contact type image sensors and operational amplifiers in electronic printing. On the other hand, because of higher carrier

mobility of polysilicon, they are being used in the fabrication of integrated logic circuit with adequate speed as well as individual switching elements.

(e) Thin Film Resistors

Thin film sheet resistivity are the resistivity of a square of the thin film material when one contact is made along one entire side of the square and the other along the opposite side. With a material of a given sheet resistivity, the value of any particular resistor is determined by the length/width ratio, regardless of the actual length and width (Doyle, 1966). The implication of this is that if the length of the resistor is 5 times as long as the width the value of the resistor will be 5 times the sheet resistivity and one-fifth if otherwise.

Though sheets resistivity range of 10 to 10,000Ω/sq are available, most circuits are designed with materials having sheet resistivity of about 100 to 300 0hms/sq. in order to save cost which is proportional to the resistivity range.

However, due to the limitations of single metal films, alloys have been resorted in producing these resistors. About 500 Ω/sq. have been achieved with nickel – aluminum alloy. Resistors exhibiting good stability and power dissipation capabilities have been fabricated using chromium-silicon monoxide. Sheet resistivity range from 10 to 1000 Ω/sq. is attainable with this. Resistors made from metal-dielectric mixtures are called cermet resistors (Sze, 1981).

The major set back of the thin film resistor is end – to – end shunt capacitance which is even small (picofarad). Temperature affects the performance also. These resistors are better high frequency resistors than most discrete types.

(f) Thin Film Capacitors

The thin film capacitors are classified into four depending on the method of preparation of their dielectric layers. These include: (i) anodized (ii) evaporated (iii) reactively sputtered and (iv) polymerized capacitor.

An anodized thin film capacitor is formed from wet electrolytic cell having metals like tantanium, tungsten, titanium, aluminium and niobium as anode of the electrode and which is converted to oxide by anodization. As a result of the insulating properties of the oxide, the thickness of the layer formed depends on the applied voltage only and not on the length of time it is applied.The capacitor is most successful when tantanium is used as anode.

Evaporated film capacitors are usually formed in a vacuum. Due to its high dielectric strength, silicon monoxide is the most commonly used.

Polymer-film dielectrics may be formed by immersing a substrate in the appropriate monomer which is present as a gas at low pressure. Irradiation of the substrate surface by ultraviolet light or with an electron or ion beam causes local polarization to occur. Capacitors made from such dielectric films appear promising for application where several low-temperature cycling is anticipated (Doyle, 1966).The fabrication of reactively sputtered capacitors from metal oxides is still on.

It has been observed that thin film capacitors are highly stable when operated at a temperature below 150^0C and at voltage below 20 volts. The high frequency performances of capacitors are limited by series resistance of the two thin film electrodes.

(g) Thin Film Inductors

The thin film inductor could be fabricated by forming large spiral – turns of conductive material in order to achieve appreciable inductance. The most widely used method however is to wind small toroids on high-permeability ferrite these conductors are attached to the substrates by suitable lead.

(h) Micro Electronics

The film is used in the fabrication of semiconductor integrated circuits popularly called thin film integrated circuit.

Problems such as degradation and even inter-diffusion in integrated circuits are solved by using thin films with controlled texture.

(i) Metallurgical Coating

A coating is a near-surface region having properties different from the bulk material. Metallurgy is the science of procuring shaping, treating and use of metals. Metallurgical coatings are desirable and important for economic, aesthetic, achieving unique properties and for engineering designs. The coating process may be deformative chemical interaction which affects the solid state properties of the material. If the process involves the deposition of new materials on the substrate, the method is known as deposited or overlay coating but if it involves altering the entire surface material to produce a surface made up of the new material and the substrate it is called conversion coating (Nodeem*et al*., 2005).

The application of coating is categorized as: decorative, protection against corrosion, protection from friction, material conservation, cutting tools etc.

(j) Decorative Coatings

All kinds of consumer products are bearing aesthetically pleasing coatings today for variety of purposes. In order to increase gas mileage in automobiles, heavy metals parts are replaced with light weight plastic coated with chromium by sputtering to give it the accustomed and acceptable appearance.

(k) Protection Against Corrosion

During the operation of certain machines parts, some engine parts may be exposed to a high corrosive environment. To protect such parts carefully selected coating alloys which are resistant to corrosion are used to coat such parts. For instance, in gas turbine engine where blades and vanes used in the turbine are subjected to high stresses in a highly corrosive environment of gases containing oxygen, sculptures and chlorine. They are made corrosion resistant by coating (overlay process) the bulk material alloy at high temperature with M – Cr – Al alloy (M ≡ N_i, Co, Fe or Ni + Co). Replacement of cadmium coating with thick ion-plated aluminium coatings on aircraft, spacecraft and fastener parts protect them from galvanic corrosion and provide them good brazeability

(l) Protection from Friction

Dry film lubricant coatings of materials such as gold, MoS_2 WSe_2 and other laminar materials are deposited on bearings and other sliding parts by sputtering or ion-plating to reduce wear. Such dry film lubricants are especially important for critical parts used in long term applications, since conventional organic fluid are highly susceptible to irreversible degradation and creep over a long time.

(m)Materials Conservation

Very thin steel strips are being coated today continuously with aluminum in place of very scarce and costly tin until the strips go to lacquer line. The strips are then used to produce steel cans.

(n) Cutting Tools

Cutting tools are usually made of high-speed steel or cemented carbides. The degradation in these tools are usually as a result of abrasive and adhesive wears. High temperatures and forces at the tool tip promote micro-welding between the tool and the steel chips from work piece. This causes the tool tip to wear. A thin layer of a refractory compound such as TiC, TiN, Al_2O_3 prevents the micro welding by introducing a diffusion barrier.

(o) Nuclear Fuel

Pyrolytic carbon is deposited on nuclear fuel particles used in gas cooled reactors by chemical vapour deposition in fluidized beds. The coatings retain the fission products and protect the fuel from corrosion (Bunshah and Mattox, 1980,).

(p) Biomedical Uses

Metal parts are coated with carbon by ion- plating to obtain parts for implants such as heart valves. These coatings give the parts biological compatibility.

2.8 Optical Properties

The radiant energy impinging on a thin film surface may be reflected, absorbed or transmitted as well as minimally scattered. Our interest is to measure the transmittance and absorbance of the sample from the Ultraviolet (UV) regions to near infra-red (NIR) regions of the electromagnetic spectrum using the spectrophotometer and then deducing the reflectance value from the measurements. The double beam spectrophotometer isnormally used to measure the spectral transmittance of the film samples.

The optical properties measured and calculated in this work are the transmittance (T), absorbance (A), reflection (R), reflective index (n) extinction coefficient (k), complex dielectric constant ($\in$) and optical conductivity (σ_o). The solid state properties under consideration are the compositions of the films and the thickness computations and the energy band gap. These properties are important for the characterization of this work and they are briefly explained below.

(a)Transmittance

The transmittance, T of a sample is the ratio of the radiant power passing through the surface of the sample to the radiant power incidence on it (Wooten, 1972),

$$T = \frac{I_x}{I_0} \quad (2.24)$$

where I_x is the transmitted radiation and I_o is the incidence radiation.

Usually, when transmission is corrected for reflection (and probably scattering), then the reflection of the incident and exit surfaces mustbe taken into consideration. If the radiation reaching the first interface is (I-R) I_0 while that on the second is (I-R) I_0exp (-αx), then the only fraction that emerges is (I-R)(I-R) I_0exp (-αx) while the internally reflected portion

emerging is attenuated considerably. The resultant transmission becomes

$$T = \frac{(1-R)^2 \exp(-\alpha x)}{(1-R^2)\exp(-2\alpha x)} \quad (2.25)$$

while account has been taken of the multiple reflections in the thin film samples. Neglecting the second term in the denominator when the product αx is large, gives

$$T = \frac{I_x}{I_0} = (I-R)^2 \exp(-\alpha x) \quad (2.26)$$

When two samples of different thicknesses x_1 and x_2 are considered, then

$$\frac{T_1}{T_2} = \exp[\alpha(x_2 - x_1)] \quad (2.27)$$

(b) Absorbance

The absorbance, A of a sample is the fraction of incident light of a given wavelength that is absorbed as it strikes the surface of the sample. It is defined as the common logarithm of the ratio of incident radiation to the transmitted radiation i.e.

$$A = log_{10}\ {}^{1}/_{T} \quad (2.28)$$

where T is the transmittance of the film.

It is usually possible to measure the absorbance from a spectrophotometer calibrated in this logarithmic unit (Lothian, 1958) and then calculating the transmittance from it or vice versa.

(c) Reflectance

The reflectance, R of a solid is the fraction of the incident intensity of a given wavelength that is reflected when it strikes the surface of the solid material. The incident light on a sample can experience little scattering and we then obtain

$T + R + A + S = 1$(2.29)

where L = (A + S) is optical loss. If the value of S is negligible, then L = A and equation (2.29) reduces to

$R = 1 - (T + A)$(2.30)

The quality of a thin film sample for optical application is usually determined by the value of the scattering S.

(d)Absorption Coefficient

Absorption coefficient, α is the rate of decrease (or attenuation) of radiation intensity when it passes through a thin film sample of thickness, x. Using the diffusion (penetration) equation (Thewlis, 1962).This becomes

$$I_x = I_0 \exp(-\alpha x) \qquad (2.31)$$

From equation (2.31),

$$\alpha = \frac{\ln\frac{1}{T}}{x} \quad (2.32)$$

where thickness value in nm is assumed. The calculation of α is done from transmittance values using the above relation. Since transmittance can only be measured on an extremely thin sample, the α values for typical semiconductors are in the 10^5 to 10^6/m range.

(e)Complex Refractive Index

The behaviour of light as it passes from air (or vacuum) into a solid is determined not only by the energy configuration but the refractive index, n of the solid as well. The value of n is usually taken to be a real number, which increases with frequency, but at certain frequencies (e.g near absorption resonances and for X-rays), the refractive index will usually be smaller than one and it becomes convenient to represent the absorbance as an imaginary contribution. Therefore the complete optical characterization of a semiconductor both in bulk and in thin film is possible by determining the complex refractive index (Born and Wolf, 1975),

$n_c = n - ik$ (2.33)

The real part of the refractive index, n is related to the important physical properties of the semiconductor such as the reflectance spectrum, which is connected with the band structure. The knowledge of this parameter is also important for thin film, semiconductor applications like multilayer structures and antireflection coatings. On the other hand, the imaginary part of the refractive index (extinction coefficient, k) is directly related to the absorption coefficient, α. The energy dependence of the absorption coefficient from a practical point of view, allows the determination of the semiconductor band gap value, E_g and the nature of the optical transmissions – direct or indirect.

The value of n and k can also be obtained indirectly based on the measurement of the change in the polarization of light due to the reflection from a sample surface. However, the refractive index of most transparent media (n>>k) can be obtained directly by the use of a prism through interferometry.

In experimental work, the simultaneous measurement of transmittance and reflectance from a monochromatic beam is the most reliable (usually common) method for determining these

constants. Although they are called constants, the quantities n and k are not true constants in reality because they are strongly dependent on frequency (and wavelength), the angle of incidence and the thickness of the materials (thin film and substrate) through which the beam passes.

If the effects of reflection of the incident and emergent surfaces are not ignored, then the intensity of radiation transmitted through the sample in any direction cannot be justifiably represented by the equation T = exp (-αx). However, in the boundary between vacuum (or air) and an absorbing layer specified by the refractive index, n, the extinction coefficient, k and thickness, x at normal incidence, the reflectance (reflection coefficient) in terms of the optical constant becomes (Ashcroft andMermin, 1976),

$$R = \frac{(n-1)^2 + k^2}{(n+1)^2 + k^2} \quad (2.34)$$

where multiple reflections inside the thin film sample is ignored. In the case of semiconductors and insulators for materials within therange of frequencies in which absorption is weak $k^2 << (n-1)^2$, the relation then reduces to (Meinel and Meinel, 1976),

$$R = \frac{(n-1)^2}{(n+1)^2} \quad (2.35)$$

In which case, n becomes,

$$n = \frac{1+\sqrt{R}}{1-\sqrt{R}} \quad (2.36)$$

where the value of n for any wavelength can be calculated by determining the reflectance at that point. If n=0 and R=1, the semiconductor is totally reflecting.

The relation between the extinction coefficient and absorption coefficient becomes

$$\alpha = \frac{2kw}{c} = \frac{2\pi c2k}{\lambda c}$$

$$= \frac{4\pi k}{\lambda} \quad (2.37)$$

where k is the extinction coefficient, c is the speed of light, w is the angular frequency, and λ is the wavelength. However the transmittance spectrum of a thin film is characterized by the presence of interference which can be used to deduce the value of n (Pankove, 1971).

(f)Complex Dielectric Constant

The dielectric (poor conductors of electricity) may be regarded as a continuous medium which becomes polarized under the action of an electric field, the dielectric constant, K_e is given by

$$K_e = 1 + X_e = \frac{\in}{\in_0} \quad (2.38)$$

where Є is the complex dielectric constant, $Є_0$ is the permittivity of free space and $X_e$is the electrical susceptibility of the substance.

The constant is a characteristic property of a given dielectric material, which varies not only from one substance to another but also with the physical state of substances (Animalu, 1977).

In general, the dielectric constant is a complex quantity that is related to complex refractive index through the equation

$\in = \in_1 + i\in_2 = (n+ik)^2$ (2.39)

where $\in_1$ and $\in_2$ are the real and the imaginary parts. Therefore expanding and collecting terms gives

$\in_1 = n^2 - k^2$(2.40)

$\in_2 = 2nk$ (2.41)

where the real part, $\in_1$ relates to the refractive surface properties (Fresnel reflection coefficients) and the imaginary part, $\in_2$ gives the radio absorption coefficient (Bekefi and Barret, 1987). The physical implication is that electromagnetic waves incident on a medium can propagate through it when the real part is positive but are totally reflected from the medium if it is negative.

(g) Optical Conductivity

The optical response on a transparent solid is characterized by the complex refractive index given by$n_c = n - ik$, the real and imaginary parts may be expressed in terms of optical constants (ie the dielectric constant given by

$\in = \in_1 + i\in_2 = (n - ik)^2$

as well as the absorption coefficient defined by

$$\in_2 = \frac{\alpha nc}{w} \quad (2.42)$$

But we also have that

$\in_2 = (4\pi\sigma_o)/w$ (2.43)

From equation (2.42) and (2.43), we have

$$\frac{\alpha nc}{w} = (4\pi\sigma_o)/w$$

$$\sigma_o = \frac{\alpha nc}{4\pi} \quad (2.44)$$

where σ_o is optical conductivity (the frequency response of a material when irradiated by light) of the sample at the optical frequency concerned. We note that it is not generally equal to the dc or low frequency conductivity(Pankove, 1971),

The values of σ_o and k in metals are high with reflectance approaching unity and in semiconductors are low which reduce reflectance.

In insulators, the values of k and σ_o tends to zero and hence $n = \in^{1/2}$.

(h)Band Gap

A semiconductor in which the minimum of the conduction band and maximum of the valence band occur at the same value of the wave-vector, the absorption begins when the relation, $E_g = h\nu = (hc)/\lambda_o$ is satisfied where λ_0 is the minimum wavelength of absorption, h is the Planck's constant, c is the speed of light and v is the frequency for direct energy transition. Thus when the electron undergoes transition from the upper part of the valence band without a change in momentum, it causes dispersion near the fundamental absorption edge.

The absorption coefficient relationship for this direct transition is then given by (Bube,1974),

$$\alpha = A(h\nu - E_g)^n \quad (2.45)$$

where the selection rule gives $n = \frac{1}{2}$ for the allowed transition and n = 3/2 for forbidden transition. Similarly, for an indirect transition (Tsidilskovsk, 1982), the electron excitation is achieved using the energy of the photon with the momentum of the phonon. The absorption coefficient relationship in this case becomes

$$\alpha = B(h\nu - E_g + E_p)^n \quad (2.46)$$

where E_g is the band gap and E_p is the phonon energy involved in the indirect transition. If $E_p = 0$,

$$\alpha = B(h\nu - E_g)^n \quad (2.47)$$

where n = 2 is the allowed transition and n = 3 is the forbidden (Estrella*et al*, 2003) while A and B are constants which are characteristic of the crystalline and amorphous semiconductor materials.It is important to note that near the fundamental absorption edge, the dependency of the absorption coefficient on the energy of light quanta enables the plot of α^2 against hν in the direct transition deviates from being a straight line. Using the Tauc's plot technique (Tauc, 1968), an extrapolation of the straight portion of the plot cuts the hν axis at the point hν = E_g and α^2 =0 (the absorption edge). This gives the energy band gap, E_g which accurately obeys the Urbach exponential dependence on photon energy (Urbach, 1953). The same procedure is applied in the indirect transition but the extrapolation is made to cut hν axis in the determination of the energy band gap, E_g by plotting $\alpha^{1/2}$ against hν.

2.9 Review of Previous work using SILAR and SGT methods

Patil *et al.*,(2016) deposited copper oxide thin films on glass substrate using modified SILAR method. For deposition of CuO,0.1 M sodium thiosulphate ($Na_2S_2O_3$) solution was added to 0.1 M copper sulphatepentahydrate ($CuSO_4$. $5H_2O$) solution till copper sulphate solution becomes colourless (complex solution) which was used as cationic solution. 0.1 M sodium hydroxide (NaOH) solution was maintained at 70^oC temperature which was used as anionic solution. Ultrasonically cleaned glass substrates were first dipped in anionic solution for 5 s and then in cationic solution for 5 s, this completes one SILAR cycle. The CuO thin films were prepared for 90, 100, 110, 120 cycles. The X-ray diffraction spectroscopic study show that deposited CuO is polycrystalline in nature with monoclinic structure. Also it has flower like morphology which is porous in nature. The optical band gap energy varies from 2 to 2.1 eV with respect to deposition cycles. The photoluminescence show strong emission at 465 and 516 nm. The optical and

morphological properties of CuO thin films deposited using modified SILAR method show that CuO is useful for solar cell application. The maximum photoelectrochemical cell efficiency is 0.26 % for 100 SILAR cycles.

Ravichandran*et al.,* (2014), prepared thin films of copper oxide on glass substrates by SILAR method with slight modification which employs successive dipping in 1M NaOH, kept at 70 degrees copper complex solution at room temperature successively for 20 s, followed by rinsing in triple distilled water for 10 seconds. The structure of the films were studied using XRD and the films are found to be polycrystalline with mixed phases before annealing and tend to become monoclinic after having annealed. The morphology details of thin films were characterized using scanning electron microscopy and the morphology is formed by needle like grains. The optical properties of the films were studied using ultra violet- visible measurements within the energy ranges 1.45 to 2.3 eV. The band gap, was estimated using Tauc's method. The annealed sample exhibited a band gap of 1.7 eV. The films are suitable for optical applications.

Onwuemeka*et al.,* (2017) studied the deposition and characterization of Copper(I) oxide thin films prepared by solution growth technique using ammonia as complexing agent. The thin films of Cu_2O are deposited on glass substrate at 100°C of NaOH solution for 4hours. The deposited sample was annealed at 250°C using Master Chef annealing machine for 1hour. The optical properties were measured using UV-1800 Series Double Beam Spectrophotometer. The composition and thickness measurements of the films were determined using Rutherford Backscattering Spectroscopy (RBS), X-ray Fluorescence (XRF) and Quantitative Analysis. The optical band gap of the deposited films of Cu_2O is 2.61±0.05eV as annealed for 1hour at 250°C.

Other properties calculated from transmittance, using appropriate equation are absorbance, reflectance, absorption coefficient, refractive index, extinction coefficient, dielectric constant and optical conductivity were also determined.

Üst*et al.*, (2015) studied the electrochemical approaches for rearrangement of lead sulfide thin films prepared by SILAR method. A clean substrate was immersed into S^{2-} precursor solution for 20s, and then rinsed with deionized water for 20 store move the unattached ions. Then this sulfur-modified substrate was immersed into Pb^{2+} precursor solution for 20s and rinsed again with deionized water for 20s to completeone cycle of SILAR process. The dipping cycle was repeated many times to obtain PbS thin films for electrochemical approaches and the other characterizations. The production process of PbS thin films by the SILAR technique was repeated a number of times and confirmed that reproducible PbS thin films are obtained. Morphological studies showed that both electrochemical approaches result with morphological transformation from irregular film to regular cubic-like film formation. XRD patterns revealed that as prepared amorphous PbS thin films turning to polycrystalline structure with diffraction peaks at $2\theta = 26.40°$, 30.50°, 43.70°, 51.30°, and 53.90° which are associated with (111), (200), (220), (311), and (222) crystalline faces of PbS after electrochemical processes. UV–vis–NIR investigation of the PbS thin films demonstrated that optical properties of the thin films are protected after electrochemical applications. All of the results indicate that potentio-dynamic process results with more crystalline structure than that of potentio-statically processed samples. These electrochemical approaches are hope ful for reorganization of PbS thin films and may be considered as a supporting process to increase crystallinity of thin films not only for PbS but also other semiconductive materials e.g.CdTe or ZnSe.

Preetha*et al.,* (2012) deposited lead sulfide on glass substrate using successive ionic layer adsorption and reaction (SILAR) method at different pH of the cationic precursor, keeping the pH of the anionic precursor invariant. In this work, we establish that the pH of the cationic precursor and in turn the size of the crystallites affects the optical and electrical properties of PbS thin films. The characterization of the film was carried out using X-ray diffraction, scanning electron microscopy, optical and electrical measurement techniques. The presence of nanocrystallites was revealed by optical absorption and structural measurements. The PbS thin films obtained under optimal deposition conditions were found to be polycrystalline with face centered cubic structure.

The lattice parameter, grain size, micro strain, average internal stress and dislocation density in the film were calculated and correlated with pH of the solution. The values of average crystallite size were found to be in the range 16nm - 23nm. Optical studies revealed the existence of direct and indirect band gap values in the range 0.99eV-1.84 eV and 0.60eV-0.92 eV, respectively. The room temperature resistivity of the synthesized PbS films was in the range of 1.2 x 10^7 to 3.5 x $10^7 \Omega$ cm.

Daniel-Umeri*et al*., (2016) deposited copper oxide thin films on glass substrate. The effects of bath pH and temperature on the structural, morphological and optical properties of the films were investigated. The films were prepared by successively dipping them for 20s each in a solution of 1M NaOH and then in a solution of 0.1M copper complex. Temperature of the NaOH solution was varied from room temperature to 70^{o}C, while that of the copper complex solution was

maintained at room temperature. The films were characterized by X-ray diffraction (XRD), scanning electron microscopy (SEM), ultraviolet-visible spectroscopy (UV-VIS) and fourier transform infrared (FTIR) spectroscopy. XRD studies confirmed that the films were polycrystalline with both Cu_2O and CuO crystallographic phases existing depending on the pH of the solution bath. The calculated crystallite size from the XRD measurement was found to be in the range~1.52 -1.67A. SEM micrograph revealed that the grains were distributed evenly over the substrate surface. The bandgap value was found to be in the range, 1.6eV-2.0eV.

Onwuemeka and Nwulu (2017), studied the Deposition and Characterization of CdO thin films by solution growth technique using ammonia (NH_3) as a complexing agent. Thin films of CdO are deposited onto glass substrates using chemical bath deposition (CBD) at room temperature for 3hours and 1hour. X-ray florescence (XRF) which determines the cationic compositions and Rutherford Backscattering spectroscopy (RBS) analysis which reveals that the thin films have percentage compositions of the elements Cd/O, 47/53 for 3hours annealed sample at 200°C and the thicknesses are 100nm for 3hours and 200nm for 1hour.

It was found that CdO thin film exhibits n-type conduction. Optical band gap values of direct transitions are 2.48 ± 0.05eV and 2.20 ± 0.05eV for 1hour and 3hours annealed samples respectively. Optical properties were measured using Double Beam UV- Spectrophotometer with serial number UV061514. Transmittance was measured and other properties were calculated from it using appropriate equations.

Koao*et al.*,in 2014 who deposited lead sulphide (PbS) powders by chemical bath deposition (CBD) method by varying the synthesis temperatures. The influence of the synthesis temperature and the different molar concentration of lead acetates on the structure, morphology and optical properties of PbS nanostructures were investigated, respectively. The X-ray diffraction (XRD) patterns of the PbS nanostructures correspond to the various planes of a single phase cubic PbS. It was observed that a decrease in the synthesis temperature resulted into extra diffraction peaks due to the presence of impurity phases. It was observed that the estimated average grain sizes from XRD analysis increased slightly with an increase in the synthesis temperature and molar concentrations of lead acetate, respectively.

The crystallinity of the cubic PbS improved significantly with an increase in synthesis temperature and the molar concentration of lead acetate. The surface morphology study revealed nanorod structures at low synthesis temperatures but a cubic structure at the high synthesis temperatures. It was also observed that by increasing the molar concentration of lead acetate does not influence the morphology of PbSnanorods but the grain sizes increases slightly with an increase in lead acetate content. The reflectance spectra showed a partially increase in percentage reflectance and shift of the absorption edge to a higher wavelength with an increase in the synthesis temperature and molar concentration of lead acetate. An additional absorption band in the visible region (647 nm) emerged with an increase in the synthesis temperature. The band gap energy of PbS was found to decrease with an increase in the synthesis temperature and molar concentration of lead acetates, respectively. The luminescence intensity was found to decrease with an increase in the synthesis temperature and molar concentration of lead acetates, respectively. The maximum luminescence intensity was found at a synthesis temperature of 55ºC and at 0.12M of lead acetate, respectively.

Çetinkaya*et al.*,(2013) deposited CuO inter-layers in the CuO/p-Si Schottcky diodes using CBD and sol-gel methods. Deposited CuO layers were characterized by Scanning electron microscopy (SEM) and X- diffractometer (XRD) techniques. From the SEM images, it was seen that the film grown by CBD method is denser than the film grown by sol-gel method. This result is compatible with X-ray diffractometer (XRD) results which show that the crystallization in Chemical bath deposition (CBD) method is higher than it is in sol-gel method. For the electrical investigations, current-voltage characteristics of the diodes have been studied at room temperature. Conventional *I-V* and Norde's methods were used in order to determine the ideality factor, barrier height, and series resistance values. It was seen that the morphological and structural analysis are compatible with the results of electrical investigations.

The review of other works show that no substantial researches have been carried out in the area of metallic oxide alloyed thin films and the need to add to existing binary thin films of CdO, Ga_2O_3 and $In_2O_{3,}ZnO$, SnO_2 draw my interest to find the possibility of generating transparent metallic oxide alloyed thin film.

CHAPTER THREE
MATERIALS AND METHODS

3.1 Materials

The materials used include the following: sodium hydroxide (NaOH),de-ionized water, Copper (II) tetraoxosulphate (VI) pentahydrate ($CuSO_4.5H_2O$) salt, ammonia solution (NH_3)as complexing agent,lead (II) nitrate ($Pb(NO_3)_2$), glass substrates, hydrochlorine acid (HCl), tin(II) chloride ($SnCl_2$), trioxonitrate (V) acid (HNO_3), cadmium chloride ($CdCl_2$), zinc chloride ($ZnCl_2$), digital electronic balance and beakers pH metre, water bath, thermometer, electronic balance for weighing the reactants before and after deposition,the reagents and glass substrates for deposition processes to take place,thepH meter to determine the pH values of the solution during deposition, UV-1800 double beam spectrophotometer for the collection of optical data.X-ray spectrophotometer for determination of structuralproperties and scanning electron microscope (SEM) for microstructure and RBS for determination of compositionsand thicknesses of the deposited samples.

3.2 Methods

The dual approach involved in carrying out this work are successive ionic layer adsorption and reaction (SILAR) and solution growth deposition technique (SGT). SILAR deposition works on the principle of adsorption process and SGT deposition, is based on the principle of condensation process.

3.2.1 Pre-deposition Process

In order to obtain good and quality deposits using SILAR and SGT methods, the substrates were soaked in aqua regia (HCl and HNO_3) for 24 hours in the ratio 3:1 concentration to degrease the surface of the substrates and also to create nucleation centers on the surface of the

substrates where captures occur. The substrates were washed with detergents and rinsed in de-ionized water and were allowed to dry in air.

The reagents were weighed usingdigital electronic balance in order to determine the masses of the required reactants**.** The set-ups are shown in Figure. 3.1and 3.2 for SILAR and solution growth technique respectively.

3.3 Deposition of PbO Thin Films by SILAR Method

The dual approach employed in the deposition of PbO:SnO_2 involves the deposition of PbO thin films using SILAR method followed by SGT. The synthesis of PbO thin films using SILAR method constituted**:** 3ml of 3M solution of ammonia used as complexing agent and measured with a syringe and was added into separate beakers containing 16.56g of 0.2M solution of $Pb(NO_3)_2$ dissolved in 250cm^3 water and 16g of 2M solution of NaOH dissolved in 200cm^3 of watter, 3ml of 99% of 3M solution of ammonia used as complexing agent. The initial stage here is the formation of white precipitate and in addition of excess NH_3, and stirring vigorously the dissolution of the precipitate occurred leading to a complex solution called lead tetra-amine complex ion as given in equation (3.1). This reaction was made in 50ml beaker and de-ionized water was added up to 50ml in order to free the ions in the solution.

$$Pb(NO_3)_2 + 4NH_3 \rightleftharpoons [Pb(NH_3)_4]^{2+} + 2NO_3^- \quad (3.1)$$

PbO thin films were deposited as given in equation (3.2), on the substrates in cycles; one cycle is completed by dipping the substrate first into the beaker containing the cationic precursor followed by rinsing in de-ionized water for 5 seconds and finally immersing it in the third beaker of ionic precursor.

In Figure 3.1, adsorption took place in the first beaker containing $[Pb(NH_3)_4]^{2+}_{(aq)}$ when the substrates were immersed in it for 6 seconds and then rinsed in a beaker of de-ionize water in the

second beaker for 5 seconds, followed by reaction in the third beaker, containing the anionic precursor,which is 16g of 2M solution of NaOH dissolved in $200cm^3$ of water kept at constant temperature of 60^0C for 6 seconds after which the substrates were rinsed in de-ionized water for 5 seconds and this was repeated based on the number of chosen cycles and dip-time for the samples as depicts in Table 3.1**.** The reaction equation for SILAR deposition of PbO thin films is given in equation (3.2).

$$[Pb(NH_3)_4]^{2+}{}_{(aq)} + 2NaOH_{(aq)} \rightarrow PbO_{(s)} + 2Na^{+}{}_{(aq)} + H_2O_{(l)} + 4NH_{3(l)} \quad (3.$$

Table 3.1 The deposition of PbO thin films by SILAR Method

Sample	Dip-time(s)in each reactant	No. of cycle	Dip-time(s) in each Beaker of H_2O
A_7	6	15	5
A_8	6	15	5
A_9	6	15	5
A_{10}	6	15	5
A_{11}	6	15	5
A_{12}	6	15	5

3.4 Deposition of $PbO:SnO_2$ Using Solution Growth Technique

The constituent materials that make-up the deposited samples of $PbO:SnO_2$**,** on the substrates includes: 20mlof 13.52g of 0.24M complex solution of hydrated tin(II) chloride, 3ml of 3M solution of NH_3 and 15ml of 16g of 2M solution of NaOH and the substrates containing the deposited samples of suspected PbO thin filmsprepared by SILAR method. Ammonia ($NH_{3(aq)}$) in this reaction is the complexing agent. It controls the rate of ion – by – ion interaction, thereby moderating the rate of formation of precipitate. It also creates an alkaline medium for good formation of deposits. The process was performed at the constant parameters such as concentration, volume of complexing agent, temperature, time of growth and pH except the annealing temperatures as given in Table 3.2. By immersing the substrates containing the suspected PbO thin films in already prepared solution mixture containing 0.24M solution of hydrated tin (II) chloride complexed with NH_3 solution given in equation (3.3), and withNaOH solution as the anionic precursor given in Figure 3.2and was kept for 12 hours for optimum deposition of $PbO:SnO_2$ to occur after which the samples were removed and rinsed in de-ionized water and was allowed to dry in air by hanging it in slanting order by the aid of a clip.

Several bath compositions were employed, but the optimum result was achieved with the specification noted above for all the samples in Table 3.2. Equally good and uniform depositions were obtained using 0.1M, 0.25M 0.4M, 0.5M, solutions of tin chloride. The solutions for the depositions were made in 50ml beakers and on glass substrates at the pH value of 10. The resultant equation from the reaction is given in equation (3.4).

$$SnCl_2.2H_2O + 4NH_3 \longleftrightarrow [Sn(NH_3)_4]^{2+} + 2H_2O + 2Cl^- \quad (3.3)$$

$$2PbO_{(s)} + [Sn(NH_3)_4]^{2+}{}_{(aq)} + 4NaOH^-{}_{(aq)} \rightarrow SnPb_2O_{4(s)} + 4Na^+ + 2H_2O_{(l)} + 4NH_{3(aq)} \quad (3.4)$$

The samples were annealed at varying temperatures ranging from100°C-250°C in order to remove the water of crystallization, thereby obtaining adherent white deposit on the substrates as given in equation(3.5).

$$SnPb_2O_{4(s)} + 2H_2O_{(g)} \xrightarrow[100^0C\text{-}250^0C]{\text{heat}} SnPb_2O_{4(s)} \quad (3.5)$$

Table 3.2 The different parameters for the deposition of PbO:SnO_2 thin films of 0.24M solution of $SnCl_2.2H_2O$

Samp-les	Annealing Temp.(°C) (for1hour)	$Pb(NO_3)_2$ Conc. (mol)	NH_3 Conc. (mol)	NaOH Conc. (mol)	$SnCl_2$ Vol. (ml)	NH_3 Vol. (ml)	NaOH Vol. (ml)	Dep. Temp of (NaOH) (°C)	Dep. Time (hr)
A_7	150	0.20	3.00	2.00	20.00	5.00	15.00	60.00	12.00
A_8	100	0.20	3.00	2.00	20.00	5.00	15.00	60.00	12.00
A_9	150	0.20	3.00	2.00	20.00	5.00	15.00	60.00	12.00
A_{10}	200	0.20	3.00	2.00	20.00	5.00	15.00	60.00	12.00
A_{11}	250	0.20	3.00	2.00	20.00	5.00	15.00	60.00	12.00
A_{12}	200	0.20	3.00	2.00	20.00	5.00	15.00	60.00	12.00

3.5 Deposition of CuO Thin Films by SILAR Method

The dual approach employed in the deposition of CuO:SnO_2 involves the deposition of CuO thin films using SILAR method followed by SGT. The synthesis of CuO thin films using SILAR method constituted**:** 3ml of 99% of 3M solution of ammonia used as complexing agent and measured with a syringe and was added into separate beakers containing 19.97g of 0.4M of $CuSO_4.5H_2O$ dissolved in 200cm^3 of water and 16g of 2M solution of NaOH dissolved in 200cm^3 of water kept at constant temperature of 60^0C.

The initial stage here occurred when $CuSO_4.5H_2O$ solution was made to react with NH_3 solution, leading to the formation of blue gelatinous precipitate, which dissolved in excess NH_3, solution leading to the formation of complex solution called copper tetra-amine complex ion as given in equation (3.6). This reaction was made in 50ml beaker and de-ionized water was added up to 50ml in order to free the ions in the solution.

$$CuSO_4.5H_2O + 4NH_3 \rightarrow [Cu(NH_3)_4]^{2+} + 5H_2O + SO_4^{2-} \qquad (3.6)$$

CuO thin films were deposited as given in equation (3.6), on substrates in cycles; one cycle is completed by dipping the substrate first into the beaker containing the cationic precursor of $[Cu(NH_3)_4]^{2+}$and anionic NaOH precursor for 5 seconds followed by rinsing in de-ionized water for 4 seconds between the two reactants. The complete deposition occurred after 20 cycles for all the sample as demonstrated in Figure 3.1.

In Figure 3.1, the reaction process involves adsorption of Cu cation from the complex solution in the first beaker for 5 secondsand then followed by rinsing in a beaker of de-ionize water in order to remove unadsorbed Cucations on the surface of the substrates for 4 seconds.

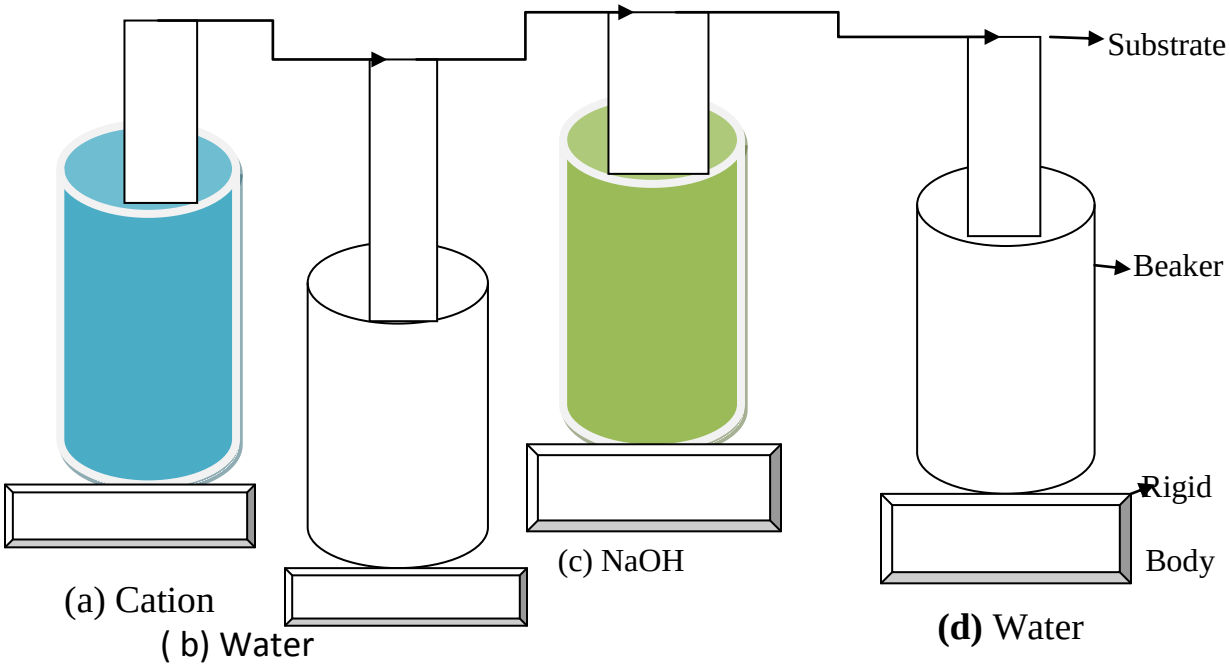

Figure 3.1Experimental Set up of SILAR deposition method.

However, the formation of CuO occurred when the substrates were immersed in the third beaker containing anionic precursor of 16g of 2M solution of NaOH dissolved in 200cm^3 of water kept at constant temperature of 60^{0}C, for 5 seconds after which the substrateswas rinsed in de-ionized water for 4 seconds and this was repeated based on the number of chosen cycles and dip-time for the samples as depicted in Table 3.3**.** The reaction equation for SILAR deposition of CuO thin films is given in equation (3.7).The parameters for the deposition of CuO are given in Table 3.3.

$$[Cu(NH_3)_4]^{2+}{}_{(aq)} + 2NaOH_{(aq)} \rightarrow CuO_{(s)} + 2Na^{+}{}_{(aq)} + H_2O_{(aq)} + 4NH_{3(l)} \quad (3.7)$$

Table 3.3 The deposition of CuO thin films by SILAR Method.

Sample	Dip-time(s) in each Reactant	No. of cycle Beaker of H_2O	Dip-time(s) in each
A_{19}	5	20	4
A_{20}	5	20	4
A_{21}	5	20	4
A_{22}	5	20	4

3.6 Deposition of CuO:SnO_2Alloyed Thin Films by Solution Growth Technique

The constituent materials that make-up the deposited samples of CuO:SnO_2, on different substrates: 20ml of 0.24M solution of hydrated tin chloride, 3ml of 3M solution of NH_3 solution and 15ml of 2M solution of NaOH and the substrates containing the deposited samples of suspected oxides of CuO prepared by SILAR method. Ammonia ($NH_{3(aq)}$) in this reaction is the complexing agent. It controls the rate of ion – by – ion interaction, thereby moderating the rate of formation of precipitate. It also creates an alkaline medium for good formation of deposits.

The process was performed at the constant parameters such as concentration, volume of complexing agent, temperature, time of growth and pH as given in Table 3.2 by immersing the substrates containing the suspected CuO thin films into already prepared solution mixture containing 0.24M solution of hydrated tin (II) chloride complexed by NH_3 solution, and with anionic precursor of 16g of 2M solution of NaOH dissolved in 200cm^3 of water kept at constant temperature of 60^0C, given in Figure 3.2**.** It was kept for 9 hours for optimum deposition of CuO:SnO_2 to occur after which the samples were removed and rinsed in de-ionized water and were allowed to dry in air by hanging it in slanting order by the aid of a clip. Several bath

compositions were employed, but the optimum result was achieved with the specification given in Table 3.4. The solutions for the depositions were made in 50ml beakers and on glass substrates at the pH value of 11. The resultant equation from the reaction is given in equation (3.8).

$$2CuO_{(s)} + [Sn(NH_3)_4]^{2+}{}_{(aq)} + 4NaOH_{(aq)} \rightarrow Cu_2SnO_{4(s)} + 4Na^{+}{}_{(aq)} + 2H_2O_{(l)} + 4NH_{3(aq)} \quad (3.8)$$

The samples were annealed at varying temperatures ranging from 100°C-250°C in order to remove the water of crystallization, thereby obtaining adherent white deposit on the substrates as given in equation (3.9).

$$Cu_2SnO_{4(s)} + 2H_2O_{(g)} \uparrow \xrightarrow[100^{o}C\text{-}250^{o}C]{heat} Cu_2SnO_{4(s)} \quad (3.9)$$

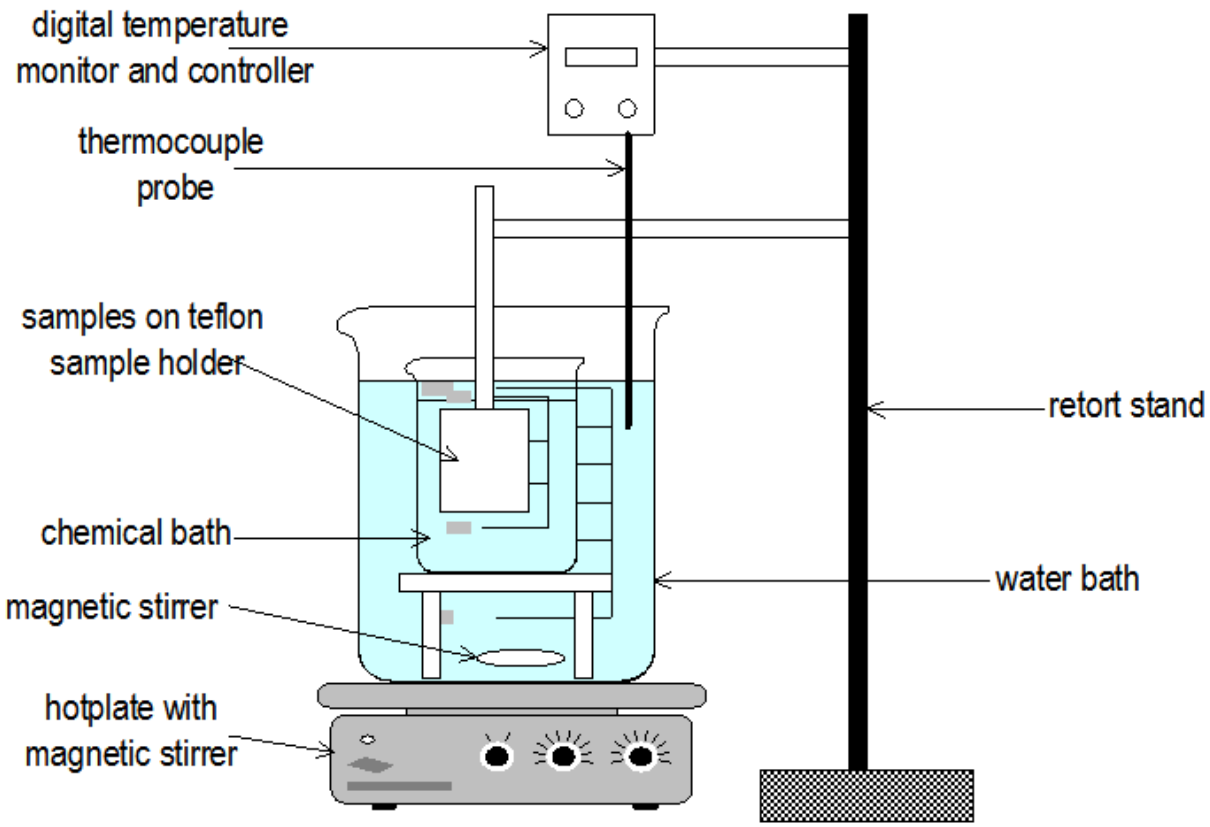

Figure3.2 Experimental setup of Solution Growth Technique (Hodes, 2002).

Table 3.4 The different parameters for the deposition of CuO:SnO_2 thin films of 0.24M solution of $SnCl_2.2H_2O$

Samples	Annealing Temp.(°C) (1hour)	$CuSO_4$ Conc. (mol)	NH_3 Conc. (mol)	NaOH Conc. (mol)	$SnCl_2$ Vol. (ml)	NH_3 Vol. (ml)	NaOH Vol. (ml)	Dep. Temp (NaOH) (^OC)	Dep. Time (hr)
A_{19}	100	0.40	3.00	2.00	20.00	5.00	10.00	60.00	9.00
A_{20}	200	0.40	3.00	2.00	20.00	5.00	10.00	60.00	9.00
A_{21}	150	0.40	3.00	2.00	20.00	5.00	10.00	60.00	9.00
A_{22}	250	0.40	3.00	2.00	20.00	5.00	10.00	60.00	9.00

3.7 Deposition of ZnO Thin Films by SILAR Method

The dual approach employed in the deposition of ZnO:SnO_2 involves the deposition of ZnO thin films using SILAR method followed by SGT. The synthesis of theZnO thin films using SILAR method constituted: 3ml of 3M solution of ammonia used as complexing agent, 20.45g of 1M solution of $ZnCl_2$ dissolved in 150cm^3 water and 16g of 2M solution of NaOH dissolved in 200cm^3 of water and3ml of 99% of 3M solution of ammonia used as complexing agent.

The initial stage here occurred when $ZnCl_2$ solution was made to react with NH_3 solution, leading to the formation of white gelatinous precipitate, which dissolved in excess NH_3, solution leading to the formation of complex solution called zinc tetra-amine complex ion as given in equation (3.9). This reaction was made in 50ml beaker and de-ionized water was added up to 50ml in order to free the ions in the solution.

$$ZnCl_2 + 4NH_3 \rightleftharpoons [Zn(NH_3)_4]^{2+} + 2Cl^- \qquad (3.10)$$

In Figure 3.1, the reaction process involves adsorption of cations of Zn^{2+} from the complex solution in the first beaker through immersion of the substrates for 8 seconds and subsequently followed by rinsing in the second beaker of de-ionize water for 3 seconds in order to remove unadsorbed Zn-ions on the surface of the substrates.

However, the formation of ZnO occurred when the substrates were immersed in the third beaker containing anionic precursor of 16g of 2M solution of NaOH dissolved in $200cm^3$ of water kept at constant temperature of 60^0C for 8 seconds after which the substrates were rinsed in de-ionized water for 3 seconds and this was repeated based on the number of chosen cycles and dip-time for the samples as depicts in Table 3.5**.** The reaction equation for SILAR deposition of ZnO thin films is given in equation (3.10).

$$[Zn(NH_3)_4]^{2+}{}_{(aq)} + 2NaOH_{(aq)} \rightarrow ZnO_{(s)} + 2Na^{+}{}_{(aq)} + H_2O_{(l)} + 4HN_{3(l)} \qquad (3.11)$$

The deposition is done successively in the same cycle times and at the same time the substrates lasts in each beaker to achieve uniform deposition.

Table 3.5 The deposition of ZnO thin films by SILAR Method.

Sample	Dip-time(s) in each reactant	No. of cycle	Dip-time(s) in each beaker of H_2O
A_{24}	8	22	3
A_{25}	8	22	3
A_{26}	8	22	3
A_{27}	8	22	3
A_{28}	8	22	3

3.8 Deposition of $ZnO:SnO_2$ alloyed thin films by Solution Growth Technique

The constituent reagent that make-up the deposited samples of $ZnO:SnO_2$ alloy on the substrates include: 20ml of 0.24M solution of hydrated tin(II) chloride, 3ml of 3M solution of NH_3 and 15ml of 2M solution of NaOH and the substrates containing freshly deposited samples of suspected ZnO thin films prepared by SILAR method. Ammonia ($NH_{3(aq)}$) in this reaction is the complexing agent. It controls the rate of ion – by – ion interaction, thereby moderating the rate of formation of precipitate. It also creates an alkaline medium for good formation of deposits.

The process was performed at the constant parameters such as concentration, volume of complexing agent, temperature, time of growth and pH as given in Table 3.6 by immersing the substrate containing the suspected ZnO thin films into already prepared solution mixture containing 0.24M solution of hydrated tin (II) chloride complexed by NH_3 solution, and with anionic precursor of 16g of 2M solution of NaOH dissolved in $200cm^3$ of water kept at constant temperature of 60^0C, given in Figure 3.2**.** It took 8 hours for optimum deposition of $ZnO:SnO_2$ to occur after which the samples were removed and rinsed in de-ionized water and were allowed to dry in air by hanging it in slanting order with the aid of a clip.

Several bath compositions were employed, but the optimum result was achieved with the specification noted above for all the samples in Table 3.6. Several bath compositions were employed as depicts in Table 3.6, but the optimum result was achieved with the specification noted above with the pH value of 11. Equally good and uniform depositions were obtained using 0.5M, 0.25M, 0.1M, solutions of tin chloride. The solutions for deposition were made in 50ml beakers as depicts in equation (3.12).

$$2ZnO_{(s)} + [Sn(NH_3)_4]^{2+}{}_{(aq)} + 4NaOH_{(aq)} \rightarrow Zn_2SnO_{4(s)} + 4Na^+ + 2H_2O_{(l)} + 4NH_{3(aq)} \quad (3.12)$$

The samples were annealed at varying temperatures ranging from,100°C-250°C in order to remove the water of crystallization, thereby obtaining adherent white deposit on the substrates as given in equation (3.13).

$$Zn_2SnO_{4(s)} + 2H_2O_{(g)} \xrightarrow[100^0C\ -250^0C]{\text{Heat}} Zn_2SnO_{4(s)} \quad (3.13)$$

Table 3.6The different parameters for the deposition of ZnO:SnO_2 thin films of 0.24M solution of $SnCl_2.2H_2O$

Samples	Annealing Temp.(°C) (for1hour)	$ZnCl_2$ Conc. (mol)	NH_3 Conc. (mol)	NaOH Conc. (mol)	$SnCl_2$ Vol. (ml)	NH_3 Vol. (ml)	NaOH Vol. (ml)	Dep. Temp (NaOH) (^OC)	Dep. Time (hr)
A_{23}	100	1.00	3.00	2.00	20.00	4.00	10.00	60.00	8.00
A_{24}	200	1.00	3.00	2.00	20.00	4.00	10.00	60.00	8.00
A_{25}	250	1.00	3.00	2.00	20.00	4.00	10.00	60.00	8.00
A_{26}	200	1.00	3.00	2.00	20.00	4.00	10.00	60.00	8.00
A_{27}	250	1.00	3.00	2.00	20.00	4.00	10.00	60.00	8.00
A_{28}	200	1.00	3.00	2.00	20.00	4.00	10.00	60.00	8.00
A_{29}	150	1.00	3.00	2.00	20.00	4.00	10.00	60.00	8.00

3.9 Deposition of CdO Thin Films by SILAR Method

The dual approach employed in the deposition of $CdO:SnO_2$ involves the deposition of CdO thin films using SILAR method followed by SGT. The synthesis of the alloyed thin films of CdOusing SILAR method constituted: 3ml of 3M solution of ammonia used as complexing agent 21.63g of 0.47M of hydrated $CdCl_2$ dissolved in $200cm^3$of water and 16g of 2M solution of NaOH at elevated temperature of 60^0C.When NH_3 solution was made to react with hydrated $CdCl_2$in a 50ml beaker, a white gelatinous precipitates, was formed which dissolved in excess NH_3 solution forming cadmium tetra-amine complex ion as given in equation (3.14).

$$CdCl_2.2^1/_2H_2O + 4NH_3 \rightleftharpoons [Cd(NH_3)_4]^{2+} + 2\ ^1/_2H_2O + 2Cl^- \quad (3.14)$$

De-ionized water was added up to 50ml and the solution was stirred vigorously in order to achieve uniformity in the mixture. CdO thin films were deposited on substrates in cycles; one cycle was completed by dipping the substrates first into the beaker containing the $[Cd(NH_3)_4]^{2+}$cationic precursor for 10 secondsand then rinsed in a beaker of de-ionize water by immersion for 4 seconds, and then immersed into the third beaker, containing the anionic precursor for 10 seconds, which is 16g of 2M solution of NaOHat elevated temperature of 60^0C, after which the substrates were rinsed in de-ionized water through immersion for another 4 seconds, as shown inFigure 3.1. This was repeated based on the number of chosen cycles. This is given in equations (3.15).

$$[Cd(NH_3)_4]^{2+}{}_{(aq)} + 2NaOH_{(aq)} \xrightarrow{CdO_{(s)}} 2Na^+{}_{(aq)} + H_2O_{(l)} + 4NH_{3(l)} \quad (3.15)$$

The deposition is done in successive cycle times and the time the substrates last in each beaker, this is given in Table 3.7.

Table3.7 The deposition of CdO thin films using SILAR Method.

Sample	Dip-time(s) in each Reactant	No. of cycle	Dip-time (s) in each Beaker of H_2O
A_{13}	10	10	4
A_{14}	10	10	4
A_{15}	10	10	4
A_{16}	10	10	4
A_{17}	10	10	4

3.10 Depositions and Reactions of $CdO:SnO_2$ Using Solution Growth Technique

The constituent reagent that make-up the deposited samples of $CdO:SnO_2$ alloy on the substrates include: 20ml of 0.24M solution of hydrated tin(II) chloride, 3ml of 3M solution of NH_3 and 15ml of 2M solution of NaOH and the substrates containing freshly deposited samples of suspected CdO thin films prepared by SILAR method. Ammonia ($NH_{3(aq)}$) in this reaction is the complexing agent. It controls the rate of ion – by – ion interaction, thereby moderating the rate of formation of precipitate. It also creates an alkaline medium for good formation of deposits.

The process was performed at the constant parameters such as concentration, volume of complexing agent, temperature, time of growth and pH except the annealing as given in Table 3.2. By immersing the substrates containing the suspected CdO thin films into already prepared solution mixture containing 0.24M solution of hydrated tin (II) chloride complexed by NH_3 solution, given in equation, and with anionic precursor of 16g of 2M solution of NaOH dissolved in $200cm^3$ of water kept at constant temperature of 60^0C. It took 6 hours for optimum deposition of $CdO:SnO_2$ to occur as given in Figure 3.2. After which the samples were removed and rinsed in de-ionized water and were allowed to dry in air by hanging it in slanting order by the aid of a clip. Several bath compositions were employed, but the optimum result was achieved with the specification noted above for all the samples in Table 3.8.

Several bath compositions were employed as depicted in Table 3.8, but the optimum result was achieved with the specification noted above with the pH value of 12. Equally good and uniformdepositions were obtained using 0.5M, 0.25M, 0.1M, solutions of tin chloride. The solutions for deposition were made in 50ml beakers as depicts in equation 3.16.

$$2CdO_{(s)} + [Sn(NH_3)_4]^{2+}{}_{(aq)} + 4NaOH_{(aq)} \rightarrow Cd_2SnO_{4(s)} + 4Na^{+} + 2H_2O_{(l)} + 4NH_{3(aq)} \quad (3.16)$$

The samples were annealed at temperature range,100°C-250°C in order to remove the water of crystallization, thereby obtaining adherent white deposit on the substrates as given in equation 3.17.

$$Cd_2SnO_{4(s)} + 2H_2O_{(g)} \uparrow \xrightarrow[100^0C\text{ -}250^0C]{Heat} Cd_2SnO_{4(s)} \quad (3.17)$$

Table 3.8 The different parameters for the deposition of CdO:SnO_2 thin films of 0.24M solution of $SnCl_2.2H_2O$

Samp-les	Annealing Temp.(°C) (for1hour)	$CdCl_2$ Conc. (mol)	NH_3 Conc. (mol)	NaOH Conc. (mol)	$SnCl_2$ Vol. (ml)	NH_3 Vol. (ml)	NaOH Vol. (ml)	Dep. Temp (NaOH) (^OC)	Dep. Time (hr)
A_{13}	150	0.47	3.00	2.00	20.00	5.00	15.00	60.00	6.00
A_{14}	100	0.47	3.00	2.00	20.00	5.00	15.00	60.00	6.00
A_{15}	200	0.47	3.00	2.00	20.00	5.00	15.00	60.00	6.00
A_{16}	150	0.47	3.00	2.00	20.00	5.00	15.00	60.00	6.00
A_{17}	150	0.47	3.00	2.00	20.00	5.00	15.00	60.00	6.00
A_{18}	250	0.47	3.00	2.00	20.00	5.00	15.00	60.00	6.00

CHAPTER FOUR

RESULTS AND DISCUSSION

It was observed that when 5ml of 3M solution of NH_3 was allowed to react with 20ml of 0.24M solution of hydrated $SnCl_2$, a white precipitatewas formed, which dissolved in excess NH_3 solution forming a colourless transparent solution of $[Sn(NH_3)_4]^{2+}$ (tin tetra-ammine complex ion).When 15ml of 2M solution of NaOH at 60°C was added to the solution of $[Sn(NH_3)_4]^{2+}$,the white precipitate reappeared.

When the substrates containing PbO, ZnO, CdO and CuO thin films deposited by SILAR method were inserted into the individual mixture, it took 12 hours, for $PbO:SnO_2$, 8 hours for $ZnO:SnO_2$, 6 hours for $CdO:SnO_2$ and 9 hours for $CuO:SnO_2$ to deposit optimally depending on the deposition parameters such as pH, volumes of reactants and the concentrations. From literature, zinc salts, tin salts, lead salts, copper salts and cadmium salts have the capabilities of forming complex solutions with ammonia.

This makes ammonia solution a suitable complexing agent for the deposition of the above named alloyed oxide thin films. Thus, the rates of reaction and the formation of precipitates are reduced, leading to a larger terminal thickness of the films.

However, the deposition of these oxide thin films is pH-dependent. OH^- from NaOH, did not take part in the complex formation therefore, the addition of OH^- precipitated the corresponding hydrous oxides of the individual ions which were deposited on the substrates.

In the case of OH^- ions taking part in the reaction processes, its addition increases the pH value, making the complex more stable, thereby reducing the concentration of free radicals. The suitable pH value for this work is 11,10, 12 and 11 for $CuO:SnO_2$, $PbO:SnO_2$**,** $CdO:SnO_2$ and

$ZnO:SnO_2$ respectively as detected by the pH meter. The deposited films of different parametric conditions were subjected to heat treatment from 100ºC-250ºC. using Master Chef Annealing Machine.

4.1 Characterization

It is often necessary to determine the elements that make up the thin film samples. In this work, atomic compositions and thicknesses of the samples were determined by Rutherford back scattering spectroscopy(RBS) analysis, XRD for crystallographic studies, scanning electron microscopy (SEM) for microstructure studies and UV double beam spectrophotometer for optical studies.

4.1.1Composition and Thickness Characterizations

It is often necessary to determine the elements and the thicknesses of the thin film samples. In this work, elemental compositions and the thicknesses of the samples were determined using Rutherford Back Scattering equipment: 2.2MeV alpha beam, obtained from CERD Ion Beam Analysis (IBA) Facility With Model: NEC 5SDH 1.7 MV Pelletron Tandem Accelerator equiped with a Radio Frequency Charge Exchange Ion Source Alphatron.

The Rutherford backscattering analysis shows that the sample A_{11} and A_{12} of $PbO:SnO_2$ alloyed thin films annealed at 250ºC and 200ºC respectively have 4.82% of lead, 1.39% of tin, 93.79% of oxygen with thickness of 105.20nm and 3.47% of lead, 1.28% of tin, 85.25% of oxygen with thickness of 109.28nm. These are shown in Figure 4.1 and Figure 4.2 and summarized in Table 4.1 and Table 4.2 respectively.

The samples A_{24} and A_{25} expected to be $ZnO:SnO_2$ thin films annealed at 200°C and 150°C respectively have 6.68% of zinc, 13.60% of tin, 79.72% of oxygen with thickness of 190.0nm and 5.14% of zinc, 13.42% of tin, 81.45% of oxygen with thickness of 388.52nm. These are shown in Figure 4.3 and Figure 4.4and respectively itemized in Table 4.3 and Table 4.4.

The samples A_{14} and A_{16} expected to be $CdO:SnO_2$ thin films annealed at 100°C and 150°C respectively have 1.35% of cadmium, 5.60% of tin, 93.05% of oxygen with thickness of 527.34nm and 1.35% of cadmium, 5.48% of tin, 93.17% of oxygen with thickness of 509.31nm . These are shown in Figure 4.5 and Figure 4.6and respectively itemized in Table 4.5 and Table4.6.

Samples A_{21} and A_{22} of $CuO:SnO_2$ alloyed thin films annealed at 150°C and 250°C respectively have 1.41% of copper, 10.28% of tin, 83.31% of oxygen with thickness of 411.44nm and 0.94% of copper, 6.02% of tin, 93.03% of oxygen with thickness of 126.22nm. These are shown in Figure 4.7 and Figure 4.8and respectively itemized in Table 4.7 and Table 4.8. These results is oxygen-rich films, which maybe as a result of exposure to air and surface hydroxide (Onwuemeka, *et al.,* 2014).

Table 4.1 The elements in sampleA_{11} of PbO:SnO_2

Elements	Layer(1)%Comp.	Layer(2)%Comp.
O	93.79	56.00
Ca	-	1.83
Fe	-	0.52
Na		12.60
Al	-	0.53
Si	-	28.00
Pb	4.82	-
Sn	1.39	

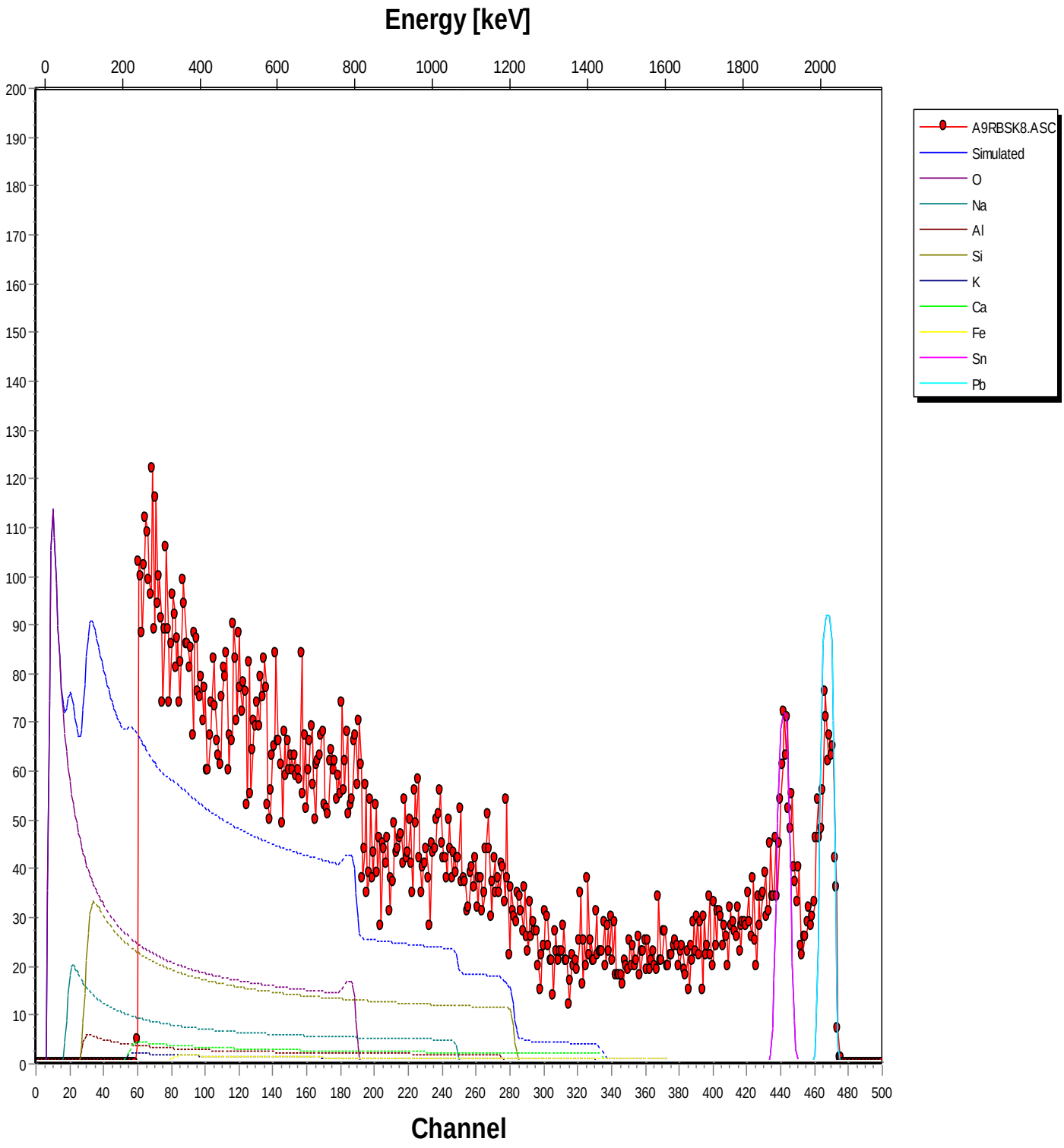

Figure 4.1 The Composition of Sample A_{11} with Thickness, 105.20nm, of $PbO:SnO_2$ Measured by Rutherford Backscattering Spectroscopy

Table 4.2 The elements in sample $A_{12}$of PbO:SnO_2

Elements	Layer(1)%Comp.	Layer(2)%Comp.
O	85.25	56.00
Ca	-	1.83
Fe	-	0.52
Na		12.60
Al	-	0.53
Si	-	28.00
Pb	3.47	-
Sn	1.28	

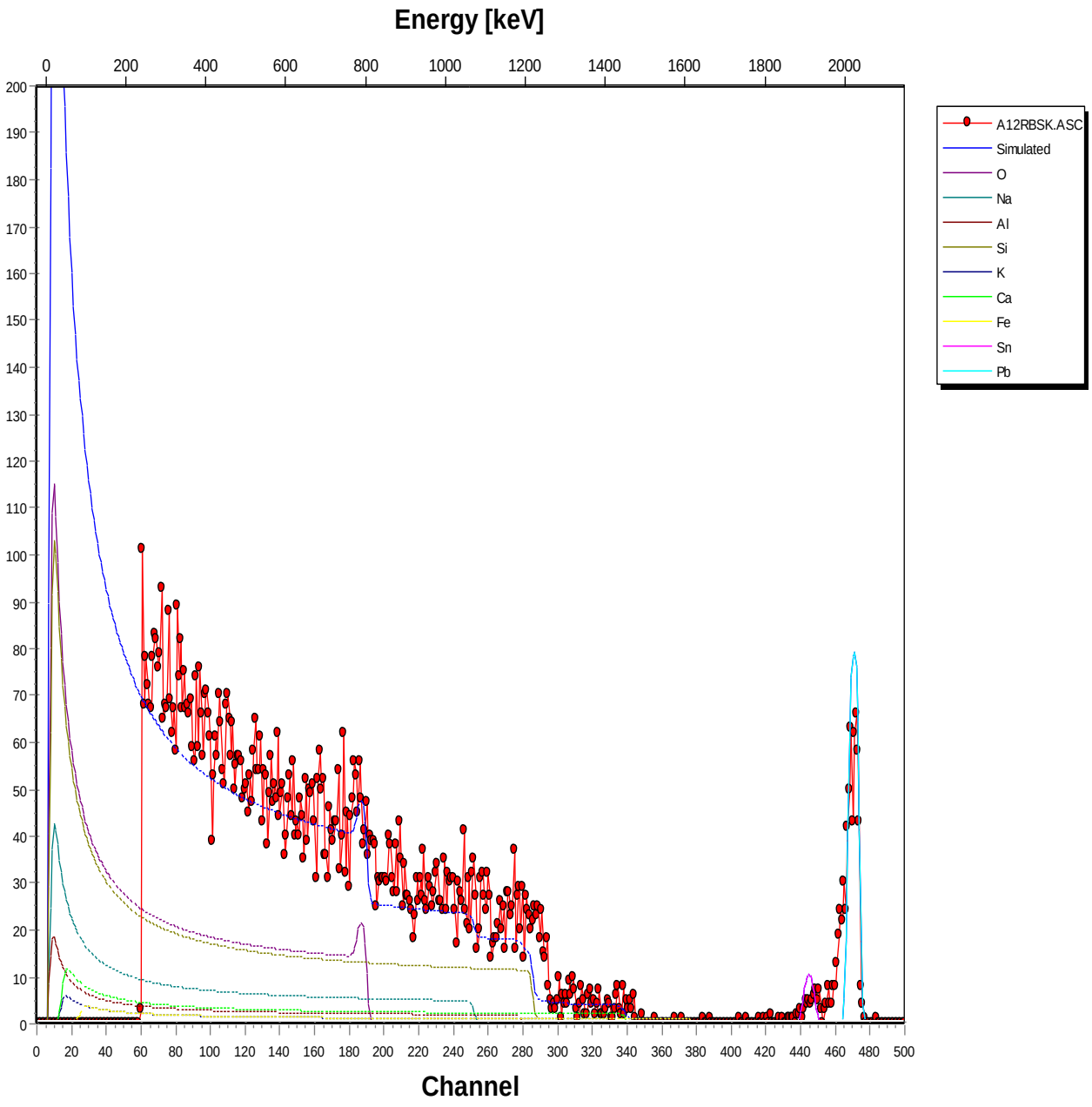

Figure 4.2 The composition of sample A_{12} of PbO:$SnO_2$with thickness, 109.28nm as measured by Rutherford backscattering spectroscopy**.**

Table 4.3 The elements in sample $A_{24}$of $ZnO:SnO_2$

Elements	Layer(1)%Comp.	Layer(2)%Comp.
O	79.72	56.00
Ca	-	1.83
Fe	-	0.52
Na		12.60
Al	-	0.53
Si	-	28.00
Zn	6.68	-
Sn	13.60	

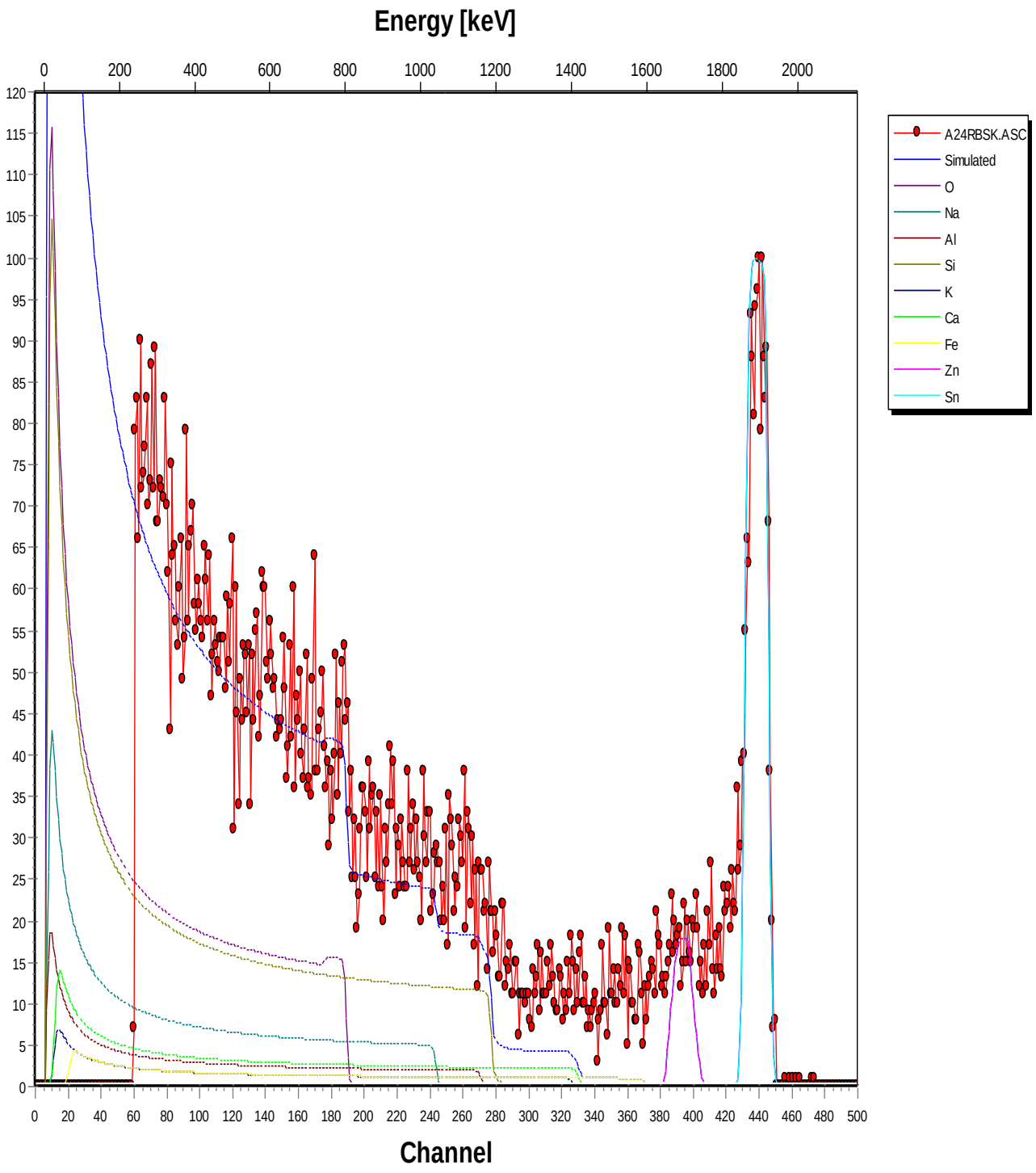

Figure 4.3 The composition of sample A_{24} of $ZnO:SnO_2$with thickness, 190.0nm as measuredbyRutherford backscattering spectroscopy

Table 4.4 The elements in sample $A_{25}$of ***$ZnO:SnO_2$***

Elements	Layer(1)%Comp.	Layer(2)%Comp.
O	81.45	56.00
Ca	-	1.83
Fe	-	0.52
Na		12.60
Al	-	0.53
Si	-	28.00
Zn	5.14	-
Sn	13.42	

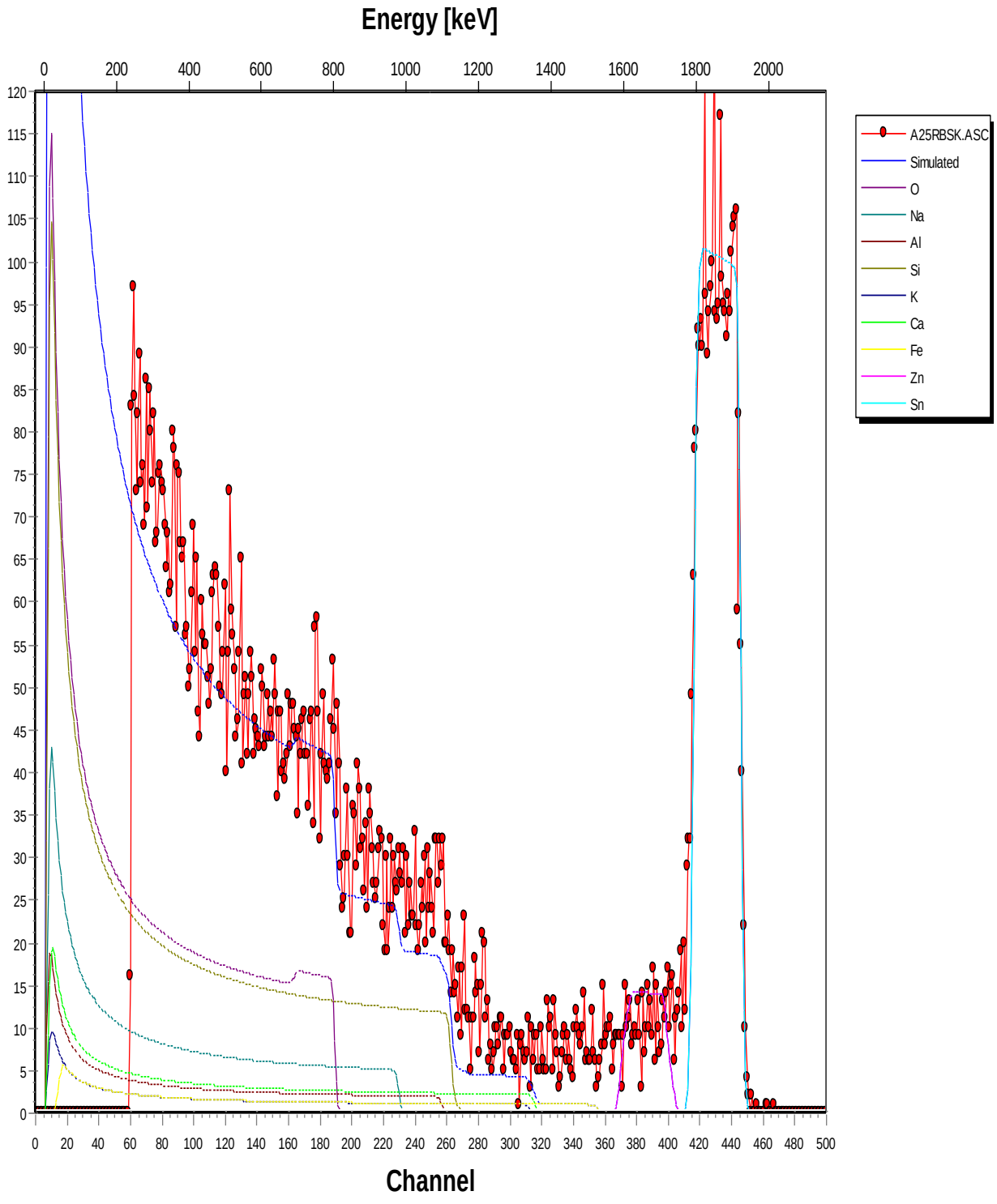

Figure 4.4 The composition of sample A_{25} of $ZnO:SnO_2$with thickness, 388.52nm as measured by Rutherford backscattering spectroscopy

Table 4.5 The elements in sample A_{14} of $CdO:SnO_2$

Elements	Layer(1)%Comp.	Layer(2)%Comp.
O	93.05	56.00
Ca	-	1.83
Fe	-	0.52
Na		12.60
Al	-	0.53
Si	-	28.00
Cd	1.35	-
Sn	5.60	

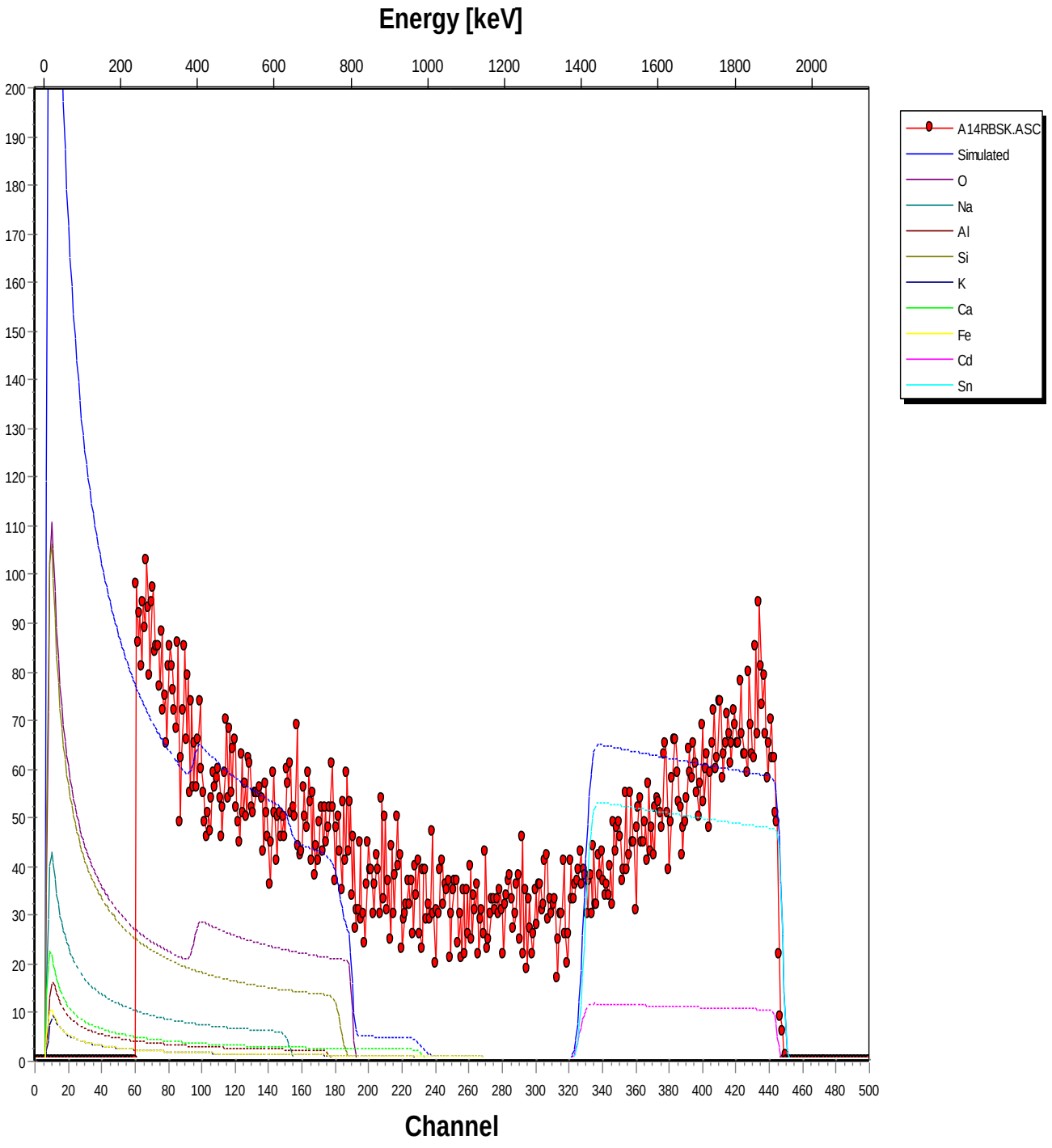

Figure 4.5 The composition of sample A_{14} of $CdO:SnO_2$with thickness, 527.34nm as measured by Rutherford backscattering spectroscopy

Table 4.6 The elements in sample A_{16} of $CdO:SnO_2$

Elements	Layer(1)%Comp.	Layer(2)%Comp.
O	93.17	56.00
Ca	-	1.83
Fe	-	0.52
Na		12.60
Al	-	0.53
Si	-	28.00
Cd	1.35	-
Sn	5.48	

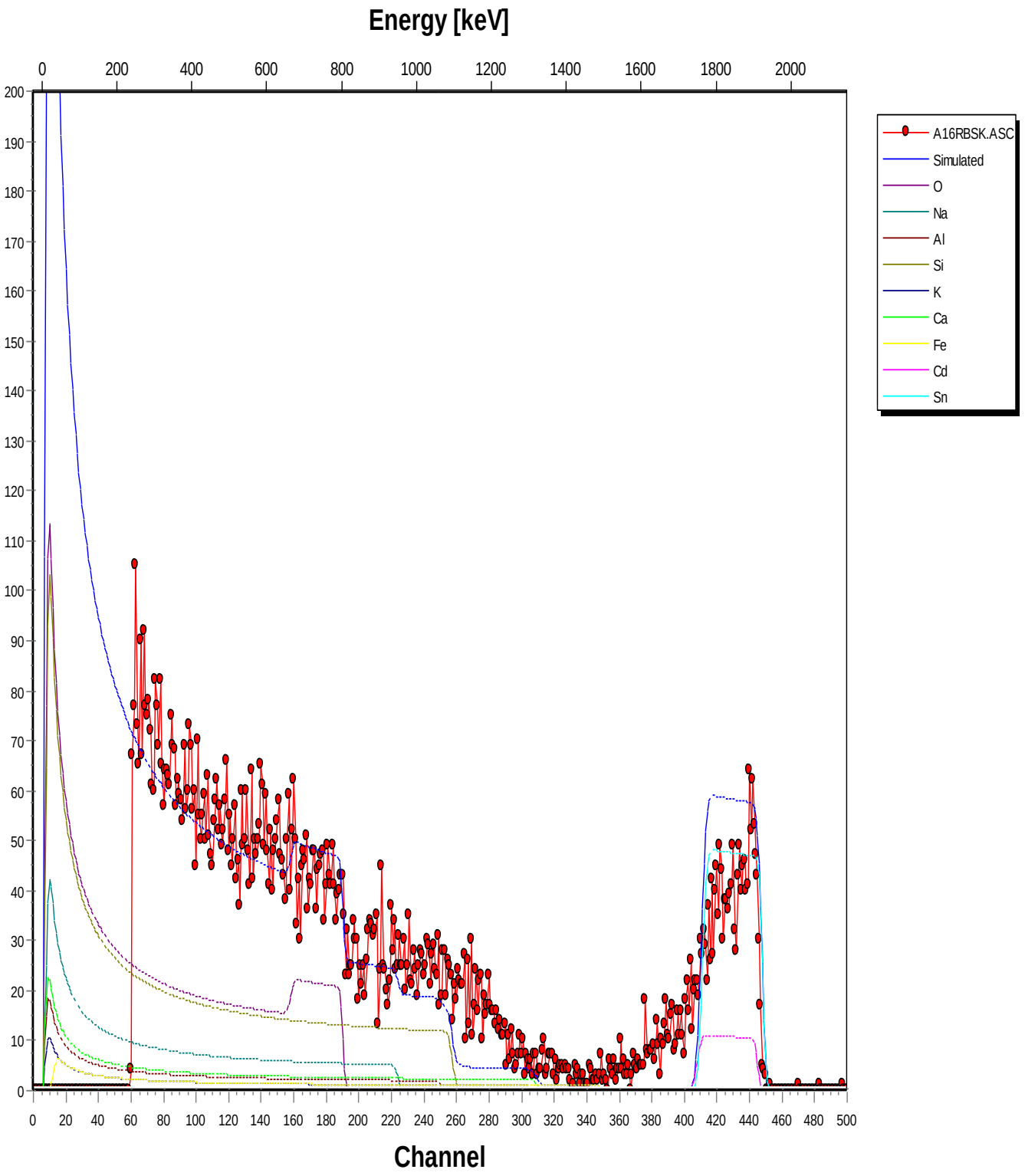

Figure 4.6 The composition of sample $A_{16}$of $CdO:SnO_2$with thickness 509.31nm as measuredbyRutherford backscattering spectroscopy

Table 4.7 The elements in sample $A_{21}$of $CuO:SnO_2$

Elements	**Layer(1)%Comp.**	**Layer(2)%Comp.**
O	88.31	56.00
Ca	-	1.83
Fe	-	0.52
Na		12.60
Al	-	0.53
Si	-	28.00
Cu	1.41	-
Sn	10.28	

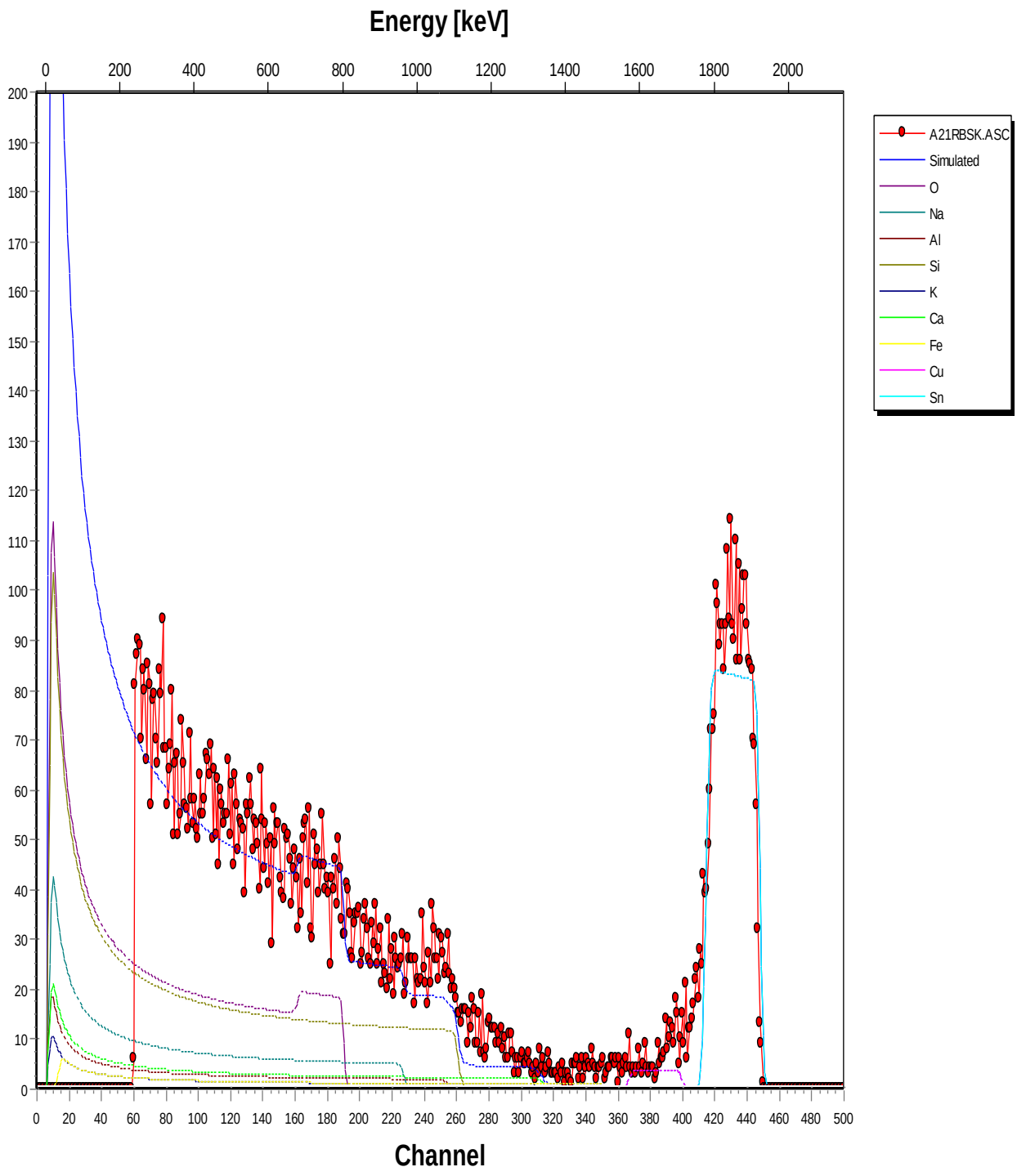

Figure 4.7 The composition of sample A_{21} of CuO:$SnO_2$with thickness 411.44nm as measured by Rutherford backscattering spectroscopy

Table 4.8 The elements in sample $A_{22}$of $CuO:SnO_2$

Elements	Layer(1)%Comp.	Layer(2)%Comp.
O	93.02	56.00
Ca	-	1.83
Fe	-	0.52
Na		12.60
Al	-	0.53
Si	-	28.00
Cu	0.94	-
Sn	6.02	

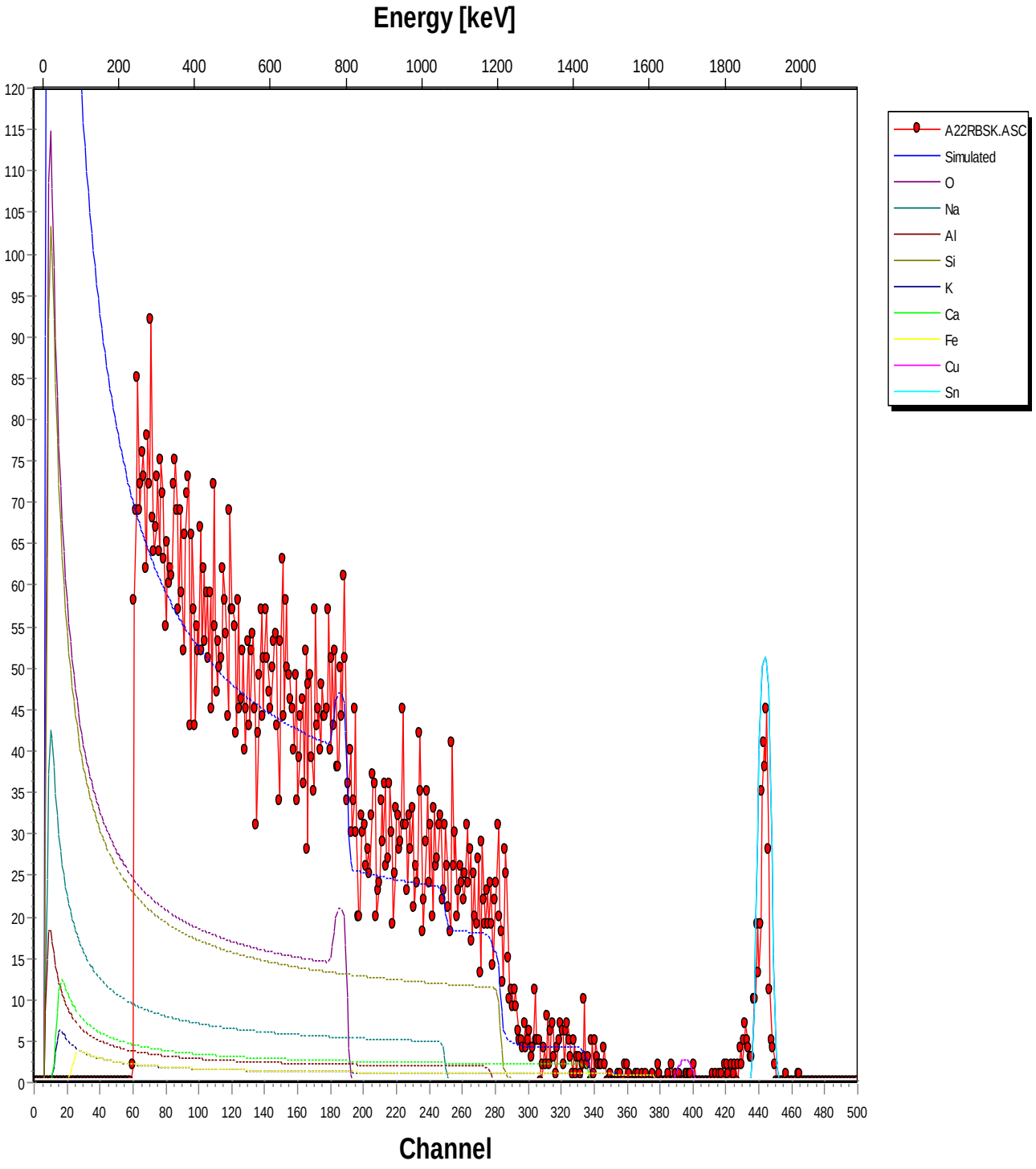

Figure 4.8 The composition of sample A_{22} of $CuO:SnO_2$with thickness, 126.22nm as measured by Rutherford backscattering spectroscopy.

4.1.2. Structural Characterizations

It is very important to examine the structures of the deposited materials, which include the crystallographic structure of the materials using X-ray diffractometer(XRD) and the microstructure of the deposited samples using scanning electron microscope (SEM).

(a) Crystallographic Studies of the Deposited Samples

The XRD analysis was carried out using X-ray diffractometer modeled GBC Enhanced Mini Material Analyzer (EMMA). XRD pattern gives information relative to the nature and structure of the alloyed thin films of PbO:SnO_2, CdO:SnO_2, CuO:SnO_2 and ZnO:SnO_2, prepared at 60^0C of sodium hydroxide solution**.** Figures 4.9, 4.10, 4.11and4.12 show x-ray diffraction of the above listed alloyed thin films.

The XRD patterns show sharp and well defined peaks which indicates the crystalline nature of alloys of PbO:SnO_2, CdO:SnO_2 and ZnO:SnO_2. The XRD pattern of CuO:SnO_2, alloyed thin films have no defined peak(s) which indicates the amorphous nature of the alloyed thin films, grown at 60^0C of sodium hydroxide solution.

The crystallite sizes given in Table 4.9 are obtained using Debye-Scherer's equation (Reka*et al,* 2014)

$$D = \frac{k\lambda}{\beta Cos\theta} \quad (4.1)$$

where k is the shape factor (k= 0.9), D is the grain size or average crystallite size, λ is the wavelength of CuKα radiation used (λ = 1.54Å), β is the experimentally observed diffraction peak width at half maximum intensity (full width at half maximum FWHM) and θ is the Bragg's diffraction angle.

Table 4.9 X-ray Diffraction Results of $PbO:SnO_2$, $CdO:SnO_2$, $CuO:SnO_2$ and $ZnO: SnO_2$ Alloyed Thin Films

Sample	2θ (degree)	d-spacing (Å)	FWHM (radian)	Grain size (nm)	Count	(hkl)
A_{12} ($PbO: SnO_{2I}$)	22.30	3.983	0.153	92.29	49	(111)
A_{16} ($CdO: SnO_2$)	15.40	5.749	0.153	91.41	41	(111)
A_{24} ($ZnO: SnO_2$)	19.552	4.537	0.350	40.18	45	(111)
	22.811	3.895	0.153	92.41	130	(200)

(b) The XRD Pattern of$PbO:SnO_2$ Alloyed Thin Films of Samples A_{11} and A_{12}

Figure4.9, shows the XRD pattern of $PbO:SnO_2$ alloyed thin films of samples A_{11} and A_{12} with one diffraction peak at $2\theta = 22.30^0$ with corresponding Miller indices (111). The patterns show well defined peaks which indicates the crystalline nature of the alloyed $PbO:SnO_2$ at 60^0C of NaOH solution. The crystallite size of both alloys is 92.29nm, using equation 4.

From the XRD results, a new compound alloyed thin films known as tin (IV) di-lead tetra oxide with orthorhombic crystal system is formed. It has a chemical formula; $SnPb_2O_4$.

The calculated data of the lattice parameters of $PbO:SnO_2$ alloy thin films of sample A_{12} are a = 8.709Å, b = 8.721Å and c = 6.292Å.

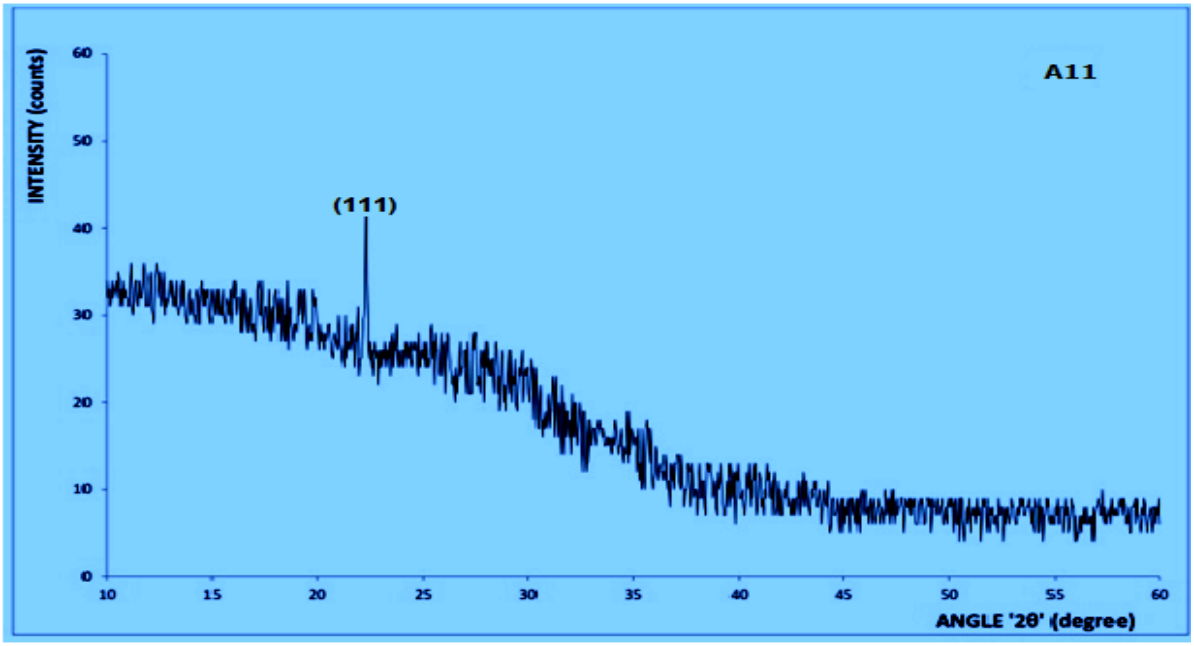

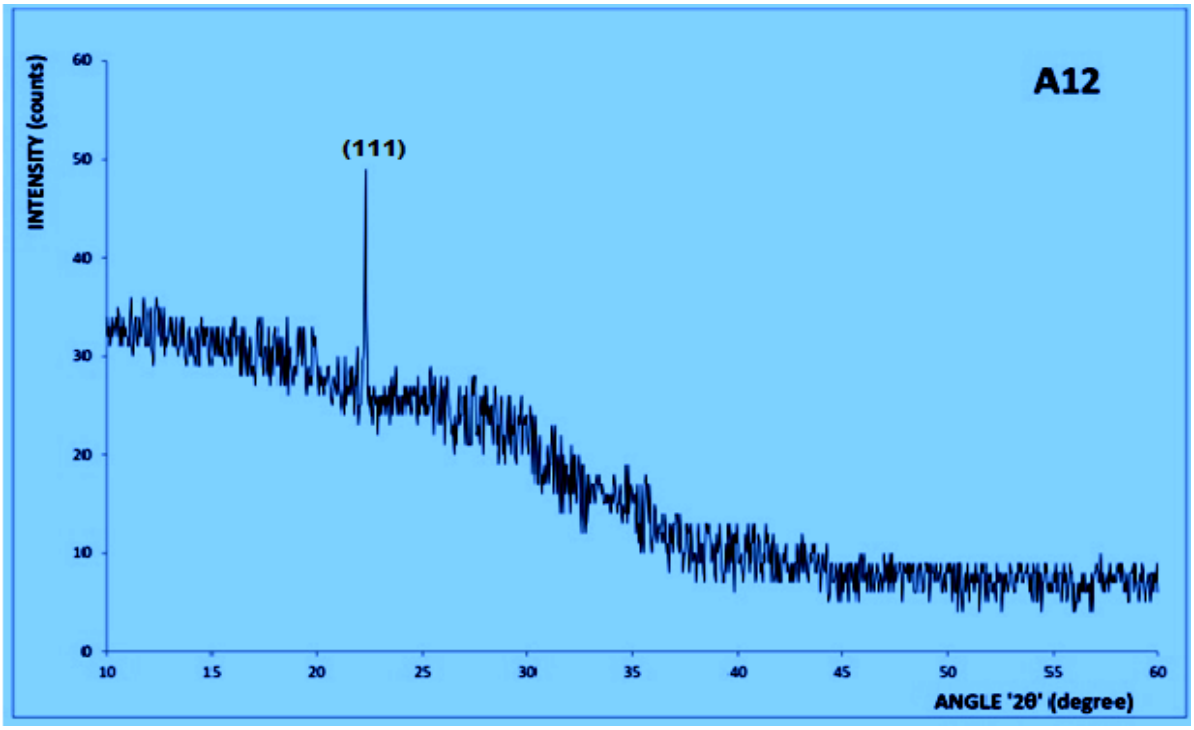

Figure 4.9 XRD Pattern of PbO:SnO_2 alloyed thin film of samples A_{11} and A_{12} at 60^0C of NaOH solution

(c) XRD Pattern of$CdO:SnO_2$ Alloyed Thin Films of A_{16}

Figure 4.10, shows the XRD pattern of$CdO:SnO_2$ alloyed thin films of samples A_{14} and A_{16} with diffraction peak at $2\theta = 15.40^0$ and with corresponding Miller indices (111). The patterns in both samples show well defined peaks, which indicate the crystalline nature of the alloy of $CdO:SnO_2$ at 60^0C of NaOH solution. The crystallite size for the alloy, is calculated using equation 4. From the observed peaks the grain size of the samples is calculated to be91.41nm. A new compound alloyed thin films known as di-cadmium tin(IV) tetra-oxide is formed. It has orthorhombic crystal system (Bowden and Cardite, 1990) with chemical formula; Cd_2SnO_4

The calculatedvalues for the lattice parameters of $CdO:SnO_2$ alloyed thin films of sample A_{16}: a= 5.569Å, b = 9.895Å, c = 3.194Å

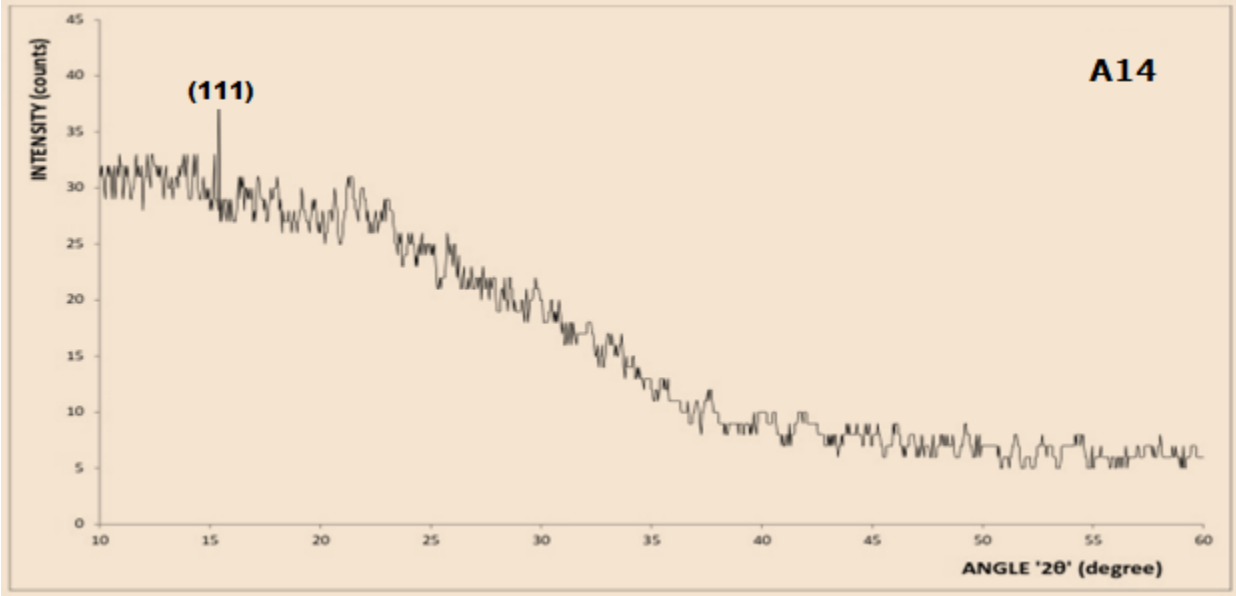

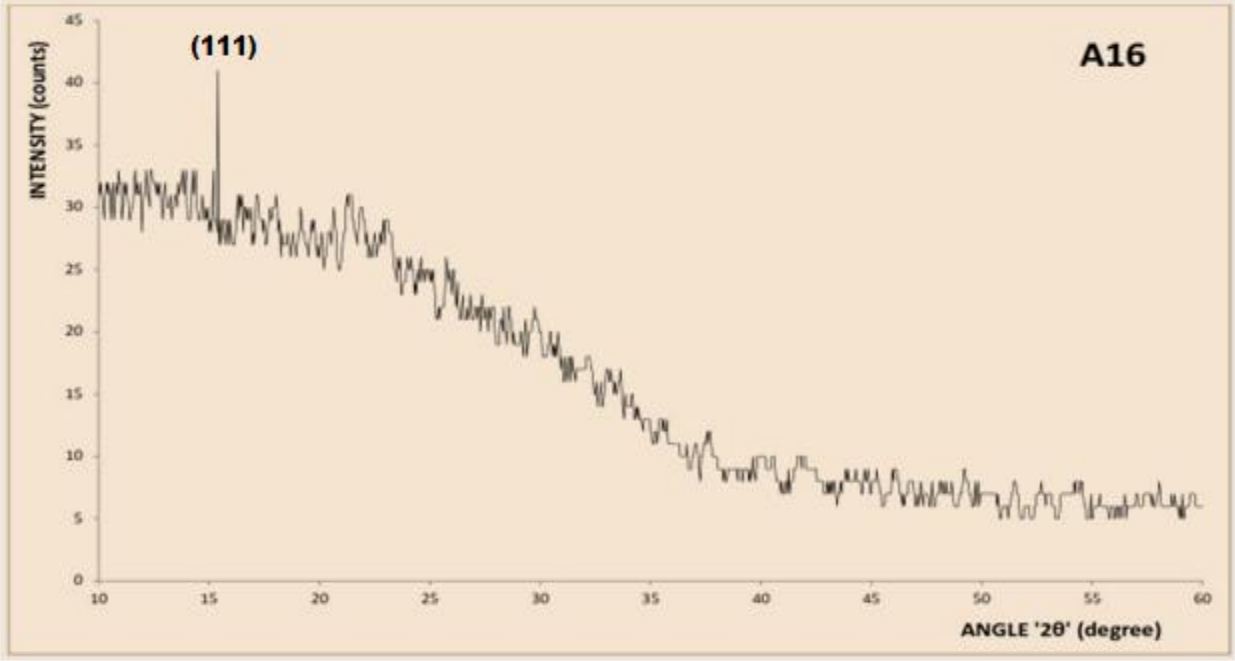

Figure 4.10 XRD pattern of CdO:SnO_2, alloyed thin films of samples A_{14} and A_{16} at 60^0C of NaOH solution

(d) XRD Pattern of$CuO:SnO_2$ Alloyed Thin Films of samples $A_{21}$and A_{22}

The XRD of $CuO:SnO_2$ alloyed thin films of A_{21} and A_{22} show no crystalline peak(s) thereby confirming the amorphous nature of the films (Eze and Okeke, 1998) which may be that the two alloying compounds films are small in amount on the substrate. It may also be that the accumulation of the individual films along the grain boundaries of the crystallites constituting the film (Centikaya*et al*, 2013)**.** This is shown in Figure 4.11**.**

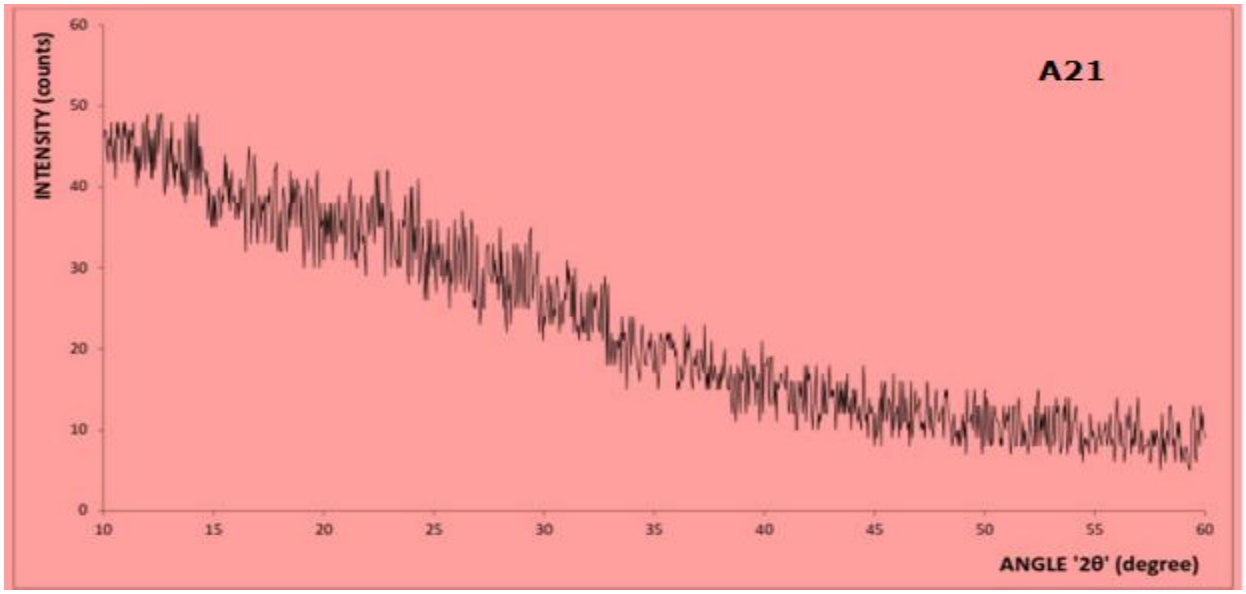

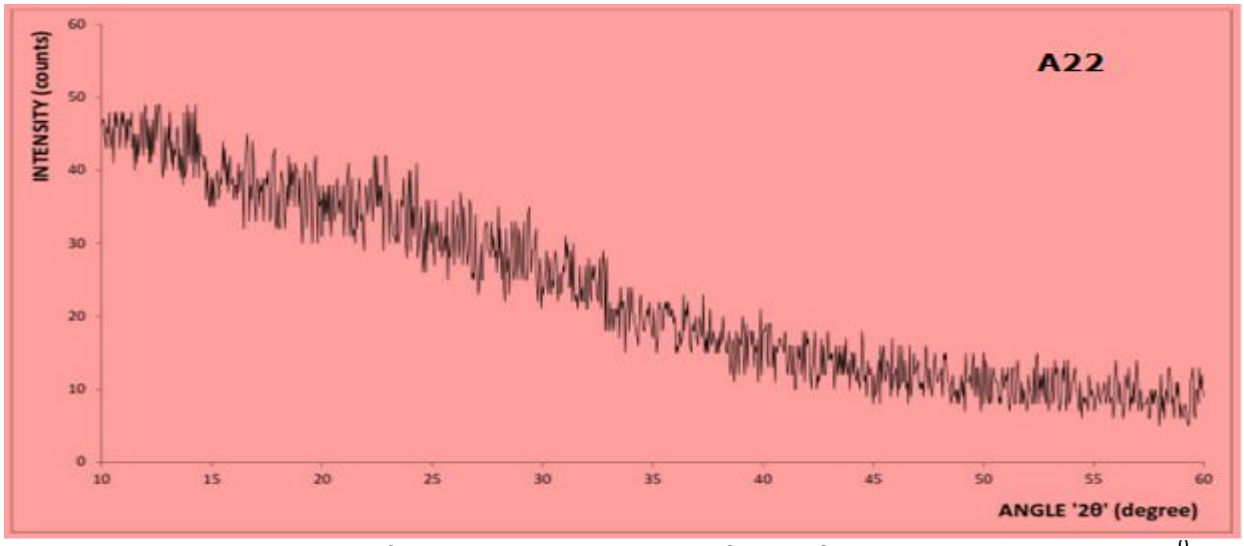

Figure 4.11 XRD pattern of $CuO:SnO_2$ alloyed thin films of samples $A_{21}$and A_{22} at 60^0C of NaOH solution

(e) XRD Pattern of$ZnO:SnO_2$ Alloyed Thin Films of A_{24} and A_{25}

Figure 4.12, shows the XRD pattern of $ZnO:SnO_2$ alloyed thin films of sample $A_{24}$and **A_{25}**with two diffraction peaks at $2\theta = 19.522^0$ and 22.811^0 with corresponding Miller indices (111) and (200). The XRD patterns show well defined peaks, which indicates the crystalline nature of the alloyed $ZnO:SnO_2$ at 60^0C of NaOH solution. The crystallite sizes for this alloy, were calculated using equation 4 and were found to be 40.522nm and 92.41nm.

From the XRD results, a new compound alloyed thin film known as di-zinc tin (IV) tetra-oxide with cubic crystal system was formed similar to spinel structure(Barth *et al*,1932). It has a chemical formula; Zn_2SnO_4.The calculated values of the lattice parameters of $ZnO:SnO_2$ alloy thin films of sample A_{24} are:a = b = c = 8.610Å.

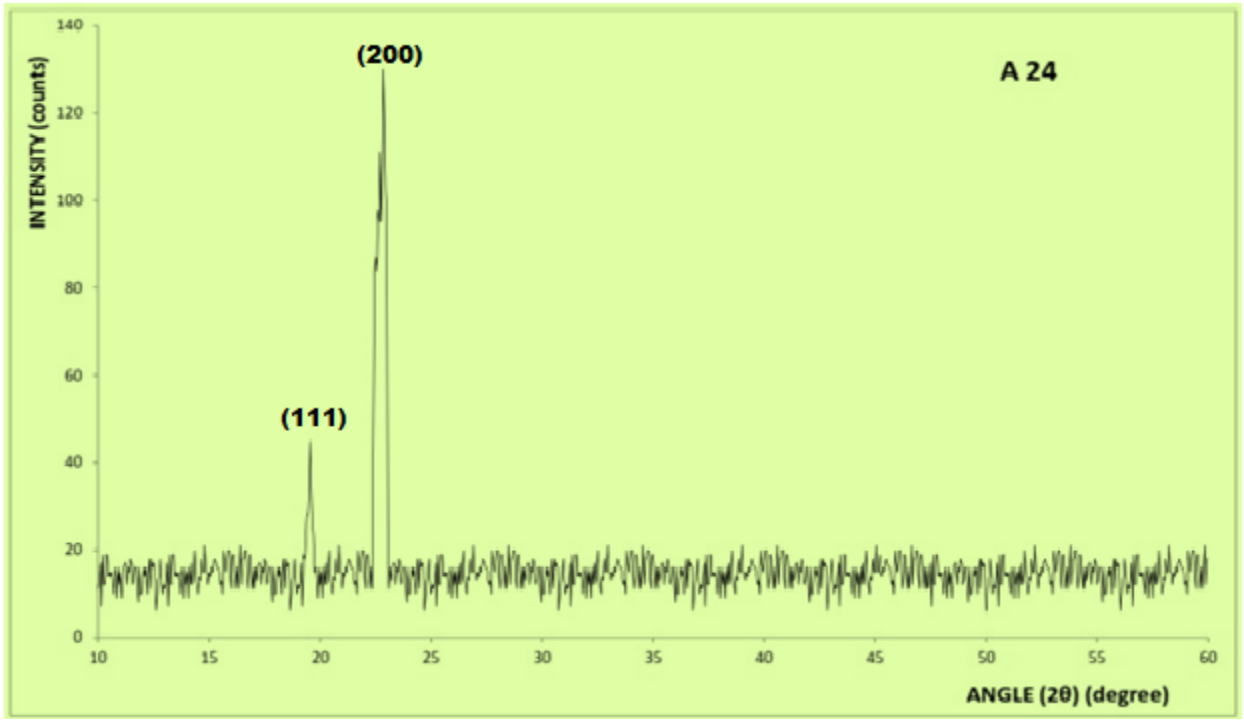

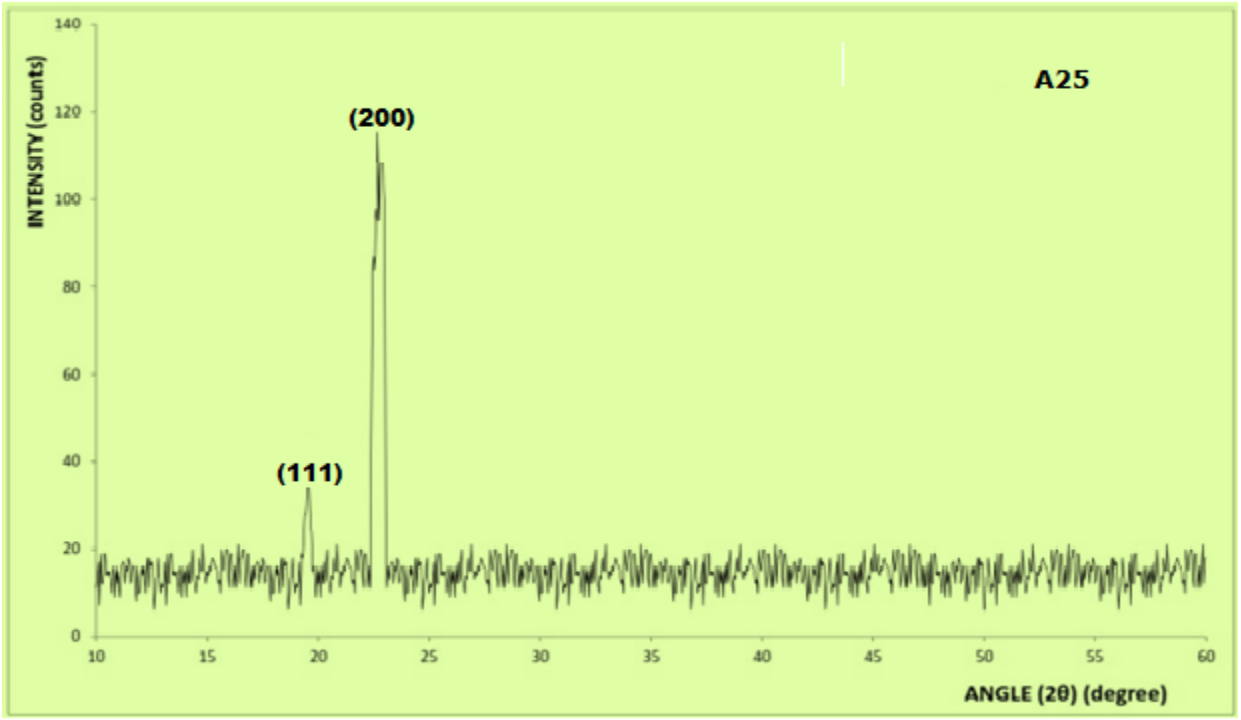

Figure 4 12 XRD pattern of ZnO:SnO_2 alloyed thin films of sample $A_{24}$and A_{25}at 60^0C of NaOH solution

(e) Microstructure of the Grown Samples

Microstructure of the thin films of $PbO:SnO_2$, $CdO:SnO_2$, $CuO:SnO_2$ and $ZnO:SnO_2$ were determined using electron microscope PhenomProx, Model number MVEO16477830 manufactured by Phenom World Eindhoven Netherland. The process of analysis is through back scattering electron imaging method.

In Figure 4.13 samples A_{11} and $\mathbf{A_{12}}$ of $PbO:SnO_2$ have coarse but well defined granular surfaces. This shows that sample A_{11} and A_{12} have high porosity and roughness which may be due to vaporization of water (Cernigoj*et al*., 2006).

SamplesA_{21} and $\mathbf{A_{22}}$, of $CuO:SnO_2$ have no cracks but rough textures. The grain crystallization was relatively good and grain sizes are uniformly covered. This is shown in Figure 4.14.

Samples A_{14} and$\mathbf{A_{16}}$, of $CdO:SnO_2$ have some cracks. They have incoherent surfaces which are due to synthesis conditions and also contain non-agglomerated morphologies. Sample A_{14} has rough texture and granular microstructures and sample A_{16}, has smooth surface. This is shown in Figure 4.15.

Figure 4.16, shows samples A_{24} and $A_{25}$of $ZnO:SnO_2$contains non-agglomerated spherical morphology. They have defined coated thin films which are due to reduction in hydrolysis and condensation of the samples. They have unit structures (Bu *et al.,* 2005).

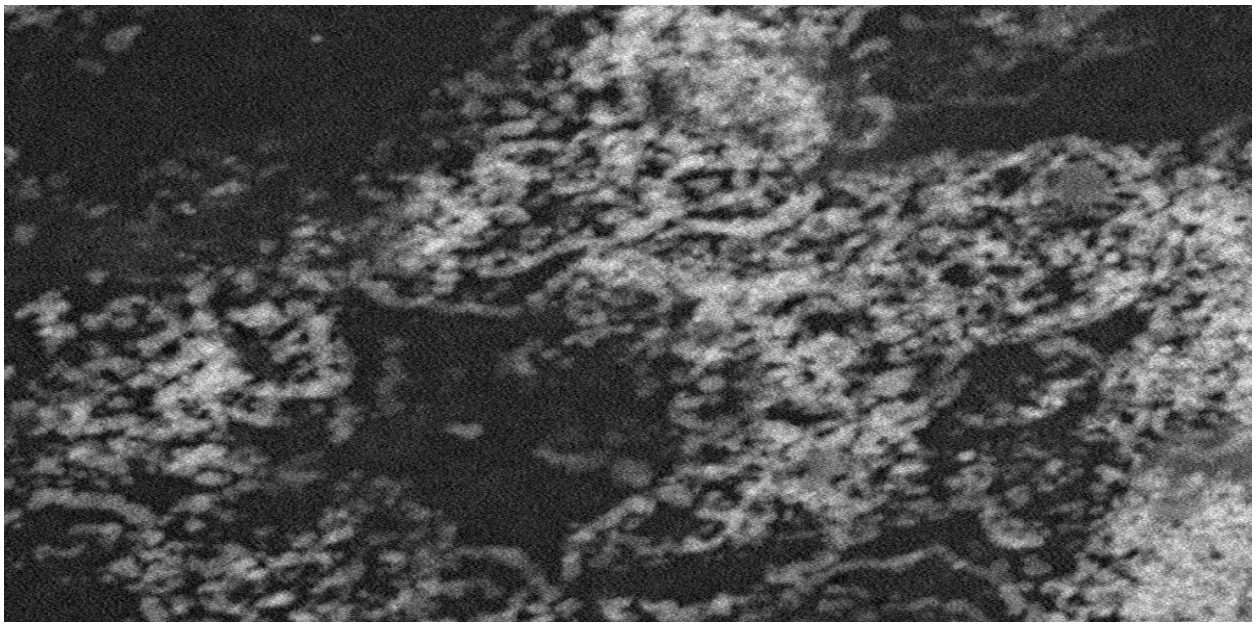

A_{11}

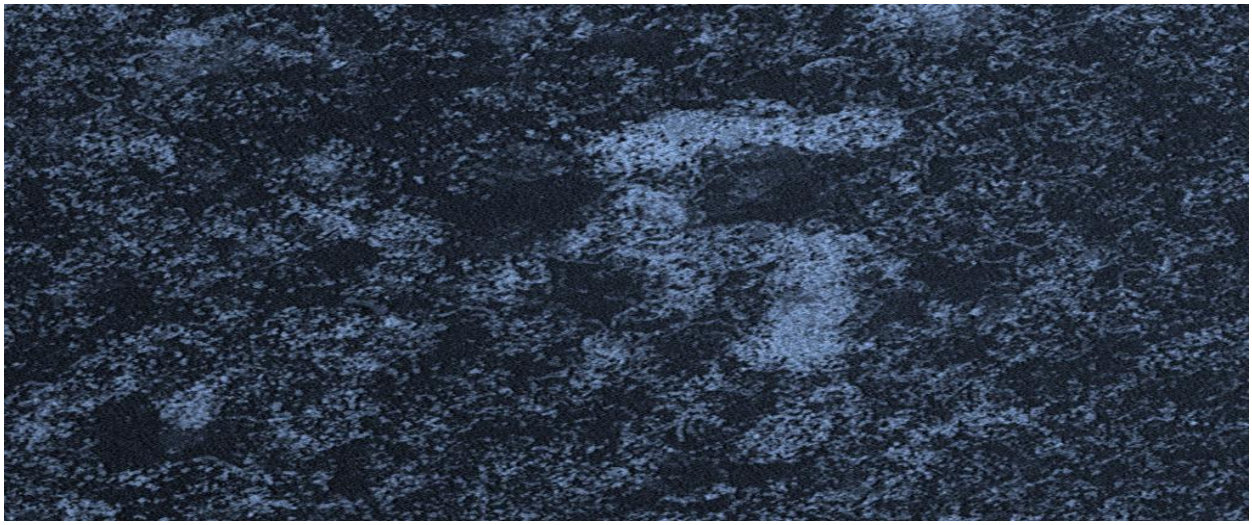

A_{12}

Figure 4.13 Scanning electron microscopy of samples A_{11} and A_{12} of $PbO:SnO_2$ alloyed thin films at constant temperature of 600C of NaOH solution.

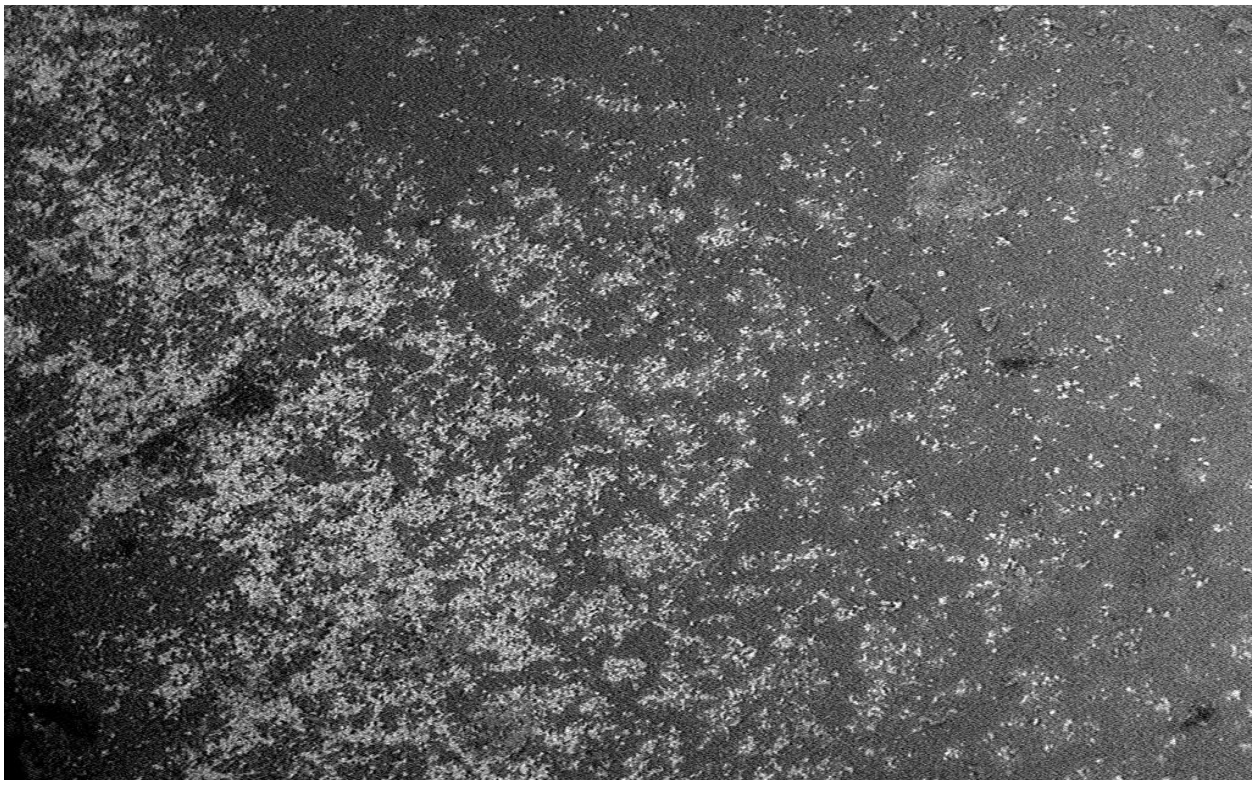

A_{21}

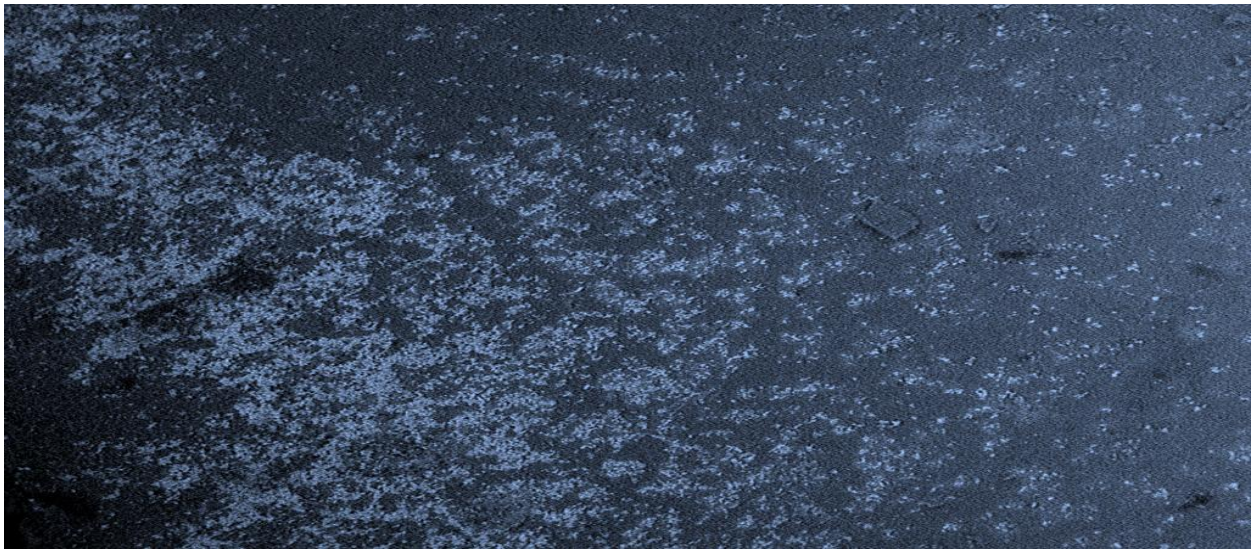

A_{22}

Figure 4.14: Scanning microscopy of sample A_{21} and A_{22} of $CuO:SnO_2$ alloyed thin films at constant temperature of 60^0C of NaOH solution.

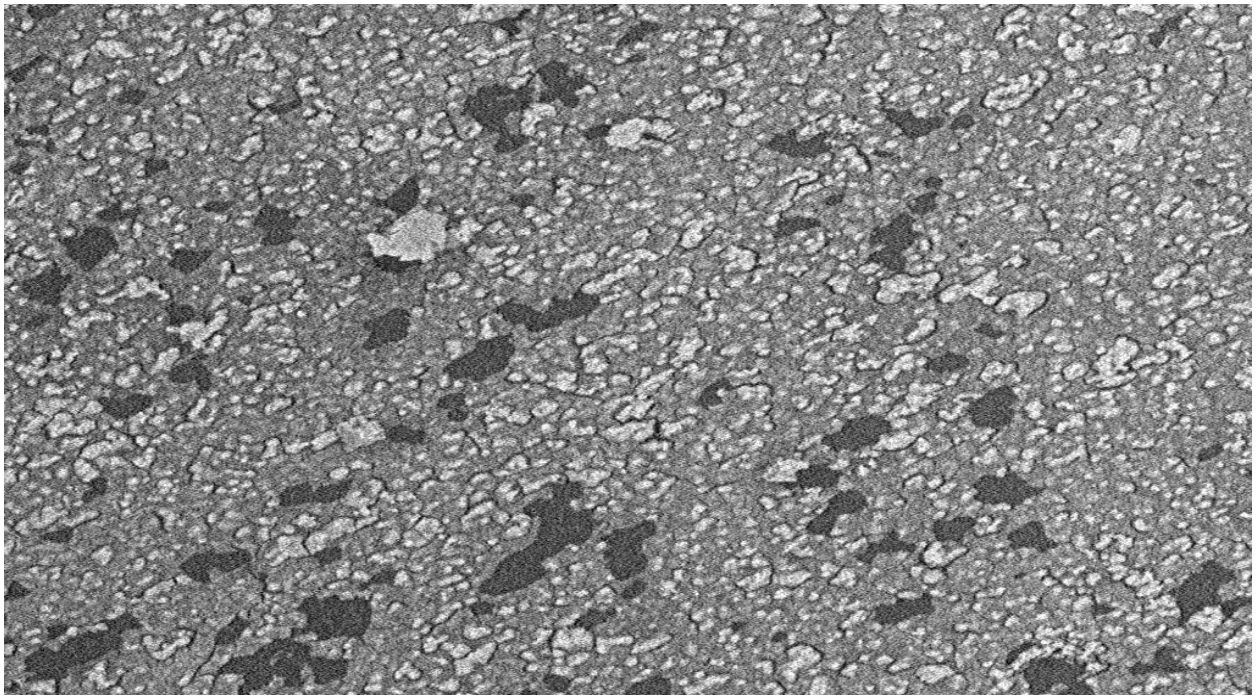

A_{14}

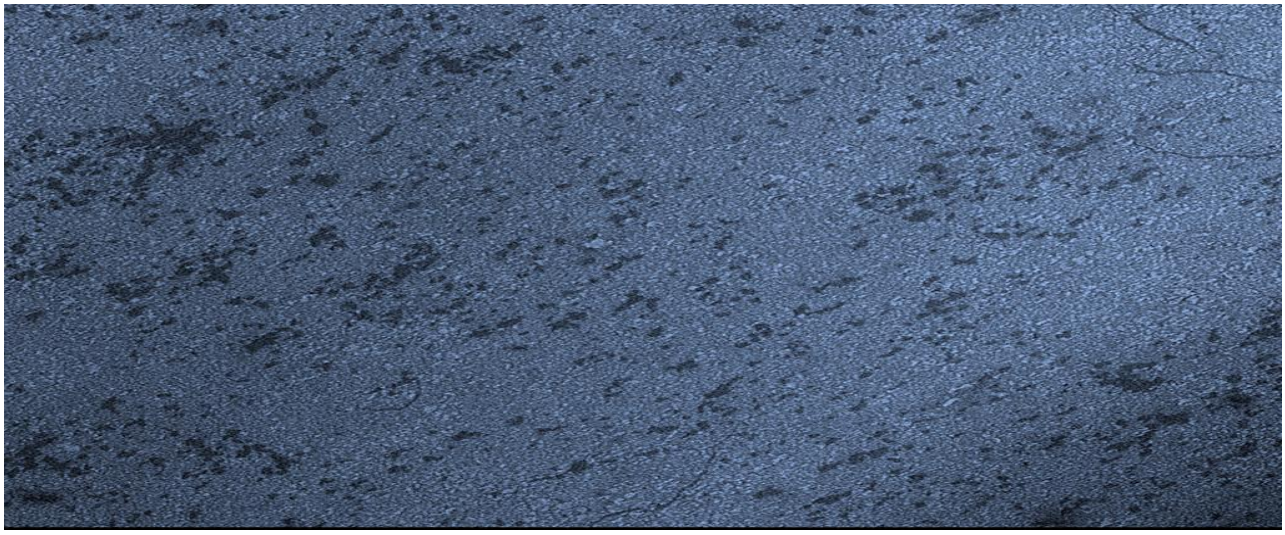

A_{16}

Figure 4.15 Scanning electron microscopy of sample A_{14} and A_{16} of $CdO:SnO_2$ alloyed thin films at constant temperature of 60^0C of NaOH solution.

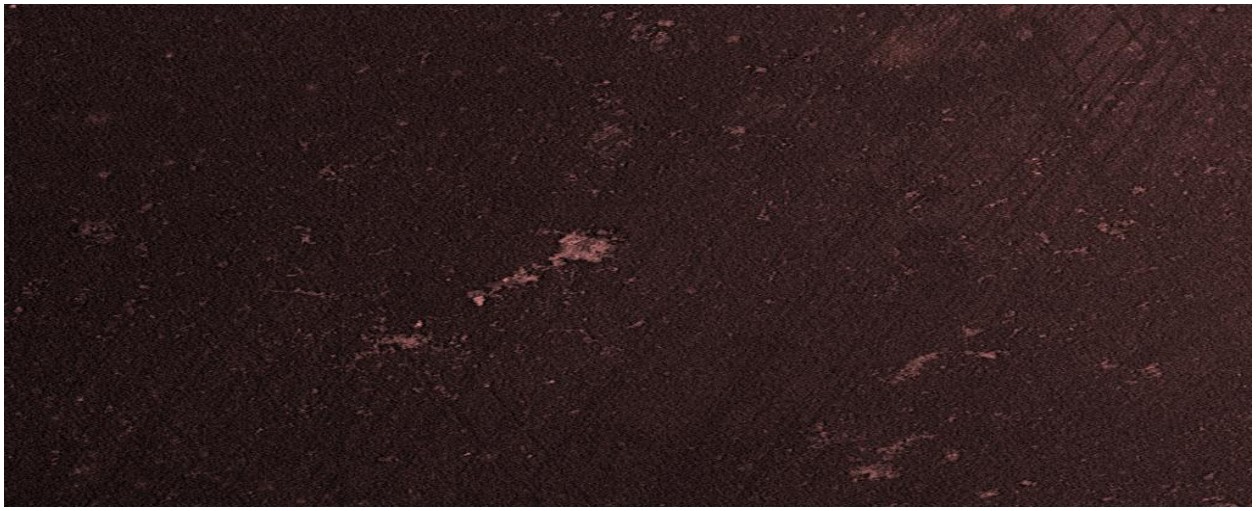

A_{24}

A_{25}

Figure 4.16 Scanning microscopy of sample A_{24} and A_{25} and of $ZnO:SnO_2$ alloyed thin films at constant temperature of 60^0C of NaOH solution.

4.1.3Optical Characterization

The transmittance spectra show that the films of samples A_{11} and A_{12} have good transparency in the UV (32%-70%) at the wavelength range (300nm-400nm) and good transmittance (21%-81%) for sample at the wavelength range (300nm-400nm) in the UV respectively. There is also high transmittances (70%-75%) for sample A_{11}at the wavelength (400nm-770nm) and (81%-75%) for sample A_{12} at the wavelength range (400nm-770nm) in the visible region of electromagnetic spectrum.In the near-infrared region, sample A_{12}falls from 75% at the wavelength of 770nm to 71% at the wavelength of 1080nm of electromagnetic spectrum. A_{11}has very high transmittance (75%-80%) at the wavelength (770nm-1080nm) at the near infrared of region of electromagnetic spectrum as shown in Figure 4.17. This behavior of the two samples is due to the effect of annealing which aided in expulsion of water of crystallization. This makes these films good materials for UV filter (Onwuemeka*et al*., 2014). See Appendix C for the data.

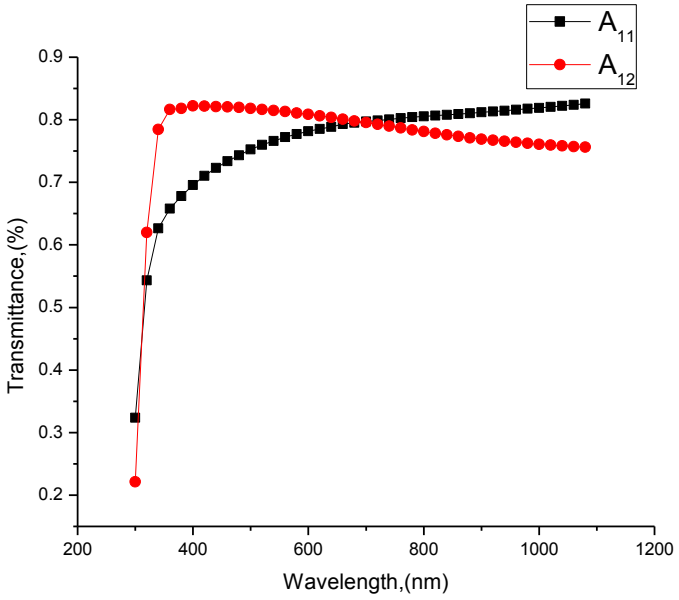

Figure 4.17 Graph of transmittance against wavelength for PbO:SnO_2 alloyed thin films of samples A_{11} and A_{12} at constant temperature of 60^0C of NaOH solution.

The two samples A_{11} and A_{12} have decreasing absorbance from the UV,0.55 and 0.65 respectively at wavelength 300nm which are obtained as their maximum values. The absorbances of samples $A_{11}$and A_{12}in the visible region decrease continually from 400nm to near infrared region of electromagnetic spectrum. This is shown in Figure 4.18, which is obtained from equation 2.28.

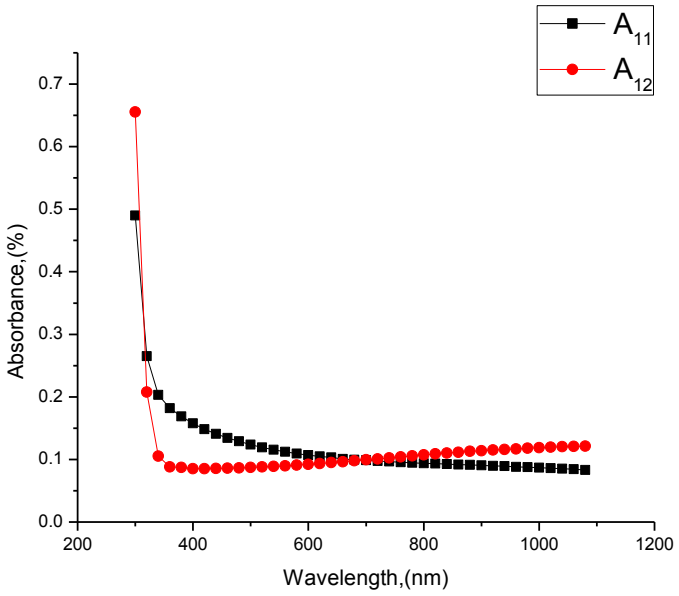

Figure 4.18 Graph of absorbance against wavelength for PbO:SnO_2 alloyed thin films of samples A_{11} and A_{12} at constant temperature of 60^0C of NaOH solution

Samples A_{11} and A_{12} have low reflectance of 0.09 – 0.19 at wavelengths at 320nm, 1080nm and 0.10-0.19 at wavelengths 340nm, 400nm respectively as depicted in Figure 4.19, The reflectance decreased as the wavelength increases from the UV through the visible to the near infrared regions of electromagnetic spectrum.

This makes PbO:SnO_2 useful in the area of multilayer solar control coating. The coating allows the visible part of the spectrum in, but either reflects the infrared (IR) radiation back into the room (energy-saving) or does not allow the infrared radiation into the room (heat-protection) depending on which side of the window has the coating (Onwuemeka*et al*., 2017).

This material can serve as front contact for solar cells or liquid crystal displays from optoelectronic applications (Roitan *et al*., 1994). The reflectance of the material is calculated using equation 2.30.

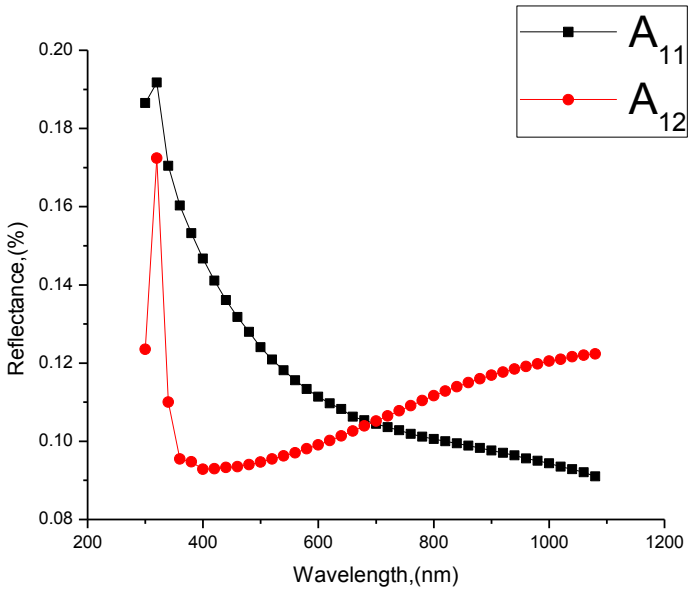

Figure 4.19 Graph of reflectance against wavelength for PbO:SnO_2 alloyed thin films of samples A_{11} and A_{12} at constant temperature of 60^0C of NaOH solution

The refraction index, as depicts in Figure 4.20 shows that sample A_{11} rises from 2.51 at λ= 300nm to its maximum value of 2.58 at λ= 320nm and falls as wavelength increases until it reaches the minimum value of 1.8 at ʎ=1080nm.

Sample A_{12} increased from 2.10 at λ= 300nm to its peak value of 2.45 at ʎ=320nm and decreases as wavelength increases up to λ=1080nm at n=2.25.The behaviour of these two samples of $PbO:SnO_2$ makes it possible for use in the area of multiple solar control coating applications where materials with high refractive index are required. The calculation of refractive index is obtained from equation 2.36

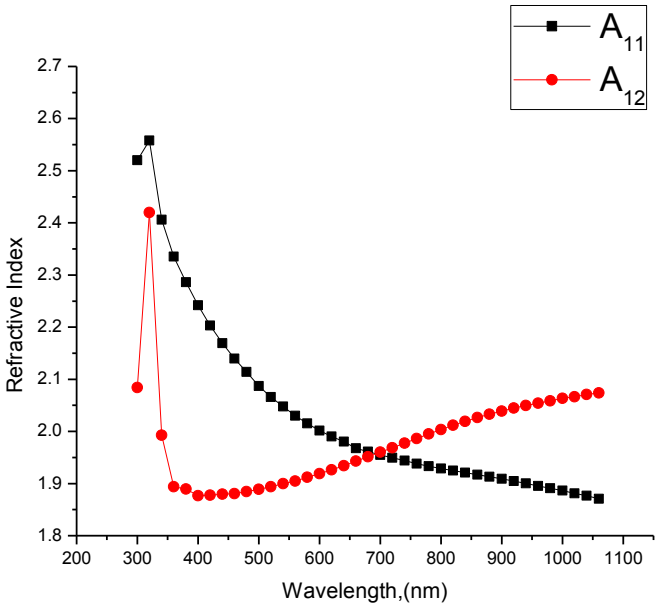

Figure 4.20 Graph of refractive index against wavelength for $pbO:SnO_2$ alloyed thin films of sample A_{11} and A_{12} at constant temperature of 60^0C of NaOH solution

Figure 4.21, shows that samples A_{11} and A_{12} have their maximum extinction coefficients of 0.026 at λ=320nm and 0.030 at λ=300nm respectively at the UV-region. The minimum values of samples A_{11} and A_{12} are 0.011 at λ=440nm and 0.005 at λ=540nm respectively at the visible region from which there were sharp increase of extinction coefficient as wavelength increases towards the infrared region . The values for Figure 4.21, is obtained from equation 2.37.

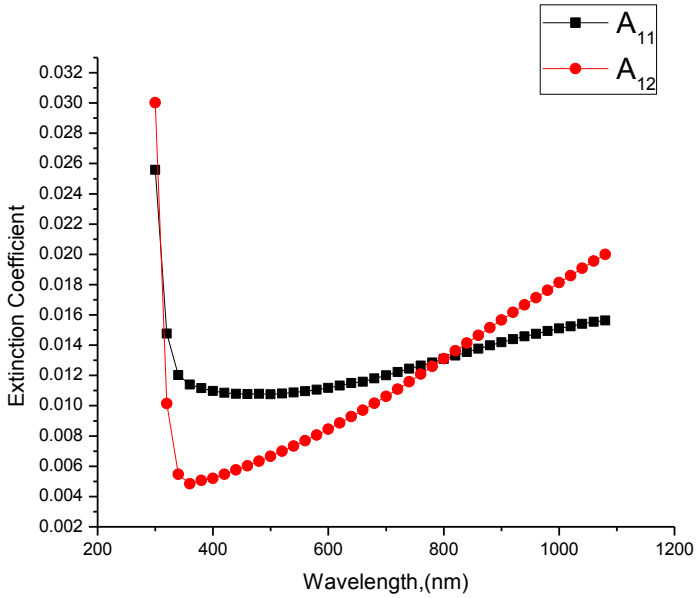

Figure 4.21 Graph of extinction coefficient against wavelength for PbO:SnO_2 alloyed thin films of samples A_{11} and A_{12} at constant temperature of 60^0C of NaOH solution.

Figure 4.22 shows samples A_{11} and A_{12} having decreasing real dielectric constants as wavelength increases. A_{11}increases from 6.25 at 300nm to 6.51 at wavelength of 320nm to its minimum value of 3.50 at wavelength λ=1080nm. Sample A_{12}, also increased from 4.50 at λ=300nm and reaches its maximum 5.58 at λ=320nm and falls as wavelength increases through the visible to near infrared region until it attains its minimum value of 3.50 at wavelength λ=400nm and rises as wavelength increases through the visible to the near infrared region of electromagnetic spectrum.

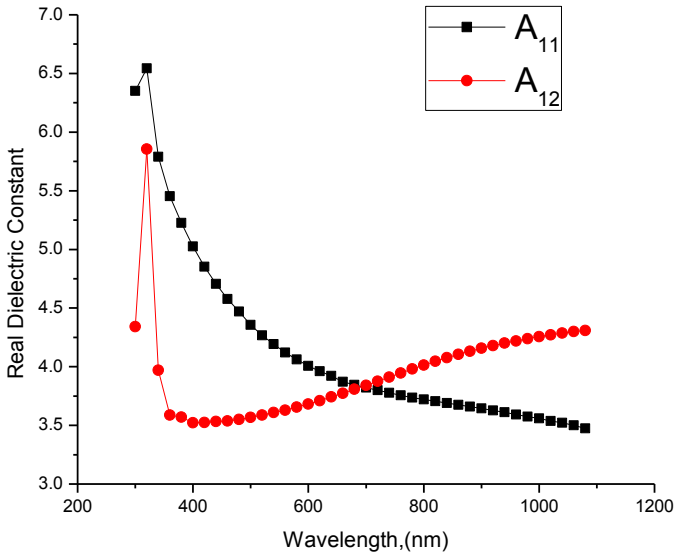

Figure 4.22 Graph of Real dielectric constant against wavelength for PbO:SnO_2 alloyed thin films of samples A_{11} and A_{12} at constant temperature of 60^0C of NaOH solution.

The imaginary dielectric constant is very low for the samples A_{11} and A_{12}. The plotted graphs fall, with increasing wavelength. Sample A_{11} falls from 0.13 at 320nm to its minimum value 0.045 at wavelength 550nm and increases up to wavelength of 1080nm at 0.05.

However, A_{12} falls from 0.12 at 320nm and reaches its minimum at 0.02 of λ = 400nm and rises slowly as wavelength increases up to maximum wavelength 1080nm as shown inFigure 4.23. The graph is obtained from equation 2.42.

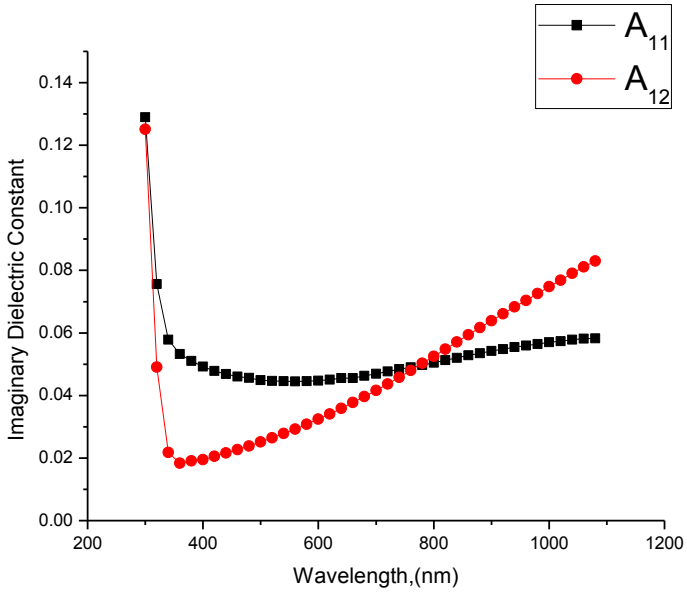

Figure 4.23 Graph of imaginary dialectic constant against wavelength forPbO: SnO_2 alloyed thin films samples A_{11} and A_{12} at constant temperature of 60^0C of NaOH solution.

Figure 4.24**,** shows the decrease of optical conductivity as wavelength increases. A_{11} decreases from its maximum value of 6.5 x $10^{14}\Omega^{-1}m^{-1}$ at 320nm to a minimum value of $1.0x10^{14}\Omega^{-1}m^{-1}$ at 1080nm. A_{12} falls from its peak value of $6.2x10^{14}\Omega^{-1}m^{-1}$at 320nm to its lowest value $1.5x10^{14}\Omega^{-1}m^{-1}$ at 1080nm. This behaviour is caused by the dependency of optical conductivity on the nature of refractive index and absorption coefficient; because at the UV region, the absorption coefficient; and refractive index are greatest and diminish as the wavelength increases. This is obtained from equation 2.43.

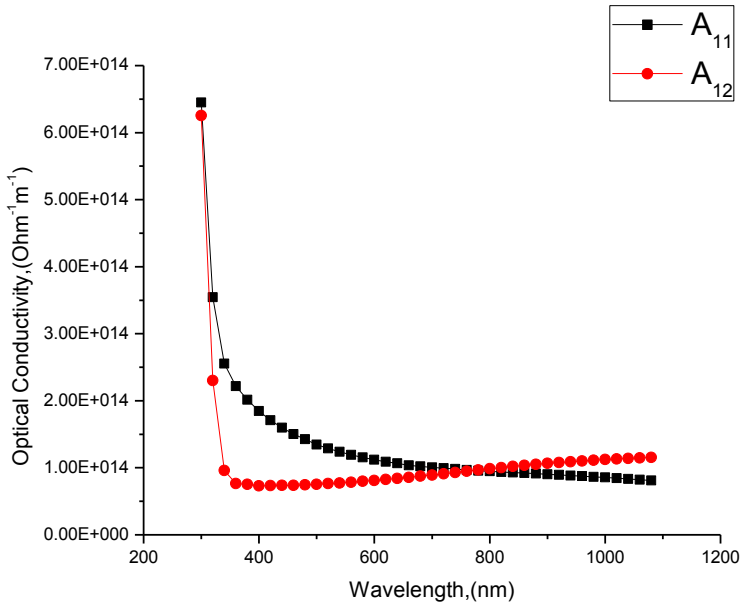

Figure 4.24 Graph of optical conductivity against wavelength for PbO: SnO_2 thin films of samples A_{11} and A_{12} at constant temperature of 60^0C of NaOH solution.

From Figure 4.25, the optical energy band gap is obtained in k space from the relation,

$$(\alpha h\upsilon)^2 = A\,(h\upsilon - E_g) \qquad (4.2)$$

where A is a constant, hv is the photon energy,E_g, is the energy band gap and α is the absorption coefficient.The energy band gaps of samples A_{11} and A_{12} are evaluated by extrapolating the linear portion of the plot $(\alpha h\upsilon)^2$ against hυ at αhυ = 0 where α is the absorption coefficient and hυ is the photon energy as shown in Figure 4.25.A direct band gap value of 3.60 ± 0.05eV is obtained for sample A_{11}. Sample A_{12} has a direct band gap of 3.70 ± 0.05eV. The two samples have in average, energy band gap of 3.65 ± 0.05e V.

The wide band gap obtained in this work makes the $PbO:SnO_2$ a good material for the production of laser diodes and light emitting diodes (LEDs) (Look, 2001).

It can also be used to produce field effect transistors where p-n junction may not be required (Roitan, 1994).

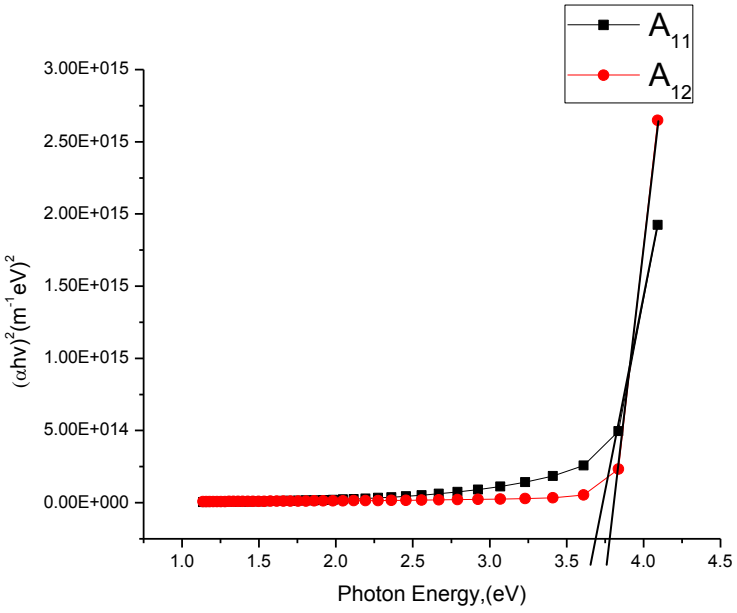

Figure 4.25 The Graph of (αhυ)2 against photon energy hυ for $PbO:SnO_2$ alloyed thin films of samples A_{11} and A_{12} at constant temperature of 600C of NaOH solution.

The transmittance spectrum shows that the films of samples A_{21} and A_{22} have good transparency in the UV(45%-64%) for sample A_{21} and good transmittance (42%-62%)for sample A_{22} in the wavelength range (320nm-400nm) in the UV. There is high transmittances (65%-74%) for sample A_{21} and (62%-69%) for sample A_{22} in the visible region of electromagnetic spectrum within the wavelength range of (400nm-700nm).

In the near-infrared region, samples A_{21} and A_{22} have very high transmittance (75%-77%) and (68%-74%)respectively within the wavelength of (770nm-1080nm) of the region of electromagnetic spectrum as shown in Figure 4.26. This makes these alloyed films good materials for UV filter and transparent electrode for flat panel displays (Onwuemeka*et al*., 2014). See Appendix A for the data.

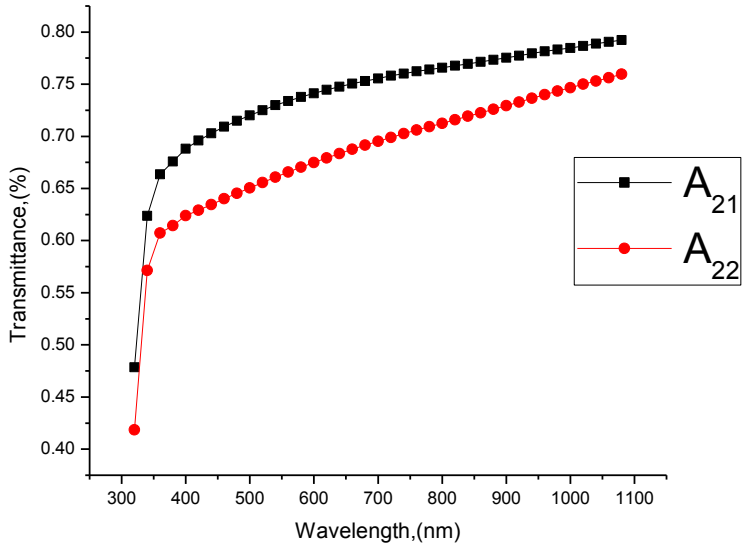

Figure 4.26 Graph of transmittance against wavelength for $CuO:SnO_2$ alloyed thin films of samples A_{21} and A_{22} at constant temperature of 60^0C of NaOH solution.

Samples A_{21} and A_{22} have decreasing absorbance from the UV, 0.32 and 0.37 respectively at wavelength 320nm which are recorded as their maximum values. The minimum absorbance of 0.10 and 0.12 were recorded at the near infrared regions of electromagnetic spectrum at wavelength 1080nm. The absorbance of samples $A_{21}$and A_{22}in the visible region decrease continually from 400nm to near infrared region of electromagnetic spectrum. This makes this material veritable in the area of optical window applications(Onwuemeka*et al.*, 2017). This is shown in Figure 4.27, which is obtained from equation 2.28.

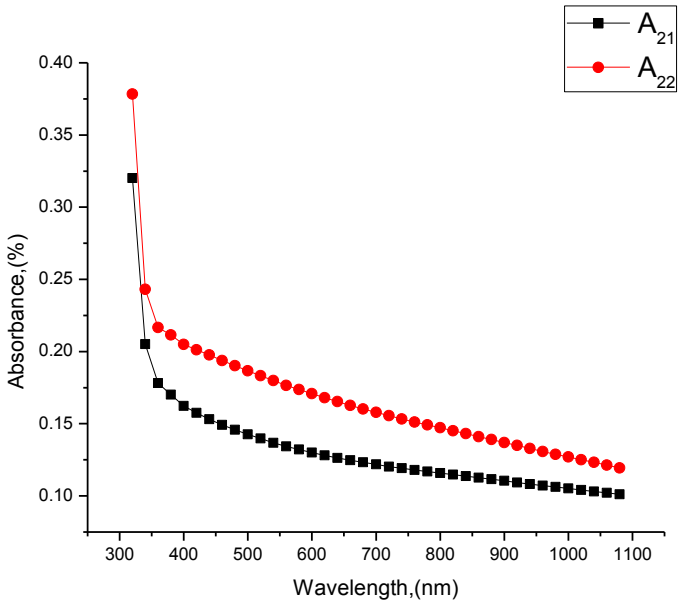

Figure 4.27 Graph of absorbance against wavelength for $CuO:SnO_2$ alloyed thin films of samples A_{21} and A_{22} at constant temperature of 60^0C of NaOH solution.

Samples A_{21} and A_{22} have low reflectance of 0.17 to 0.20 and 0.11 to 0.20 respectively as depicted in Figure 4.28. It decreased as the wavelength increases from the UV through the visible to the near infrared regions of electromagnetic spectrum.

This makes CuO:SnO_2 useful in the area of multilayer solar control coating. The coating allows the visible part of the spectrum in, but either reflects the infrared (IR) radiation back into the room (energy-saving) or does not allow the infrared radiation into the room (heat-protection) depending on which side of the window has the coating (Onwuemekaand Nwulu, 2017).

This material can serve as front contact for solar cells or liquid crystal displays from optoelectronic applications (Onwuemeka and Nwulu, 2017). The reflectance of the material is calculated using equation 2.30.

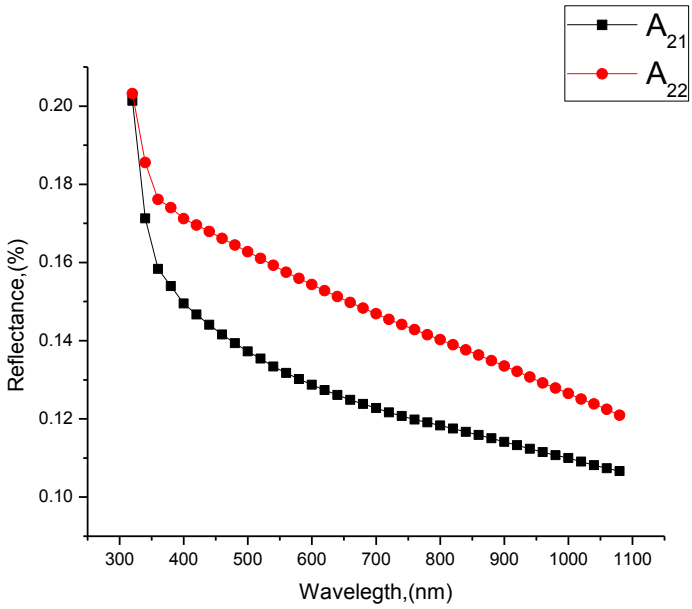

Figure 4.28 Graph of reflectance against wavelength for CuO:SnO_2 alloyed thin films of samples A_{21} and A_{22} at constant temperature of 60^0C of NaOH solution.

The refraction index, as depicts in Figure 4.29 of sample A_{21} falls from 2.65 at λ= 320nm as wavelength increases until it reaches the minimum value of 1.8 at ʎ=1080nm.

Sample A_{22} decreases from its peak value of 2.65 at ʎ=320nm as wavelength increases to its minimum value of refractive index n=2.10 at λ=1080nm.The behaviour of these two samples of $CuO:SnO_2$ makes it possible for use in the area of multiple solar control coating applications where materials with high refractive index are required. The calculation of refractive index is obtained from equation 2.36.

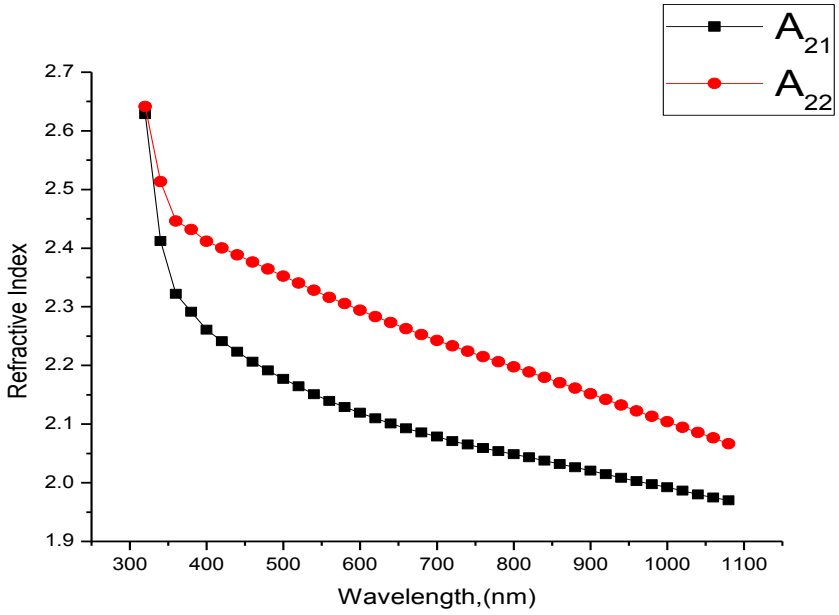

Figure 4.29 Graph of refractive index against wavelength for $CuO:SnO_2$ alloyed thin films of samples A_{21} and A_{22} at constant temperature of 60^0C of NaOH solution.

In Figure 4.30, samples A_{21} and A_{22} have their maximum extinction coefficients of 0.07 at λ=320nm and 0.18 at λ=320nm respectively at the UV-region. The minimum values of 0.012 at λ=440nm and 0.11 at λ=440nm are respectively are obtained at the visible region from which there were sharp increase of extinction coefficient as wavelength increases towards the infrared region. The values for Figure 4.30, is obtained from equation 2.37.

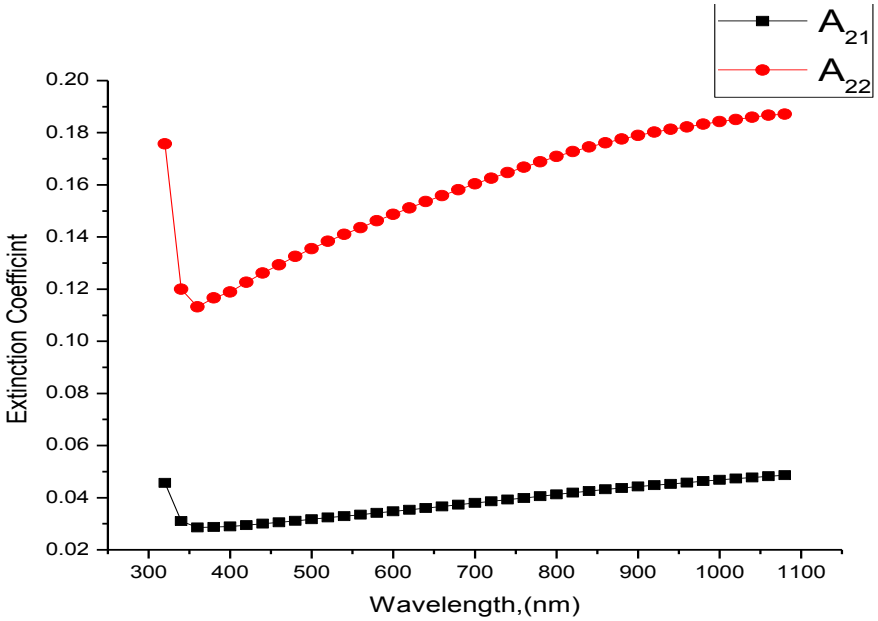

Figure 4.30 Graph of extinction coefficient against wavelength for CuO:SnO_2 alloyed thin films of samples A_{21} and A_{22} at constant temperature of 60^0C of NaOH solution.

InFigure 4.31 samples A_{21} and A_{22} have decreasing real dielectric constants as wavelength increases. A_{21} decreases from 6.68 at wavelength of 320nm to its minimum value of 5.58 at wavelength λ=1080nm. Sample A_{22}, also decreased from 6.9 at λ=320nm at the UV through the visible and reaches its minimum value 4.0 at λ=1080nm.

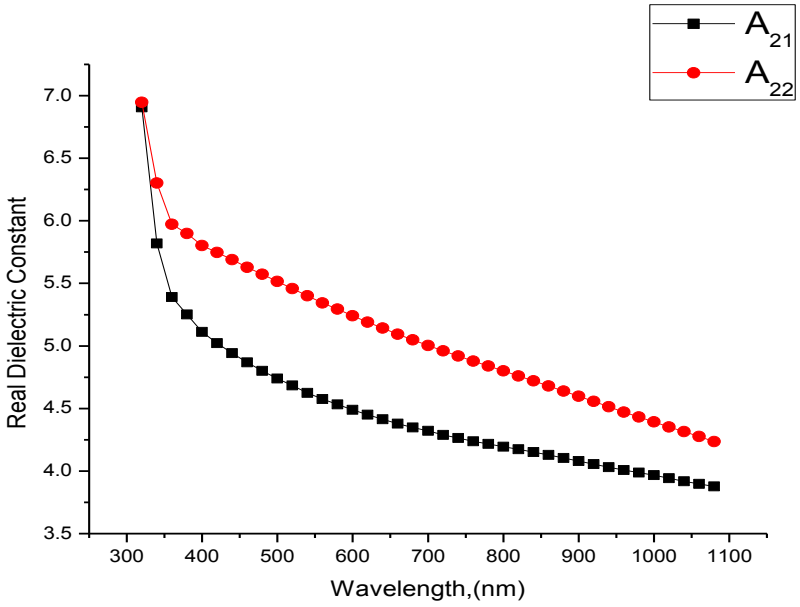

Figure 4.31 Graph of real dielectric against wavelength for CuO:SnO_2 alloyed thin films of samples A_{21} and A_{22} at constant temperature of 60^0C of NaOH solution.

Imaginary dielectric constant is very low for the samples A_{21} and A_{22}. The plotted graphs in Figure 4.32 fall, with increasing wavelength. Sample A_{21} falls from 0.23 at 320nm to its minimum value 0.15 at wavelength 360nm and increases up to wavelength of 1080nm at 0.17.

A_{12} falls from 0.91 at 320nm and reaches its minimum at 0.52 of wavelength λ = 380nm and rises slowly as wavelength increases up to maximum wavelength 1080nm. The graph is obtained from equation 2.41.

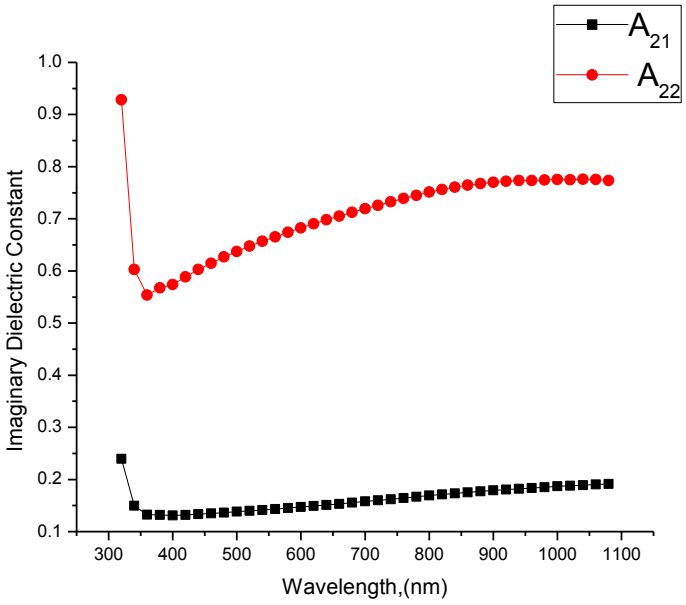

Figure 4.32 Graph of imaginary dielectric against wavelength for $CuO:SnO_2$ alloyed thin films of samples A_{21} and A_{22} at constant temperature of 60^0C of NaOH solution.

Figure4.33**,** shows the decrease of optical conductivity as wavelength increases for the two samples A_{21} and A_{22}. A_{21} decreases from its maximum value of 1.3 x $10^{14}\Omega$-m-^{1} at 320nm to a minimum value of 0.3x$10^{14}\Omega$-m-^{1} at 1080nm. A_{22} falls from its peak value of 4.4x$10^{14}\Omega$-m-^{1} at 320nm to its lowest values 1.3 x 10x$^{14}\Omega$-m-^{1} at 1080nm. This bahaviour is caused by the dependency of optical conductivity on the nature of refractive index and absorption coefficient; because at the UV region, the absorption coefficient; and refractive index are greatest and diminish as the wavelength increases. This is obtained from equation 2.43

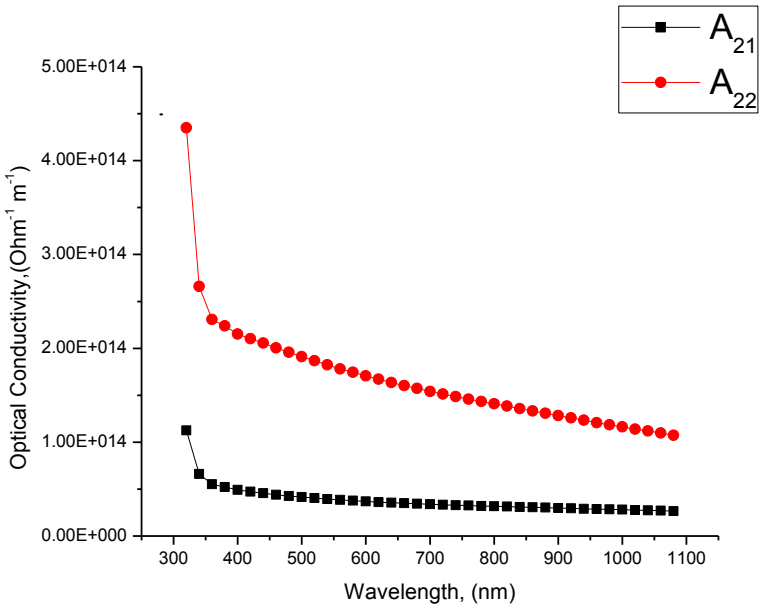

Figure4.33 Graph of optical conductivity against wavelength for CuO:SnO_2 alloyed thin films of samples A_{21} and A_{22} at constant temperature of 60^{0}C of NaOH solution**.**

The optical energy band gap is obtained in k space from the relation as obtained in equation 4.2.The energy band gaps of samples A_{21} and A_{22} are evaluated by extrapolating the linear portion of the plot $(\alpha h\upsilon)^2$ against photon energy $h\upsilon$ at $(\alpha h\upsilon)^2 = 0$ where α is the absorption coefficient and $h\upsilon$ is the photon energy as shown in Figure 4.34**.**

Direct band gap values of 3.20±0.05eV and 3.40±0.05eV are obtained for samples A_{21} and A_{22} respectively with an average band gap of 3.30±0.05eV. The wide band gaps obtained in this work make $CuO:SnO_2$ a good material for the production of laser diodes and light emitting diodes (LEDs) (Look, 2000, Liu *et al*., 2007).

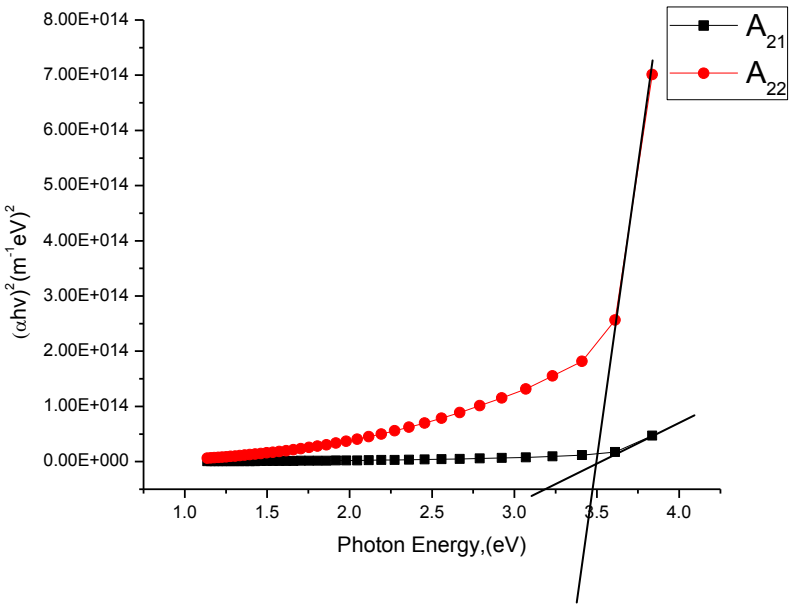

Figure 4.34 The Graph of $(\alpha h\upsilon)^2$ against photon energy $h\upsilon$for $CuO:SnO_2$ alloyed thin films of samples A_{21} and A_{22} at constant temperature of 60^0C of NaOH solution.

The transmittance spectrum shows that the films of samples A_{14} and A_{16} have good transparency in the UV (16%-60%) for sample A_{14} and good transmittance (27%-70%) for sample A_{16} in the wavelength range (320nm-400nm). The high transmittance (61%-59%) for sample A_{14} from the visible region (400nm-700nm), becomes almost linear through the near infrared region of electromagnetic spectrum.

The transmittance of sample A_{16} increases as wavelength increases up to the near infrared region of electromagnetic. In the near-infrared region, sample A_{16} has high transmittance (81%-85%) within the wavelength of 700nm- 1080nm of the region of electromagnetic spectrum as shown in Figure 4.35. This makes these alloyed films good materials for UV filter and transparent electrode for flat panel displays (Onwuemeka*et al*., 2014). See Appendix D for the data.

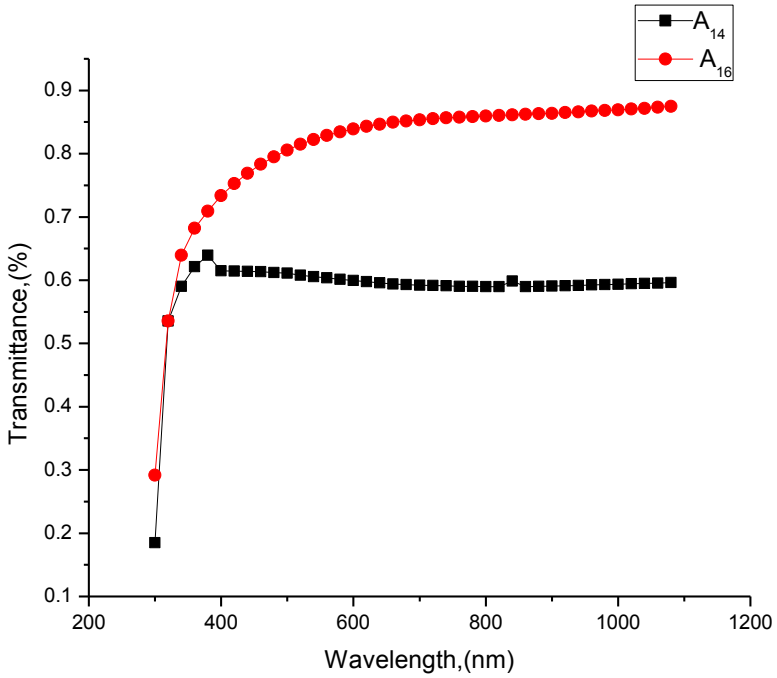

Figure 4.35 The Graph of transmittance against wavelength for CdO:SnO_2 alloyed thin films of samples A_{14} and A_{16} at constant temperature of 60^0C of NaOH solution.

Samples A_{14} and A_{16} of $CdO:SnO_2$ have decreasing absorbance from the UV, 0.75 and 0.55 respectively at wavelength 320nm which are their maximum values. The minimum absorbance of 0.22 and 0.05 were obtained at the near infrared regions of electromagnetic spectrum at wavelength 1080nm. The absorbance of sample A_{14} in the visible region decreases continually from 400nm to near infrared region of electromagnetic spectrum. This makes this material veritable in area of optical window applications. This is shown in Figure 4.36, which is obtained from equation 2.28.

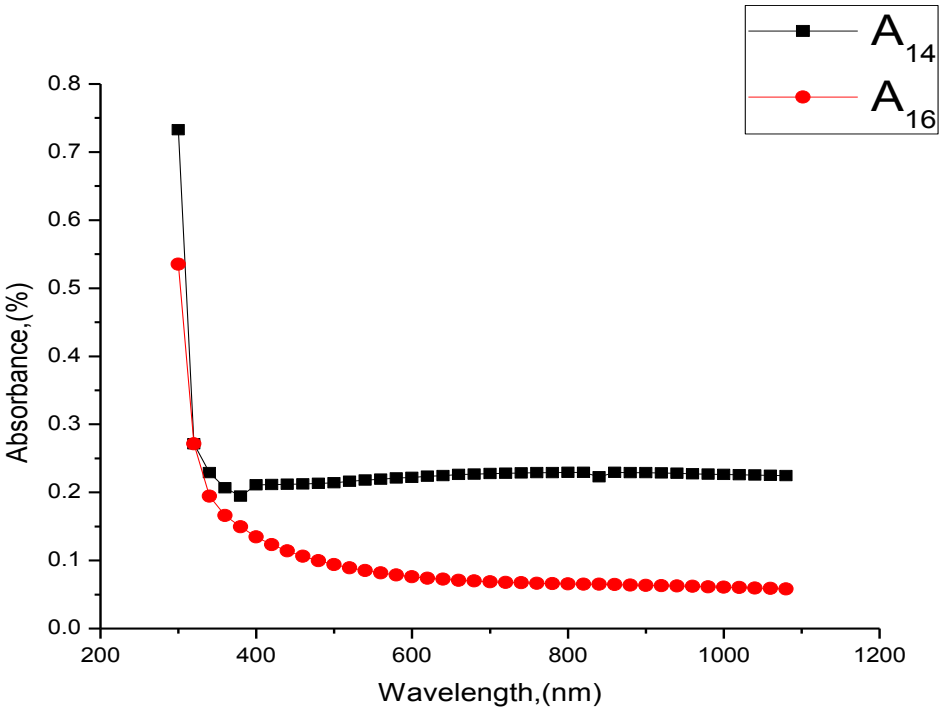

Figure 4.36 The Graph of absorbance against wavelength for $CdO:SnO_2$ alloyed thin films of samples A_{14} and A_{16} at constant temperature of 60^0C of NaOH solution.

Samples A_{14} and A_{16} have low reflectance of 0.07 to 0.20 and 0.06 to 0.21 respectively as depicted in Figure 4.37. The reflectance for both samples are highest at the UV region of the electromagnetic spectrum with values 0.20 at wavelength λ=320nm for sample A_{14} and 0.21 at wavelength λ=320nm for sample A_{16}. Sample A_{14} has linear characteristics as wavelength increases through the visible region to the near infrared region of electromagnetic spectrum. Sample A_{16} decreases from its peak value of 0.21 as wavelength increases to its lowest value 0.06 at wavelength λ=1080nm at the near infrared region of electromagnetic spectrum.

This makes CdO:SnO_2 useful in the area of multilayer solar control coating. The coating allows the visible part of the spectrum in, but either reflects the infrared (IR) radiation back into the room (energy-saving) or does not allow the infrared radiation into the room (heat-protection) depending on which side of the window has the coating(Onwuemeka*et al*., 2017).

This material can serve as front contact for solar cells or liquid crystal displays for optoelectronic applications (Roitan,1994). The reflectance of the material is calculated using equation 2.30.

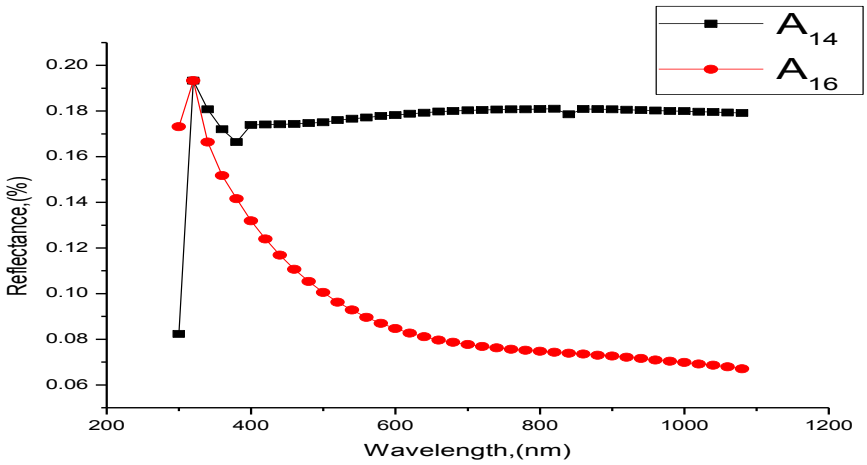

Figure 4.37 The Graph of reflectance against wavelength for CdO:SnO_2 alloyed thin films of samples A_{14} and A_{16} at constant temperature of 60^0C of NaOH solution.

The refraction index, as depicts in Figure 4.38**,** of sample A_{14} rises from n=1.8 at wavelength, λ= 320nm to its maximum value of n=2.61 at wavelength, λ= 340nm and from the visible to near infrared regions, it has linear characteristics as the wavelength increases. Sample A_{16} increases from n=2.40 at wavelength, λ= 320nm to its peak value of n=2.60 at ʎ=340nm and decreases as wavelength increases up to wavelength, λ=1080nm at n=1.7

The behaviour of these two samples of $CdO:SnO_2$ makes it possible for use in the area of multiplier solar control coating applications where materials with high refractive index are required. The calculation of refractive index is obtained from equation 2.36

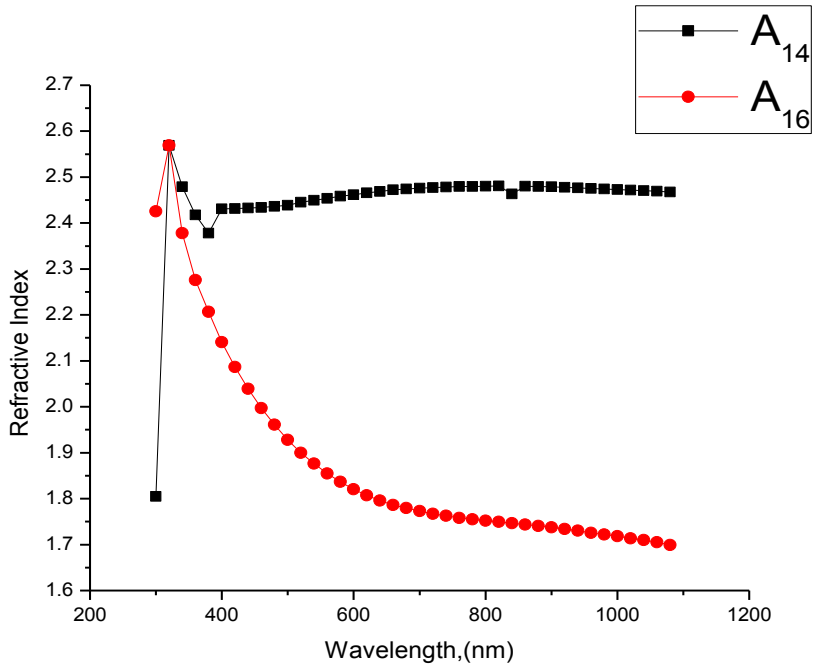

Figure 4.38 The Graph of refractive index against wavelength for $CdO:SnO_2$ alloyed thin films of samples A_{14} and A_{16} at constant temperature of 60^0C of NaOH solution.

In Figure 4.39, samples A_{14} and A_{16} have their maximum extinction coefficients of 0.09 at wavelength, λ=1080nm and 0.022 at wavelength, λ=1080nm respectively at the near infrared region. The minimum values of 0.026 at wavelength, λ=380nm at the UV region from which there was sharp decrease of extinction coefficient and increases to 0.08 at wavelength, λ=320nm for sample A_{14} andthe minimum value of 0.016 at wavelength, λ=580nm for sample A_{16} at the visible region of electromagnetic spectrum was recorded . The values for Figure 4.39, are obtained from equation 2.37.

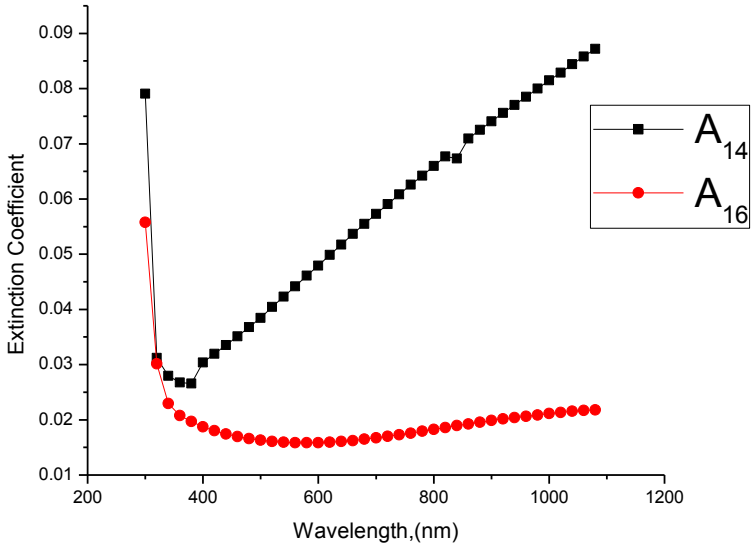

Figure 4.39 The Graph of extinction coefficient against wavelength for $CdO:SnO_2$ alloyed thin films of samples A_{14} and A_{16} at constant temperature of 60^0C of NaOH solution.

InFigure 4.40**,** samples A_{14} and A_{16} have decreasing real dielectric constants as wavelength increases. A_{14} increases from 3.2 at wavelength of 320nm to its maximum value of 6.8 at wavelength λ=360nm.It falls sharply at the visible region to 5.7 at wavelength, λ=400nm, from which it maintains a linear characteristics up to the near infrared region of electromagnetic spectrum. A_{16} increases from 5.7 at the wavelength of 320nm to its maximum value of 6.7 at the wavelength λ=360nm.It falls sharply at the visible region, from which it maintains almost a linear characteristics up to the near infrared region of electromagnetic spectrum.

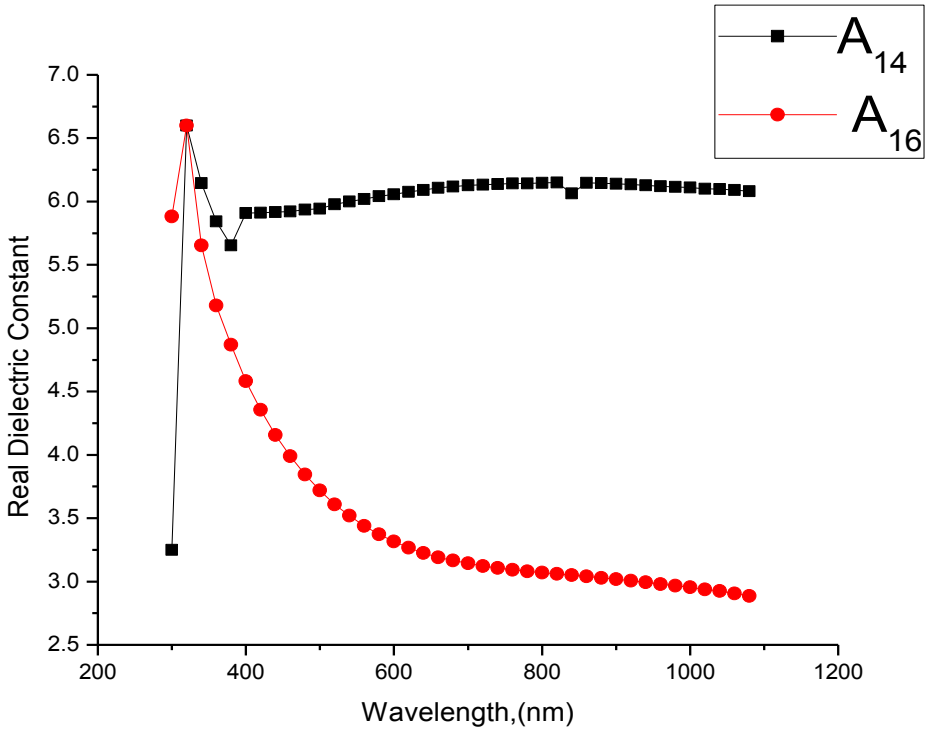

Figure 4.40 The Graph of real dielectric constant against wavelength for $CdO:SnO_2$ alloyed thin films of samples A_{14} and A_{16} at constant temperature of 60^0C of NaOH solution.

Imaginary dielectric constant in Figure 4.41, is very low for the samples A_{14} and A_{16} of $CdO:SnO_2$.The plotted graphs fall with increasing wavelength.

Sample A_{14} falls from 0.03 at 320nm to its minimum value 0.05 at wavelength, λ=360nm and increases up to 0.06 at wavelength λ=1080nm. A_{16} falls from 0.094 at 320nm and reaches its minimum at 0.018 at wavelength λ = 600nm in the visible region and rises as wavelength increases up to maximum wavelength 1080nm in the near infrared region of electromagnetic spectrum. The graph is obtained from equation 2.41.

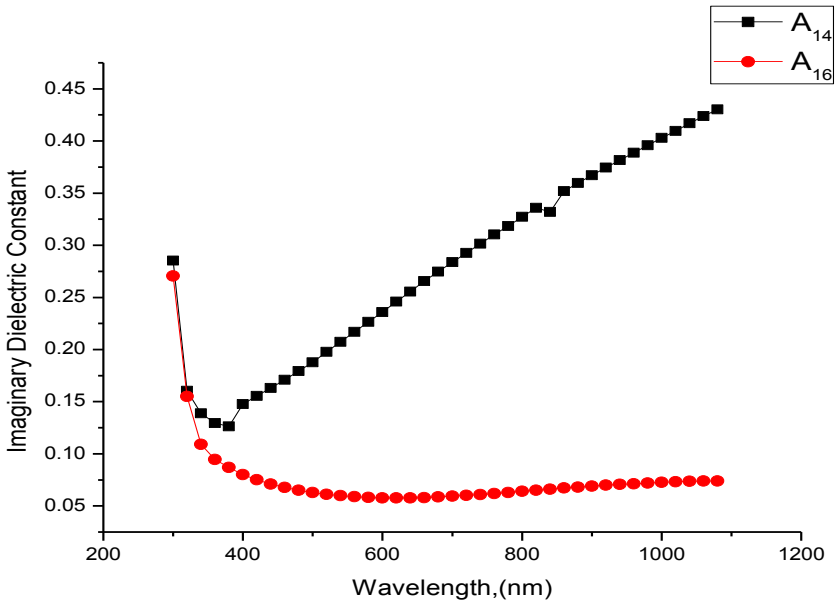

Figure 4.41 The Graph of imaginary dielectric constant against wavelength for $CdO:SnO_2$ alloyed thin films of samples A_{14} and A_{16} at constant temperature of 60^0C of NaOH solution.

Figure 4.42**,** shows the decrease of optical conductivity as wavelength increases for the two samples A_{14} and A_{16} of $CdO:SnO_2$. The two samples, have very high optical conductivity between the range of $10^{13}\Omega^{-1}m^{-1}$ to $10^{14}\Omega\text{-}m^{-1}$. A_{14} decreases from its maximum value of 1.5 x $10^{14}\Omega^{-1}m^{-1}$ at 320nm to a minimum value of $7.0x10^{13}\Omega\text{-}m^{-1}$ at 1080nm. A_{16} falls from its peak value of $4.7x10^{14}\Omega^{-1}m^{-1}$ at 320nm to its lowest values 2.5 x $10x^{13}\Omega^{-1}m^{-1}$ at 1080nm. This is as a result of the dependency of optical conductivity on the nature of refractive index and absorption coefficient; because at the UV region, the absorption coefficient; and refractive index are greatest and diminish as the wavelength increases. This is obtained from equation 2.43

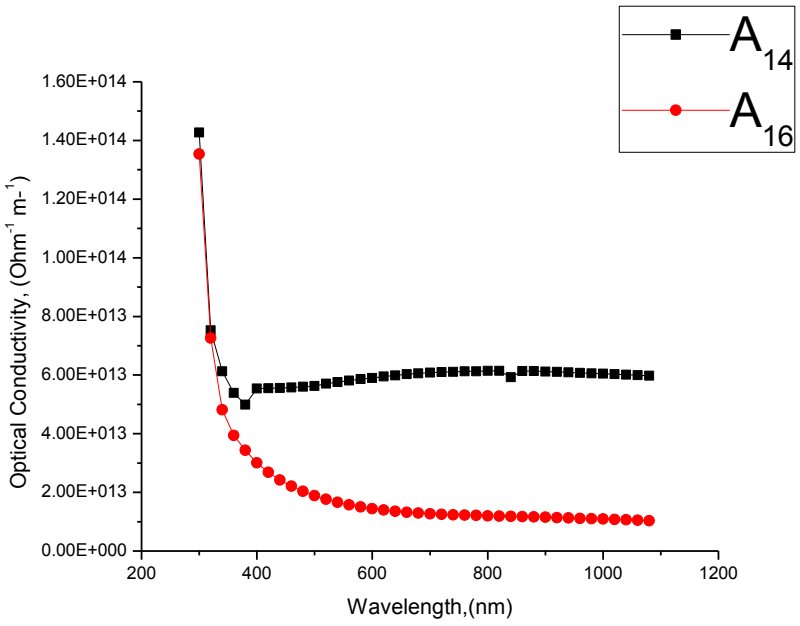

Figure 4.42 The Graph of optical conductivity against wavelength for $CdO:SnO_2$ alloyed thin films of samples A_{14} and A_{16} at constant temperature of 60^0C of NaOH solution.

The optical energy band gap is obtained in k space using equation 4.2.

The energy band gaps of samples A_{14} and A_{16} are evaluated by extrapolating the linear portion of the plot $(\propto h\upsilon)^2$ against $h\upsilon$ at $(\alpha h\upsilon)^2 = 0$ where α is the absorption coefficient as shown in Figure 4.43. Direct band gap values of 3.75±0.05eV and 3.80±0.05eV are obtained for samples A_{14} and A_{16} respectively, with an average band gap value of 3.78±0.05eV.The wide band gaps obtained in this work makes the $CdO:SnO_2$ a good material for the production of laser diodes and light emitting diodes (LEDs) (Look, 2001).

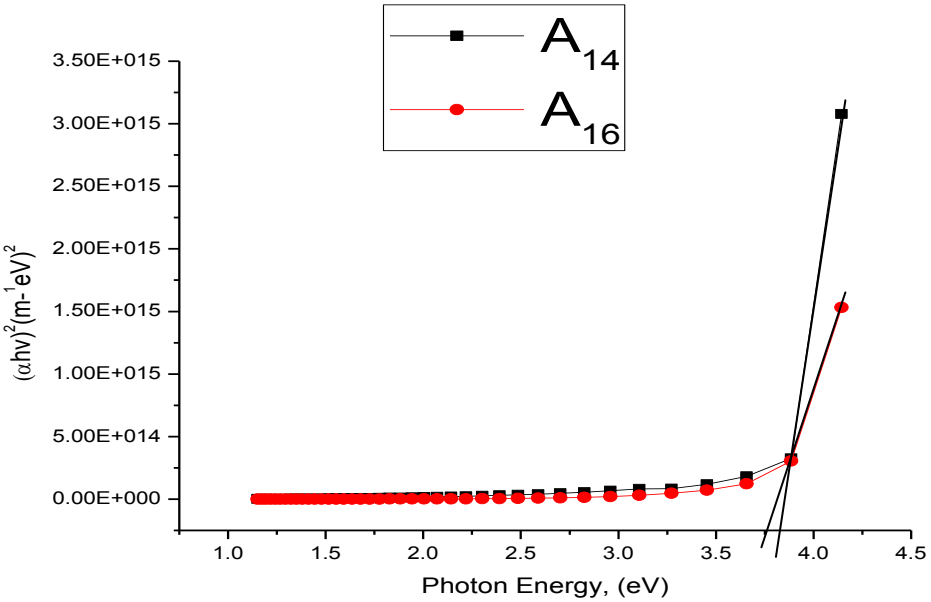

Figure 4.43 The Graph of $(\alpha h\upsilon)^2$ against photon energy $h\upsilon$ for $CdO:SnO_2$ alloyed thin films of samples A_{14} and A_{16} at constant temperature of 60^0C of NaOH solution.

The transmittance spectrum shows that the films of samples A_{24} and A_{25} have good transparency in the UV, visible and near infrared regions of electromagnetic spectrum. Sample A_{24} has transmittance range 42%-60% at the wavelength between 320nm-360nm in the UV region. Sample A_{25} has transmittance range 49%-63% at the wavelength between 320nm-400nm in the UV region.

The transmittance of sample A_{24} increases to its maximum value of 61% at wavelength, λ=450nm in the visible region. The transmittance of sample A_{25} increases as wavelength increases up to a certain value 63% at wavelength λ=480nm after which it falls and rises up to maximum value of 68% at wavelength, λ=1080nmin the near infrared region of electromagnetic spectrum. The transmittance of A_{24} falls as wavelength, increases within the visible and has almost linear characteristics in the near infrared region of electromagnetic spectrum as shown in Figure 4.44.

This makes these alloyed films good materials for UV filter (Onwuemeka*et al*., 2014). It is also a good material for solar cell application and equally a good material for transparent electrode in optoelectronic applications. See Appendix B for the data.

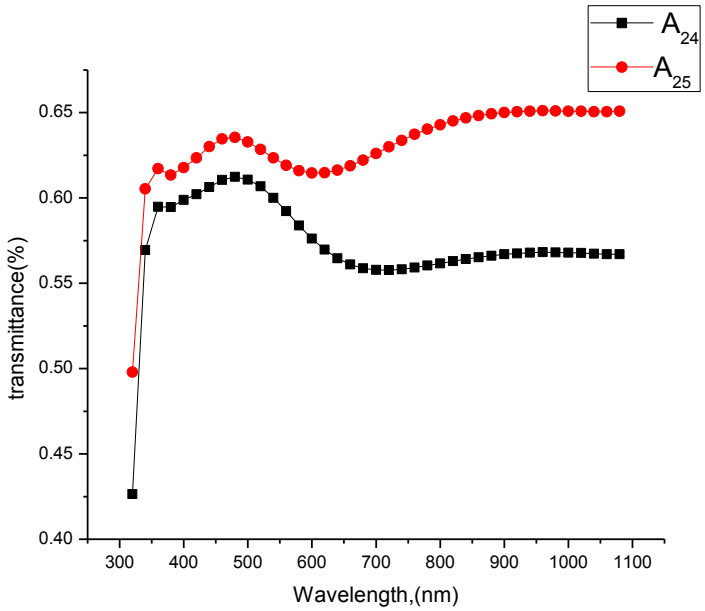

Figure 4.44 Graph of transmittance against wavelength for ZnO:SnO_2 alloyed thin films of samples A_{24} and A_{25} at constant temperature of 60^0C of NaOH solution.

Samples A_{24} and A_{25} of $ZnO:SnO_2$ have decreasing absorbance from the UV, 0.37 and 0.31 respectively at wavelength 320nm which are their maximum values. The absorbance of 0.21 at the visible region at wavelength of 480nm and 0.153 is obtained at the near infrared regions of electromagnetic spectrum at wavelength 1080nm. The absorbance of sample A_{24} in the visible region decreases continually from 400nm to near infrared region of electromagnetic spectrum. This makes the material veritable in the area of optical window coating applications (Look, 2001). This is shown in Figure 4.45, which is obtained from equation 2.28.

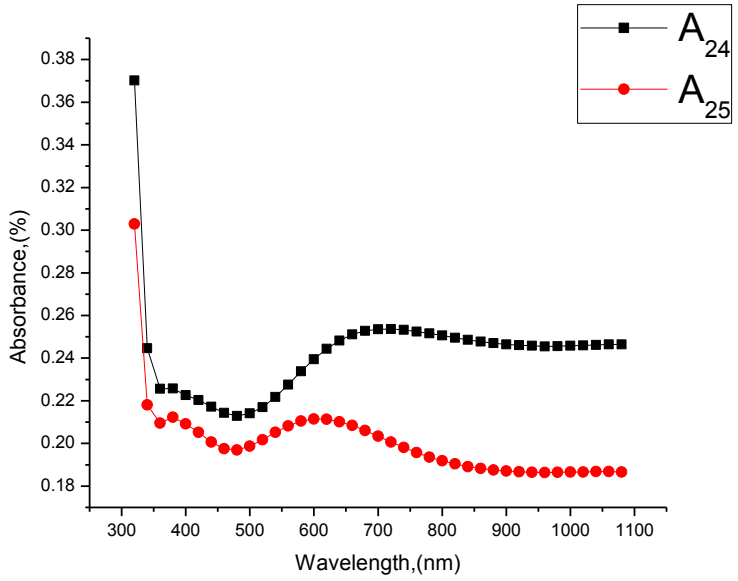

Figure 4.45 Graph of absorbance against wavelength for $ZnO:SnO_2$ alloyed thin films of samples A_{24} and A_{25} at constant temperature of 60^0C of NaOH solution.

Samples A_{24} and A_{25} have low reflectance of 0.18 to 0.204 and 0.165 to 0.20 respectively as depicted in Figure4.46. It decreased as the wavelength increases from the UV through the visible to the near infrared regions of electromagnetic spectrum.

This makes ZnO:SnO_2 useful in the area of multilayer solar control coating. The coating allows the visible part of the spectrum in, but either reflects the infrared (IR) radiation back into the room (energy-saving) or does not allow the infrared radiation into the room (heat-protection) depending on which side of the window has the coating(Onwuemeka*et al*., 2017).

This material can serve as front contact for solar cells or liquid crystal displays from optoelectronic applications (Roitan, 1994). The reflectance of the material is calculated using equation 2.30.

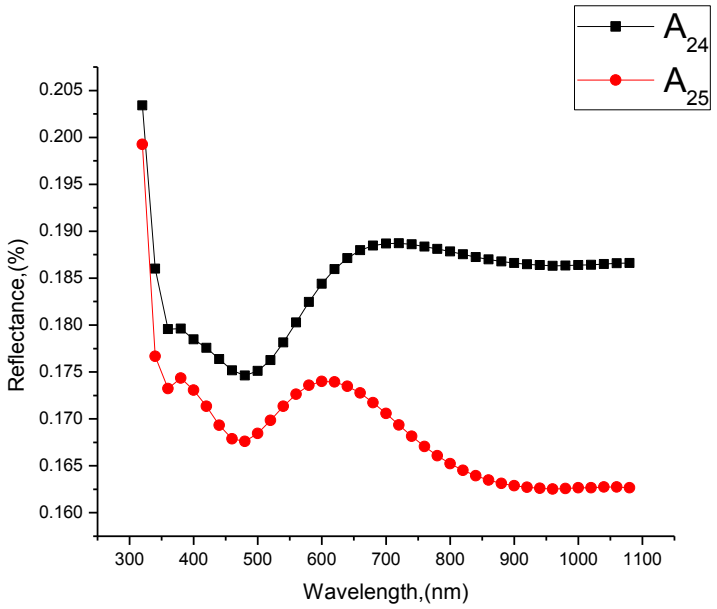

Figure 4.46 Graph of reflectance against wavelength for ZnO:SnO_2 alloyed thin films of samples A_{24} and A_{25} at constant temperature of 60^0C of NaOH solution.

The refraction index, as depicts in Figure 4.47, of sample A_{24} falls from its maximum value of 2.65 at λ= 320nm continuously to its minimum value of 2.45 in the visible region at wavelength, λ=460nm and rises as wavelength increases until it reaches a wavelength, ʎ=1080nm.

Sample A_{25} decreases from 2.63 at λ= 320nm and falls sharply to the visible region atwavelength equal to 2.40 and rises, then falls as wavelength increases to its minimum value of 2.35 at ʎ=1080nm.

The behaviour of these two samples of $ZnO:SnO_2$ makes it possible for use in the area of multiple solar control coating applications where materials with high refractive index are required. The calculation of refractive index is obtained from equation 2.36

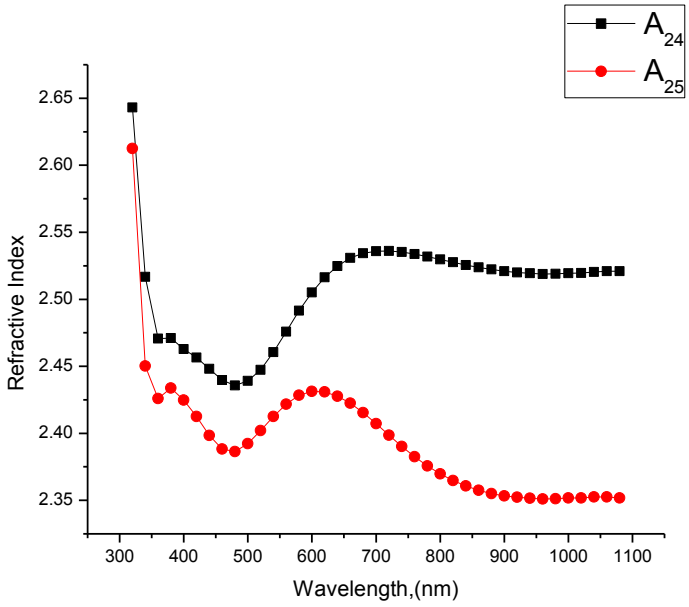

Figure 4.47 Graph of refractive index against wavelength for $ZnO:SnO_2$ alloyed thin films of samples A_{24} and A_{25} at constant temperature of 60^0C of NaOH solution.

In Figure 4.48, samples A_{24} and A_{25} have their maximum extinction coefficients of 0.025 at wavelength, λ=1080nm and 0.008 at wavelength, λ=1080nm respectively at the near infrared region. The minimum values of 0.003 at wavelength, λ=380nm and 0.008 at wavelength, λ=380nm at the UV region from which there were sharp increase of extinction coefficient from the visible as the wavelength increases to 0.025 at wavelength, λ=1080nm for sample A_{24} and 0.008 at wavelength, λ=1080nm for sample A_{25} at the near infrared region of electromagnetic spectrum . The values for Fig. 4.48, is obtained from equation 2.37.

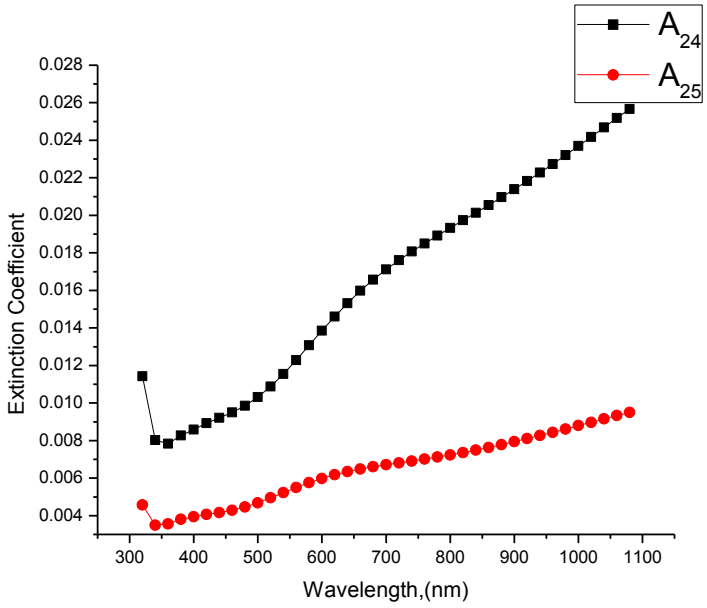

Figure 4.48 Graph of extinction coefficient against wavelength for ZnO:SnO_2 alloyed thin films of samples A_{24} and A_{25} at constant temperature of 60^0C of NaOH solution.

InFigure 4.49**,** samples A_{24} and A_{25} of $ZnO:SnO_2$ thin films have decreasing real dielectric constants as wavelength increases. A_{24} increases from 7.0 at wavelength of 320nm to its minimum value of 5.8 at wavelength λ=460nm. It rises sharply at the visible region to 6.5 at wavelength, λ=660nm, from which it maintains a linear characteristics up to the near infrared region of electromagnetic spectrum.

A_{25} decreases from 5.8 at the wavelength of 320nm to its minimum value of 5.5 at the wavelength λ=1080nm in the near infrared region. It falls sharply at the visible region, then rises, from where it maintains almost a linear characteristics up to the near infrared region of electromagnetic spectrum.

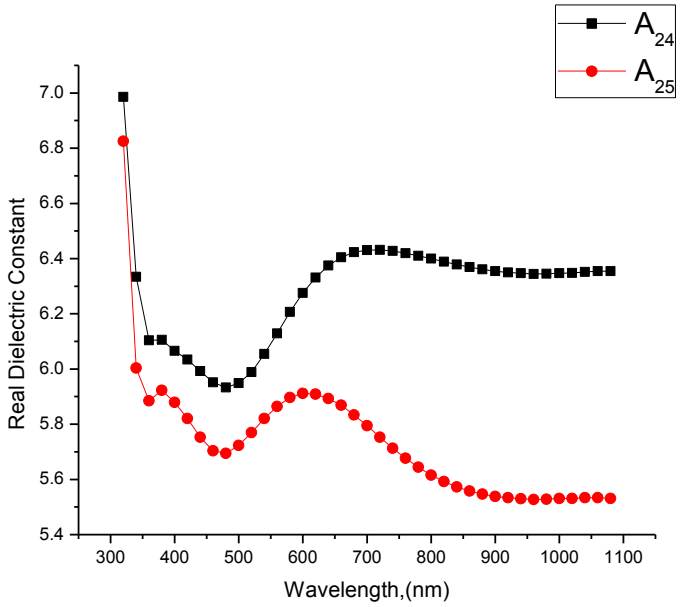

Figure 4.49 Graph of real dielectric against wavelength for $ZnO:SnO_2$ alloyed thin films of samples A_{24} and A_{25} at constant temperature of 60^0C of NaOH solution.

Imaginary dielectric constant in Figure 4.50is very low for the samples A_{24} and A_{25} of $ZnO:SnO_2$ thin films. The plotted graphs fall to the minimum values from 0.060 to 0.048for sample A_{24} and from 0.025 to 0.015 for sample A_{25} at the wavelength 320nm in the UV region.

The two samples A_{24} and A_{25} increase from these points mentioned above and reaches their maximum 0.098 at wavelength, λ =1080nm and 0.041at wavelength, λ =1080nm respectively in the near infrared region of electromagnetic spectrum. The graph is obtained from equation 2.41.

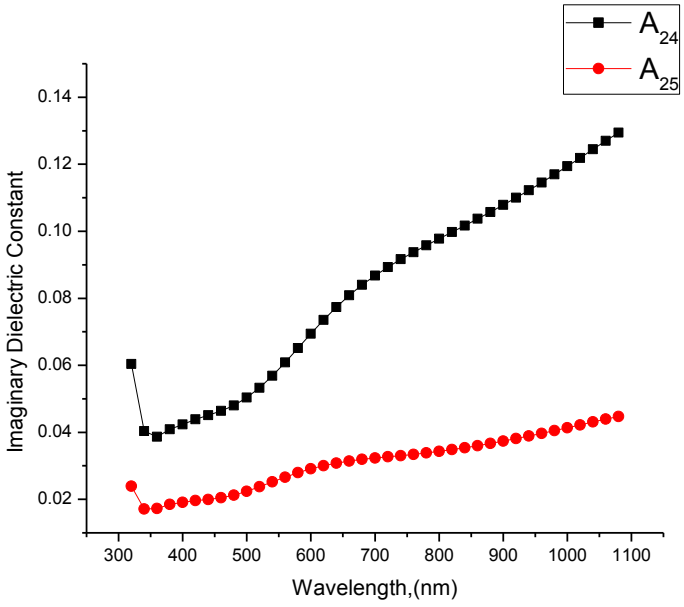

Figure 4.50 Graph of imaginary dielectric against wavelength for $ZnO:SnO_2$ alloyed thin films of samples A_{24} and A_{25} at constant temperature of 60^0C of NaOH solution.

Figure 4.50**,** shows the decrease of optical conductivity as wavelength increases for the two samples A_{24} and A_{25} of $ZnO:SnO_2$ alloyed thin films. The two samples, have very high optical conductivity between $10^{13}\Omega\text{-m}^{-1}$ to $10^{14}\Omega\text{-m}^{-1}$.

Sample A_{24} decreases from its maximum value of 2.58 x $10^{14}\Omega^{-1}\text{m}^{-1}$ at 320nm to the minimum value of $1.50\text{x}10^{14}\Omega\text{-m}^{-1}$ at 460nm in the visible region. A_{25} falls from its peak value of $1.30\text{x}10^{14}\Omega^{-1}\text{m}^{-1}$ at 320nm to its lowest values 6.0 x $10\text{x}^{13}\Omega^{-1}\text{m}^{-1}$ at 1080nm in the visible region. This is as a result of the dependency of optical conductivity on the nature of refractive index and absorption coefficient; because at the UV region, the absorption coefficient; and refractive index are greatest and diminish as the wavelength increases. This is obtained from equation 2.43.

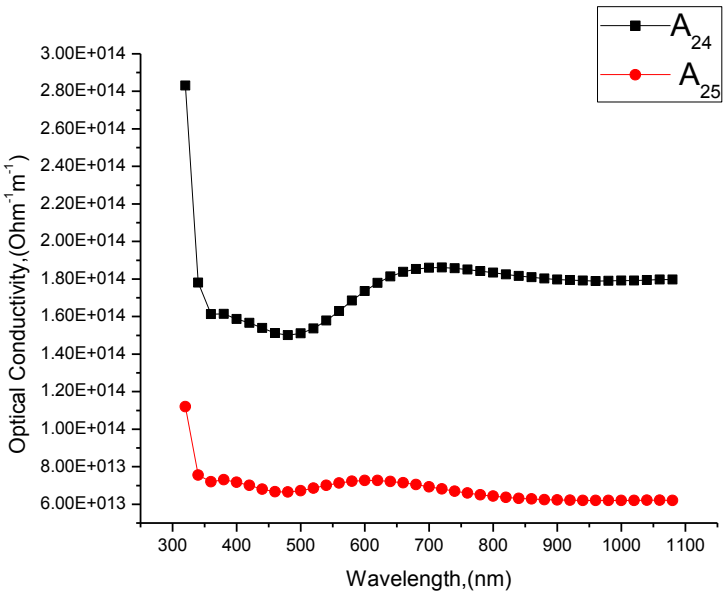

Figure 4.51 Graph of optical conductivity against wavelength for $ZnO:SnO_2$ alloyed thin films of samples A_{24} and A_{25} at constant temperature of 60^0C of NaOH solution.

The optical energy band gap is obtained in k space using equation 4.2.

The energy band gaps of samples A_{24} and A_{25} are evaluated by extrapolating the linear portion of the plot $(\alpha h\upsilon)^2$ against photon energy $h\upsilon$ at $(\alpha h\upsilon)^2 = 0$ where α is the absorption coefficient as shown in Figure 4.52.

The direct band gap values of 3.49 ± 0.05eV and 3.24± 0.05eV are obtained for samples A_{24} and A_{25}respectively.The average band gap value 3.37± 0.05eV.

The wide band gap obtained in this work makes the alloy of $ZnO:SnO_2$ a good material for the production of laser diodes and light emitting diodes (LEDs) (Look, 2001).

It can also be used to produce field effect transistors where P-n junction may not be required if produced for solar applications (Onwuemeka*et al*., 2017).

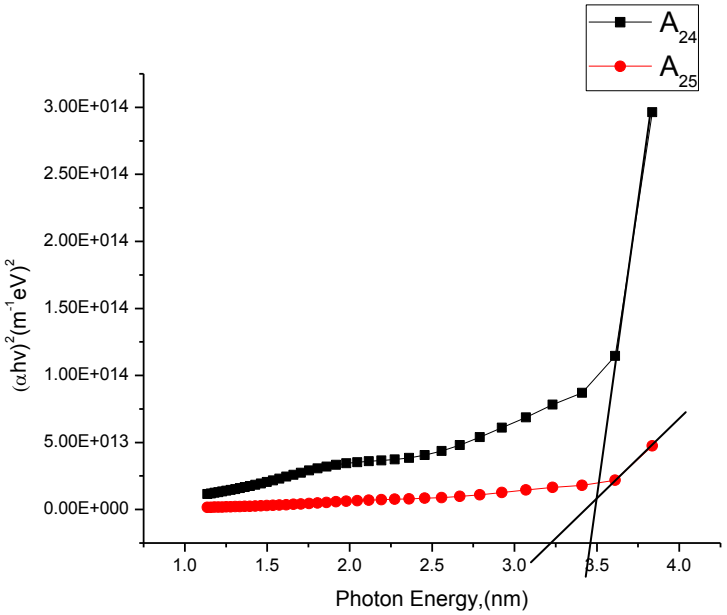

Figure 4.52 The Graph of $(\alpha h\upsilon)^2$ against photon energy $h\upsilon$ for $ZnO:SnO_2$ alloyed thin films of samples A_{24} and A_{25} at constant temperature of 60^0C of NaOH solution.

CHAPTER FIVE

SUMMARY, CONCLUSION AND RECOMMEDATIONS

5.1 Summary

In this dissertation, an uncommon materials alloyed transparent thin films formed from oxides of Pb^{2+}, Cu^{2+}, Cd^{2+} and $Zn^{2+}$with oxide of Sn^{2+} were developed using dual solution synthesis. The developed materials are $SnPb_2O_4$, Cd_2SnO_4, Cu_2SnO_4 and Zn_2SnO_4, with wide energy band gaps and high transparencyfrom the UV to near infrared regions of electromagnetic spectrum.

It can be found useful in passive applications as dazzling coating, cold and heat windows, solar thermal-energy collector, selective absorbing layer and active applications: solar cell applications, semiconductor materials, optoelectronic applications, UV light emitting devices, laser diodes, sensors, and in optical communications etc.

In this work specifically, the alloys of $ZnO:SnO_2$ and $CdO:SnO_2$, can also be found useful in the areas of ceramics production, alternative materials for galvanization of roofing sheets and other metallic coatings for anti-corrosion purposes, as quality materials in tyre manufacturing industries as heat inhibitors. $PbO:SnO_2$ and $CuO:SnO_2$ are basically raw materials for advancement in solar cell productions.

5.2 Conclusion

The alloyed materials have been deposited.The deposited materials were uniform and adherent to the substrates. The thicknesses of the materials deposited dependent on the number of cycles, dip-time and most importantly, the annealing temperatures.The elemental compositions show different percentages of the desired elements in the deposited samples. The structural properties show that PbO:SnO_2, and CdO:SnO_2 and ZnO:SnO_2 alloyed thin films are crystalline while CuO:SnO_2 is amorphous.Optical properties show that the deposited films have good transparency from the UV to the near infrared regions of electromagnetic spectrum. Based on this, these materials can be applied in the area of optical coatings-heat and cold window applications especially ZnO:SnO_2 and CdO:SnO_2, galvanization of metal and non-metal surfaces, to prevent corrosion,solar thermal heating and transparent electrodes for optoelectronic applications.

The deposited materials, have high average optical band gaps of 3.65±0.05eV, 3.30±0.05eV, 3.78±0.05eV and 3.37±0.05eV for PbO:SnO_2, CuO:SnO_2, CdO:SnO_2 and ZnO:SnO_2 alloyed thin films respectivelyand this, makes the materials suitable for active applications in laser diodes, light emitting diodes, photovoltaic for solar energy conversion, sensors for detection of poisonous substances most especially in the oil producing areas and flat panel displays for optoelectronic applications. Other properties investigated are absorbance, reflectance, optical conductivity, optical constants and absorption coefficient.

5.3 Recommendations

1. Researchers might look into the potentials yet to be discovered in the alloys of different binary semiconductor compound thin films using dual solution synthesis for preparations, which will go a long way to improving already existing performance of transparent conducting oxides of cadmium, gallium, zinc, indium and tin and other nontransparent alloys.

2. Researchers should look into other areas of energy generations and systems that are environmental friendly, noiseless and pollution-freewhich are thin film based materials.

3. The Federal and State governments may embrace scientific research by giving adequate funding, because of its importance in the area of health, energy, social, political and economic development of the citizenry.

4. The participation of government and private organizations would go a long way in developing a blue print on how these researched materials could utilized and channeled to the various areas of applications.

5.4 Contribution to knowledge

In this dissertation, uncommon method known as dual solution synthesis was used to develop new materials alloyed thin films were reported which will further contribute to field of modern science and technology.

References

Aeger, C., (2002). Film Deposition; Introduction to Microelectronic Fabrication (2nd Ed.). Upper Saddle River, Prentice Hall.

Agbogu, A.C.N., (1993). Growth and Characterization of ZnS Thin Film by Solution Growth Technique, Unpublished M.Sc. Thesis, University of Nigeria Nsukka, Nigeria, 30 - 63.

Aldona, Z., Jan, I. and Dionizy, C., (2003). Application of the Sol-gel Method of Deposition of Thin Films. *J.Materials Science,* 21(4), 439-443.

Amuh, J.N., (1991). The Growth and Characterization of Thin Film CdSe by Solution Growth Technique, Unpublished M,Sc Thesis, University of Nigeria Nsukka, Nigeria, 10-31.

Animalu, A.O.E., (1977). Intermediate Quantum Theory of Crystalline Solids, Prentice-Hall, New Jersey.

Ashcroft, N.W. and Mermin, N.D., (1976). Solid State Physics. Holt, Reinhart and Winston, New York.

Asif, M. and Muneer, T., (2007). Energy Supply, its Demand and Security for Develop And Emerging Economies, *Renewable and Sustainable Energy Reviews*, 11 (7), 1388-1413.

Badeker, K., (1907). Thermal Oxidation of Sputtered Cadmium Thin Films, *Ann. Phys*. (Leipzig) 22, 749.

Barth, T. F.W. and Posnjak, E.Z., (1932). Spinel structure with and without variateequipoints*Kristallchem*. 82(4), 325.

Bekefi, G.and Barret, A.H., (1987). Electromagnetic Vibrations, Waves, and Radiations, MIT *Press Cambridge*.

Born, M. and Wolf, E., (1975). Principles of Optics, Pergamon, *Oxford*London.

Bowden, M.E. and Cardile, C.M., (1990). Structures of Orthorhombic and Cubic DicadmiumStannate.

Bu, S.J., Jin, Z.G, Liu, X.X; Yang L.R. Cheng Z.J., (2005). Synthesis of TiO_2 Porous Thin Films by Polyethelene Glycol Templating and Chemistry of the Process. *J.Eur.Ceram*. Soc., 25(5), 673-679.

Cabric, B., and Pavlovic, T., (2000).AnApparatus For *Crystal* Growth in the Undergraduate Laboratory. *Journal of Applied Crystallography* , *33*, 387-388.

Callister, W. D., (2007). Materials Science and Engineering: An Introduction 7th edition, John *Wiley and Sons, Inc.* New York.

Cashman, R.J., (1946). Thin Film Deposition of Lead Sulphide Thin Films, for Infrared Applications, *Journal of Opt. Phys. Am*., *36*,356.

Chandrasekaran, S. (2013). A novel single step synthesis, high efficiency and cost effective photovoltaic applications of oxidized copper nano particles. *Journal of Solar Energy Materials and Solar Cells* 109(3), 220–226.

Chandra, S.,Kainthla, R.C., Pandya, D.K., and Chopra, K.L., (1979). Photovoltaic Effect of Chemically Deposited Cu_2S, Thin Films.*Thin Solid Films*, *60*, 65.

Chen, F.S.S., Wu, Y.T., Lai, G.L. and Lai, Y.H., (2011). Disproportionation and ComproportionationReaction of Resistive Switching in NiO_x Films. *Applied Physics Letter*, 98.

Cernigoj, U., Stangar U.L.,Trebse, P., Krasove, U.O., and Gross, S., (2006).Photocatalytically Active $Ti0_2$Thin Films Produced by Surfactant- Assisted Sol- Gel Processing.*Thin Solid Films*, 495(2), 327-332.

Cetinkaya, S.,Cetinkaya, H.A., Bayansal, F., and Kahraman, S., (2013). Growth and characterization of CuO nanostructures on si for fabrication of CuO/p-Si Schotky Diodes.*Scientific World Journal*, 12(2), 1-6.

Chopra, K.L., Paulson, P.D., Dutta., (2004). Thin film Solar Cell: An Overview, *Progress in Photovoltaic Research and Applications*, 12(2-3), 69-92.

Chopra, K.L., Major, S., and Pandya, D.K., (1983). Indium-doped Zinc Oxide Thin Films as Transparent Electrode for Solar Cells, *Thin Solid Films*, *102*, 1-46.

Chopra, K.L., and Das, S.R., (1983). Thin Film Solar Cells,*Plenum Press*, New York.

Cointea , L., Nasiu, M., Petrisor, Jr. R.B., Mos, M.S., Gabor, R.A., Varga, T.P., (2010). Synthesis, Crystal Structure and Decomposition of $[La_2(CH_3COO)_6.(H_2O)_3].3.5H_2O$ Precursor for High-k La_2O_3 Thin Films*Material Research Bulletin*, 45 (9), 1203-1206.

Daniel-Umeri, R., Osuji, R. U., Ezema, F.I (2016).Synthesis and characterization of Copper Oxide Thin Films UsingSuccessive Ionic Layer Adsorption Reaction (SILAR) Method. *Journal of Chemistry and Materials* 8 (6), 65-87

De Wit, H.J., and Crevecoeur, C., (1972), Construction to the Problem of the Influence of Electric Field on the Conductivity of Amorphous Semiconductors.
J.Appl. Phys., *15*, 729.

Dorval- Dion, C. A., and Tavares, J.R., (2013). Photo-Initiated Chemical Vapour Deposition as Scalable Particle Functionalization Technology. A practical Review "Powder Technology", *239*, 484-491.

Doyle, J.M., (1966). Thin Films and Semiconductor Integrated Circuitry, *McGraw-Hill Book Company*, New York.

Eom, C. B., and Susan McKinstry, T., (2012). Thin Film Piezoelectric.
Journal of Material Science.,. 37(11), 1007-1017.

Eslamian, M. (2017). Inorganic and Organic Solution-Processed Thin Film Devices. *Journal of Nano-Micro Letter* 9(3), 1-23.

Estrella, V., Nair, M.T.S., and Nair, P.K., (2003). Solution Growth and Optical Properties of Lead Silver Sulphide Thin Films.*Semicond. Sci. Techol*., (18), 190 – 194.

Eze, FC., (1999). Electroless Deposition of CoO Thin Films. *J. Phys. D. Appl. Phys.*, 32(5), 533.

Eze, F.C. and Okeke, C.E., (1993). Characteristics of Spin-coated Metal –modified Arsenic Selenide Films. *Physica B. North Holland190*, 136 -144.

Ferari, B., Sanchez-Herencia, A.J., and Moreno, R., (1998). Aqueous Electrophoretic Deposition of AlO_3/ZrO_2 Layered Ceramics. *Mater. Lett*., 35(6), 887-897.

Girase, K.D., (2013).Effect of Gel Parameters on the Growth and Nucleation of Lead Iodate Crystals. *International Journal on Cybernetics & Informatics*, 2(4), 57-64

Hodes, G., (2002). Chemical Solution Deposition of Semiconductor Films. *Marcel Dekker, Inc*, New York.

Kuanr, B. K Maat, S. Chandrashekariaih, S.Veerakumar, V. Camley, R. E Celinski, Z. (2008). Determination of exchange and rotational anisotropies in IrMn⁄ Fe (t)⁄IrMn exchange coupled structures using dynamic and static techniques: Application to microwave devices .*Journal of Applied Physics*103 (2), 77, 100.

Koao L.F., F. B. Dejene and H.C. Swart., (2014). Synthesis of PbS nanostructures by chemical bath deposition method. *International Journal of Electrochemical Science*, 9(9), 1747 .

Kaur, I., (1980). Growth of Compound Semiconductor Films. A Ph.D. Thesis, Indian Institute of Technology, Delhi, 56-59.

Lanje, A.S., Ningthoujam, R.S., Sharma, S. J., Pode, R. B., and Vatsa, R. K. (2010). "Luminescence properties of Sn1-xFe_xO_2 Nanoparticles. *International Journal of Nanotechnology*, 7(9), 979–988.

Lewis, B.G. and Paine, D.C., (2000).Applications and Processing of Transparent Conducting Oxides. www.mrs.org/publication/bulletin.

Li, C..M., Sun, C.Q., Chen, W., and Pan, L., (2004). Electrochemical Thin Film Deposition of Polypyrrole on different Substrates. *Surface and Coating Technology*, (198), 474-477.

Liu, Y., Liao L, Li, J and Pan, C. (2007). "From copper nanocrystallineto CuOnanoneedle array: synthesis, growth mechanism, and properties. *Journal of Physical Chemistry* 111 (13) 5050–5056.

Look, D.C., (2001). Recent Advances in ZnO Materials and Devices. *Mat. Sci Eng*., 80(1-3),383-387.

Lothian, G.F., (1958). Absorption Spectrophotometry, *Hilger and Watts Ltd. London*.

Manea, E., Budianu, E., Purica, M., Pudaru, C., Popesu, A., Gernica, I., Babarad, F. and Parvulescu, C.C., (2007). SnO_2 Thin Films Prepared by Sol-gel Method for Honeycomb Texture Silicon Solar Cells. *Romanian Journal of Information, Science and Technology*, 10 (1), 25-33.

Meinel, A.B. and Meinel, M.P., (1976). Applied Solar Energy, An Introduction, *Addison-Wesley*Massachussetts.

Morteza, E., (2016). Inorganic and Organic Solution-Processed Thin Film Devices. *Journal of Thin Films,* 9 (3), 1-24.

Neamen, D.A., (2003). Semiconductor Physics and Devices, Basic Principles, (3rd ed.).

Nicolau, Y.F. and Minnard, J.C., (1988).Solution growth of ZnS, CdS and Zn 1- xCd_xS thin films by the successive ionic-layer adsorption and reaction process; growth.*Journal of Crystal Growth,* 92(1), 128.

Nadeem, M.Y, Ahmed, W., and Wasiq, M.F., (2005).ZnS Thin Films – An Overview. *Journal of Research (Science);* BuhauddinZakaniya University, Multan, Pakistan, 16(2), 105 – 110.

Ohring, M., (2002). Materials Science of Thin Films: Deposition and Structure 2nd edition *Elsevier, Inc*.

Onwuemeka, J.I., Eze, F.C. and Ndukwe, I.C., (2017).The study of chemically deposited *ZnO* thin films for possible device applications. *Journal of Innovation in Science and Mathematics*, 5(3), 100-110.

Onwuemeka, J.I., Nwofor, O.K. Nwulu, N.C.,Nwosu, I.E., Ezike,F.M. and Obizo C.G., (2014). The Optical Study of ZnO Thin Films at Different Times of Annealing and Varying Temperatures. *Journal of Applied Physics* (IOSR-JAP), 6(1), 47-51.

Onwuemeka J.I. and Nwulu N.C., (2017). The Study of the Deposition, Composition and Optical Properties Of Cu_2OThin Films at 100^{o}C Of NaOH Solution and Annealed at 250^{o}C for 1hour Prepared by Solution Growth Technique. *Journal of Innovative Research And Knowledge*, 2(5), 59-71.

Onwuemeka, J.I. and Nwulu, N.C., (2017). The Study of the Deposition, Compositions and Optical Properties Of *CdO* Thin Films at 60^{o}C-100^{o}C of NaOH Solution and Annealed at 200^{o}c for 1hour and 3hours, Prepared by Solution Growth Technique. *Journal Of Innovative Research And Knowledge*, 2(5), 29-35.

Ottone, C., Laurenti, M., Bejtka, K., Sanginario, A. and Cauda, V., (2014). The Effect Thin Film Thickness and Roughness in the Anodization Process of very Thin Al-Films. *Journal of Materials Science and Nanotechnology*, 1(1), 1-9.

Pankove, J.I., (1971). Optical Processes in Semiconductors, *Prentice-Hall New York*.

Pathan, H. M and Lokhande, C. D., (2004). Deposition Of Metal Chalcogenide Thin Films By Successive Ionic Layer Adsorption and Reaction (SILAR) Method. *Journal of Material Science*, 27(2), 85-111.

Patil, A.S., Lohar, G.M., Fulari, V.J (2016). Structural, Morphological, Optical and Photoelectrochemical Cell Properties of Copper Oxide Using Modified SILAR Method. *Journal of Material Science* 27(3), 9550–9557

Perillo, P.M. and Rodriquez D.F., (2014), Formation of TiO2 by Anodization of Ti-Films. *Open Access Library Journal*, 65(1), 1-9.

Preetha, K.C., Murali, K.V., Rajina, A.J., Deepa, K. and Remadevi, T.C., (2012).Effect of cationic precursor pH on optical and transport properties of SILAR deposited nano crystalline PbS thin films. *Current Applied Physics*, 12(1), 53-59.

Rao, M. C., (2013).A Brief Survey On Basic Properties Of Thin Films For Device Application. *International Journal of Modern Physics*, Conference Series,*22*, 576–582.

Reka, M., Devi, B., Lawrence, N., Prithirivikumaran, N., (2014). Synthesis and Characterization of Conducting Polymer Polyaniline Doped with Salicylic Acid. *International Journal of Chem. Tech. Research*, 6(13), 5400-5403.

Ravichandran, A. T., Dhanabalan, K., Chandramohan, R., Vasuhi, A., Parameswaran, P. (2014). Optical Properties Of Modified- Silar Grown Copper Oxide Nanocrystalline Thin Films. *International Journal of Information Research* 1(1) 007-011.

Roitan, F.B., (1994), Deposition Techniques for Films and Coatings; Science Technology and Applications (2nd Ed.), Noyes, Park Bridge, NJ, USA.

Rosenburg, R., Kuan, T.S., and Havel, H.I., (1980). Application of Thin Films in Energy, *Optics and Electronic Physics Today*, Philadelphia (USA).

Savale, P.A., (2016). Physical Vapour Deposition Method for Synthesis of Thin Films; A Comparative Study. *Archive of Applied Science Research*, 8(5), 1-8.

Seshan, K., (2002). Handbook of Thin Film Deposition Processes and Techniques; Principles, Methods, Equipment and Applications (2nd Ed.).

Srivastava, S.K., Palit, D., (2005). Defect Studies by X-Ray Diffraction, Electrical and Optical Properties of Layer Type Tungsten Mixed Molybdenum Sulphoselenide. *Journal of Solid State Ionics* (176), 513-521

Sze, S.M., (1981). Physics of Semiconductor Devices (2nd edition), *John Willey and Sons Inc.* New York.

Tauc, J., (1968).Optical Properties and Electronic Structure of Amorphous Ge. And Si, *Material Research Bulletin*, *3*, 37 – 46.

Thewlis, J., (1962). (ed) Encyclopedia Dictionary of Physics,*Pergamon Press, Oxford*. London

Thun, R.E., (1985). Thin films, The Encyclopedia of Physics (3rd edition) VanNostrand Reinhold, New York., 1239.

Tsidilskovsk, I.M.,(1982). Band Structure of Semiconductors, *Pergamon Press Oxford*.

Üst, U.C., Dağcı, K., Alanyalıoğlu, M. (2015). Electrochemical approaches for rearrangement of lead sulfide thin films prepared by SILAR method. *Journal of Materials Science in Semiconductor Processing*. (41), 270–276.

Urbach, F., (1953). Long Wavelength Edge of Photographic Sensitivity and Electronic Absorption of Solids, *Phys. Rev*., (92), 1324.

Verhoeven, J.D., (2007). Steel Metallurgy for the Non-metallurgist. ASM International, 56.

Wiley, R.R., (2007). Practical Equipment, Materials and Processes for Optical Thin Films. *Wiley Optical Con*sultant.

Wooten, F., (1972). Optical Properties of Solids, *Academic Press*, New York.

Wu, X., Sheldon, P., Mhathongdy, Y. Rihelin, R. Mason, A. Moutino, H.R. and Coult, T.J,(1999). A.I.P. Conf. CPV Photovoltaic Review American Institute of Physics.Woodbury N.Y., 462.

Yacobi, B. G., (2004). Semiconductor Materials: An Introduction to Basic Principles, 1-3, 154-157, 107.

Yamatoto, T. and Katayama-Yoshida, H., (1999). P-type Properties of $CuAlO_2$ and $CuSnO_2$ *Jpn. J. Appl.*, 38(28), 37.

Yram, D. B., (2015).Investigating The Optical Band Gap And Crystal Structure Of Copper Sulphide And Copper Selenide Thin Films Deposited By Chemical Bath Deposition. Unpublished M.Sc.Thesis, 20-35.

.

Appendix A

λ	T_{21}	T_{22}	A_{21}	A_{22}	R_{21}	R_{22}
320	0.47852	0.41852	0.3201	0.378284	0.20138	0.203196

340	0.62367	0.57141	0.205045	0.243052	0.171285	0.185538
360	0.66345	0.60727	0.178192	0.216618	0.158358	0.176112
380	0.67592	0.61446	0.170105	0.211506	0.153975	0.174034
400	0.68814	0.62393	0.162323	0.204864	0.149537	0.171206
420	0.69586	0.62923	0.157478	0.201191	0.146662	0.169579
440	0.70277	0.63449	0.153187	0.197575	0.144043	0.167935
460	0.70923	0.64015	0.149213	0.193718	0.141557	0.166132
480	0.71489	0.64526	0.145761	0.190265	0.139349	0.164475
500	0.72014	0.65059	0.142583	0.186693	0.137277	0.162717
520	0.72488	0.65562	0.139734	0.183348	0.135386	0.161032
540	0.72989	0.66078	0.136743	0.179943	0.133367	0.159277
560	0.73392	0.66586	0.134351	0.176617	0.131729	0.157523
580	0.73766	0.67032	0.132144	0.173718	0.130196	0.155962
600	0.74118	0.67488	0.130076	0.170773	0.128744	0.154347
620	0.74454	0.67928	0.128112	0.167951	0.127348	0.152769
640	0.74756	0.68335	0.126354	0.165357	0.126086	0.151293
660	0.75052	0.68759	0.124638	0.16267	0.124842	0.14974
680	0.75298	0.69145	0.123217	0.160239	0.123803	0.148311
700	0.75537	0.6953	0.12184	0.157828	0.12279	0.146872
720	0.75809	0.69901	0.120279	0.155517	0.121631	0.145473
740	0.76013	0.7025	0.119112	0.153354	0.120758	0.144146
760	0.76224	0.70602	0.117908	0.151183	0.119852	0.142797
780	0.76405	0.70932	0.116878	0.149158	0.119072	0.141522
800	0.76584	0.71255	0.115862	0.147185	0.118298	0.140265
820	0.76765	0.71588	0.114837	0.14516	0.117513	0.13896
840	0.76953	0.71925	0.113774	0.14312	0.116696	0.13763
860	0.77141	0.72258	0.112715	0.141114	0.115875	0.136306
880	0.77339	0.72603	0.111601	0.139045	0.115009	0.134925
900	0.77536	0.72946	0.110497	0.136999	0.114143	0.133541
920	0.77742	0.73293	0.109344	0.134938	0.113236	0.132132
940	0.77945	0.73643	0.108212	0.132869	0.112338	0.130701
960	0.78139	0.74005	0.107132	0.130739	0.111478	0.129211
980	0.78311	0.7433	0.106177	0.128836	0.110713	0.127864
1000	0.78477	0.74654	0.105258	0.126947	0.109972	0.126513
1020	0.78676	0.74994	0.104158	0.124973	0.109082	0.125087
1040	0.78885	0.75301	0.103006	0.123199	0.108144	0.123791
1060	0.79054	0.75623	0.102076	0.121346	0.107384	0.122424
1080	0.79221	0.75966	0.10116	0.119381	0.10663	0.120959

Appendix A

λ	α_{21}	α_{22}
320	1791409	6900892
340	1147516	4433911

360	997233.6	3951686
380	951974.9	3858433
400	908426.4	3737261
420	881311.5	3670246
440	857295.4	3604292
460	835055.9	3533931
480	815736.4	3470939
500	797952.7	3405765
520	782007.5	3344747
540	765267	3282636
560	751884.2	3221960
580	739530.1	3169070
600	727959.8	3115357
620	716966.5	3063872
640	707127.9	3016543
660	697523.3	2967537
680	689569.8	2923185
700	681867.5	2879194
720	673131.4	2837032
740	666599.8	2797575
760	659862.5	2757976
780	654097.9	2721031
800	648410.5	2685036
820	642673	2648096
840	636727.9	2610888
860	630797.4	2574292
880	624567	2536555
900	618383.8	2499214
920	611935	2461615
940	605596.8	2423872
960	599555	2385022
980	594210.8	2350305
1000	589064.3	2315846
1020	582908.9	2279845
1040	576460.9	2247479
1060	571259.5	2213672
1080	566130.6	2177819

Hv	$(\alpha hv)^2$(sampleA_{21})	$(\alpha hv)^2$(sampleA_{22})
3.836806	4.72421E+13	7.01052E+14
3.611111	1.71711E+13	2.56363E+14
3.410494	1.15672E+13	1.81635E+14
3.230994	9.4607E+12	1.55415E+14
3.069444	7.77498E+12	1.31591E+14
2.92328	6.63743E+12	1.15115E+14
2.790404	5.72262E+12	1.01152E+14
2.669082	4.9677E+12	8.89693E+13
2.55787	4.35368E+12	7.88227E+13
2.455556	3.83932E+12	6.99405E+13
2.361111	3.40922E+12	6.23676E+13
2.273663	3.02746E+12	5.57054E+13
2.19246	2.71747E+12	4.99004E+13
2.116858	2.45073E+12	4.50036E+13
2.046296	2.21897E+12	4.06399E+13
1.980287	2.01583E+12	3.68127E+13
1.918403	1.84024E+12	3.34887E+13
1.860269	1.68372E+12	3.0475E+13
1.805556	1.55017E+12	2.7857E+13
1.753968	1.43035E+12	2.55027E+13
1.705247	1.31757E+12	2.34047E+13
1.659159	1.22323E+12	2.15447E+13
1.615497	1.13637E+12	1.98515E+13
1.574074	1.06007E+12	1.8345E+13
1.534722	9.90284E+11	1.69809E+13
1.49729	9.25959E+11	1.5721E+13
1.46164	8.66141E+11	1.45632E+13
1.427649	8.11003E+11	1.3507E+13
1.395202	7.59333E+11	1.25246E+13
1.364198	7.11657E+11	1.16242E+13
1.334541	6.66921E+11	1.07921E+13
1.306147	6.25678E+11	1.00231E+13
1.278935	5.8797E+11	9.30426E+12
1.252834	5.54203E+11	8.67034E+12
1.227778	5.23076E+11	8.08461E+12
1.203704	4.92312E+11	7.53095E+12
1.180556	4.6314E+11	7.03986E+12
1.158281	4.37819E+11	6.57437E+12
1.136831	4.14214E+11	6.12965E+12

AppendixB

λ	T_{24}	T_{25}	A_{24}	A_{25}	R_{24}	R_{25}	α_{24}	α_{25}
320	0.42639	0.49786	0.370193	0.302893	0.203417	0.199247	4486320.308	1795111
340	0.56941	0.60526	0.244575	0.218058	0.186015	0.176682	2963971.273	1292333
360	0.59485	0.6172	0.225593	0.209574	0.179557	0.173226	2733926.348	1242052
380	0.59465	0.6134	0.225739	0.212256	0.179611	0.174344	2735696.22	1257948
400	0.59886	0.61775	0.222675	0.209187	0.178465	0.173063	2698565.427	1239760
420	0.60211	0.62347	0.220324	0.205184	0.177566	0.171346	2670079.611	1216037
440	0.60638	0.63005	0.217255	0.200625	0.176365	0.169325	2632886.456	1189015
460	0.61052	0.63466	0.2143	0.197459	0.17518	0.167881	2597074.873	1170251
480	0.61243	0.63553	0.212944	0.196864	0.174626	0.167606	2580634.888	1166725
500	0.61079	0.63287	0.214108	0.198685	0.175102	0.168445	2594747.778	1177520
520	0.60677	0.6284	0.216976	0.201764	0.176254	0.169836	2629502.486	1195764
540	0.60004	0.62346	0.22182	0.205191	0.17814	0.171349	2688205.049	1216078
560	0.59218	0.6192	0.227546	0.208169	0.180274	0.172631	2757603.349	1233725
580	0.58377	0.61598	0.233758	0.210433	0.182472	0.173587	2832885.312	1247145
600	0.57613	0.61458	0.23948	0.211422	0.18439	0.173998	2902220.786	1253002
620	0.56969	0.61478	0.244361	0.21128	0.185949	0.17394	2961383.82	1252164
640	0.56461	0.61635	0.248251	0.210173	0.187139	0.173477	3008526.588	1245599
660	0.56093	0.61879	0.251091	0.208457	0.187979	0.172753	3042942.939	1235430
680	0.55875	0.62219	0.252782	0.206077	0.188468	0.171733	3063437.542	1221326
700	0.55779	0.62602	0.253529	0.203412	0.188681	0.170568	3072488.061	1205531
720	0.55768	0.62997	0.253615	0.20068	0.188705	0.16935	3073526.094	1189342
740	0.55814	0.63377	0.253257	0.198068	0.188603	0.168162	3069186.59	1173863
760	0.55919	0.63727	0.252441	0.195677	0.188369	0.167053	3059294.584	1159688
780	0.56033	0.64032	0.251556	0.193603	0.188114	0.166077	3048575.701	1147398
800	0.56158	0.64293	0.250588	0.191836	0.187832	0.165234	3036847.576	1136928
820	0.5629	0.6451	0.249569	0.190373	0.187531	0.164527	3024490.982	1128256
840	0.56415	0.6469	0.248605	0.189163	0.187245	0.163937	3012816.344	1121084
860	0.56523	0.64832	0.247775	0.188211	0.186995	0.163469	3002750.269	1115440
880	0.56618	0.64935	0.247045	0.187521	0.186775	0.163129	2993911.738	1111354
900	0.56694	0.6501	0.246463	0.18702	0.186597	0.16288	2986851.584	1108383
920	0.56746	0.65056	0.246065	0.186713	0.186475	0.162727	2982026.404	1106563
940	0.56784	0.65089	0.245774	0.186492	0.186386	0.162618	2978503.106	1105257
960	0.56818	0.65114	0.245514	0.186326	0.186306	0.162534	2975352.679	1104269
980	0.56805	0.65102	0.245613	0.186406	0.186337	0.162574	2976557.031	1104743
1000	0.56784	0.6508	0.245774	0.186552	0.186386	0.162648	2978503.106	1105613
1020	0.5677	0.65079	0.245881	0.186559	0.186419	0.162651	2979800.888	1105653
1040	0.56731	0.65048	0.24618	0.186766	0.18651	0.162754	2983417.829	1106879
1060	0.56699	0.65048	0.246425	0.186766	0.186585	0.162754	2986387.432	1106879
1080	0.56694	0.65079	0.246463	0.186559	0.186597	0.162651	2986851.584	1105653

Appendix B

Hv	$(\alpha hv)^2 A_{24}$	$(\alpha hv)^2 A_{25}$
3.836806	2.96292E+14	4.74375E+13
3.611111	1.14559E+14	2.17786E+13
3.410494	8.69377E+13	1.79438E+13
3.230994	7.81282E+13	1.65195E+13
3.069444	6.86097E+13	1.44809E+13
2.92328	6.09241E+13	1.26367E+13
2.790404	5.39757E+13	1.1008E+13
2.669082	4.80499E+13	9.75622E+12
2.55787	4.35723E+13	8.90623E+12
2.455556	4.05966E+13	8.36058E+12
2.361111	3.85461E+13	7.97121E+12
2.273663	3.73574E+13	7.64496E+12
2.19246	3.65533E+13	7.31645E+12
2.116858	3.59618E+13	6.96975E+12
2.046296	3.52694E+13	6.57416E+12
1.980287	3.43911E+13	6.14863E+12
1.918403	3.3311E+13	5.71E+12
1.860269	3.20435E+13	5.28187E+12
1.805556	3.05942E+13	4.86279E+12
1.753968	2.90418E+13	4.47096E+12
1.705247	2.74693E+13	4.11328E+12
1.659159	2.59312E+13	3.79324E+12
1.615497	2.44261E+13	3.5099E+12
1.574074	2.30274E+13	3.26196E+12
1.534722	2.17223E+13	3.04457E+12
1.49729	2.05077E+13	2.85382E+12
1.46164	1.93922E+13	2.68508E+12
1.427649	1.83773E+13	2.53592E+12
1.395202	1.74483E+13	2.40425E+12
1.364198	1.66028E+13	2.28631E+12
1.334541	1.58375E+13	2.1808E+12
1.306147	1.51349E+13	2.08406E+12
1.278935	1.44802E+13	1.99456E+12
1.252834	1.39064E+13	1.91562E+12
1.227778	1.33732E+13	1.84266E+12
1.203704	1.28651E+13	1.77124E+12
1.180556	1.24051E+13	1.70755E+12
1.158281	1.19652E+13	1.64372E+12
1.136831	1.15297E+13	1.5799E+12

Appendix C

λ	T_{11}	T_{12}	A_{11}	A_{12}	R_{11}	R_{12}
300	0.32382	0.22116	0.489696	0.655293	0.186484	0.123547
320	0.54317	0.62003	0.265064	0.207587	0.191766	0.172383
340	0.6265	0.78464	0.203079	0.10533	0.170421	0.11003
360	0.6579	0.81654	0.18184	0.088023	0.16026	0.095437
380	0.67812	0.81805	0.168693	0.08722	0.153187	0.09473
400	0.69566	0.82205	0.157603	0.085102	0.146737	0.092848
420	0.71048	0.82172	0.148448	0.085276	0.141072	0.093004
440	0.72304	0.82111	0.140838	0.085599	0.136122	0.093291
460	0.73384	0.82069	0.134399	0.085821	0.131761	0.093489
480	0.743	0.81953	0.129011	0.086435	0.127989	0.094035
500	0.75247	0.81815	0.123511	0.087167	0.124019	0.094683
520	0.75987	0.81654	0.119261	0.088023	0.120869	0.095437
540	0.76616	0.81479	0.115681	0.088954	0.118159	0.096256
560	0.77213	0.81311	0.11231	0.089851	0.11556	0.097039
580	0.77707	0.81088	0.10954	0.091043	0.11339	0.098077
600	0.78165	0.80869	0.106988	0.092218	0.111362	0.099092
620	0.78542	0.8063	0.104898	0.093503	0.109682	0.100197
640	0.78865	0.8037	0.103116	0.094906	0.108234	0.101394
660	0.79297	0.80098	0.100743	0.096378	0.106287	0.102642
680	0.795	0.79814	0.099633	0.097921	0.105367	0.103939
700	0.79703	0.79539	0.098525	0.09942	0.104445	0.10519
720	0.79889	0.79259	0.097513	0.100951	0.103597	0.106459
740	0.80063	0.78964	0.096568	0.102571	0.102802	0.107789
760	0.80255	0.78679	0.095528	0.104141	0.101922	0.109069
780	0.80415	0.78378	0.094663	0.105806	0.101187	0.110414
800	0.8055	0.78101	0.093934	0.107343	0.100566	0.111647
820	0.80678	0.77829	0.093245	0.108859	0.099975	0.112851
840	0.80795	0.77574	0.092616	0.110284	0.099434	0.113976
860	0.8092	0.77336	0.091944	0.111618	0.098856	0.115022
880	0.81049	0.77116	0.091252	0.112856	0.098258	0.115984
900	0.81178	0.7691	0.090562	0.114017	0.097658	0.116883
920	0.81316	0.7672	0.089824	0.115091	0.097016	0.117709
940	0.81453	0.76546	0.089093	0.116077	0.096377	0.118463
960	0.81613	0.76398	0.088241	0.116918	0.095629	0.119102
980	0.81752	0.76234	0.087502	0.117851	0.094978	0.119809
1000	0.81889	0.76076	0.086774	0.118752	0.094336	0.120488
1020	0.82068	0.75961	0.085826	0.119409	0.093494	0.120981
1040	0.82202	0.75819	0.085118	0.120222	0.092862	0.121588
1060	0.82376	0.75717	0.084199	0.120807	0.092041	0.122023
1080	0.82591	0.75639	0.083067	0.121254	0.091023	0.122356

Appendix C

α_{11}	α_{12}	n_{11}	n_{12}	hv	$(\alpha hv)^2 A_{11}$	$(\alpha hv)^2 A_{12}$
10718322	12573907	2.52012	2.084002	4.092593	1.9242E+15	2.64812E+15
5801644	3983228	2.558153	2.419914	3.836806	4.955E+14	2.33566E+14
4444929	2021086	2.406116	1.992705	3.611111	2.5764E+14	5.32661E+13
3980060	1688995	2.335138	1.894061	3.410494	1.8425E+14	3.31811E+13
3692310	1673598	2.28618	1.889264	3.230994	1.4232E+14	2.92398E+13
3449565	1632950	2.241821	1.876498	3.069444	1.1211E+14	2.51227E+13
3249187	1636296	2.203051	1.877554	2.92328	9.0217E+13	2.28805E+13
3082612	1642485	2.169309	1.879506	2.790404	7.399E+13	2.10057E+13
2941675	1646749	2.139666	1.880848	2.669082	6.1647E+13	1.93187E+13
2823757	1658536	2.114078	1.88455	2.55787	5.2169E+13	1.79973E+13
2703366	1672580	2.087199	1.888946	2.455556	4.4067E+13	1.68684E+13
2610341	1688995	2.065898	1.894061	2.361111	3.7986E+13	1.59034E+13
2531980	1706874	2.047588	1.899606	2.273663	3.3142E+13	1.5061E+13
2458197	1724074	2.030036	1.904913	2.19246	2.9047E+13	1.42881E+13
2397575	1746960	2.015384	1.911936	2.116858	2.5759E+13	1.36757E+13
2341713	1769497	2.001696	1.918809	2.046296	2.2962E+13	1.3111E+13
2295976	1794162	1.990353	1.926281	1.980287	2.0672E+13	1.26235E+13
2256964	1821077	1.980581	1.934376	1.918403	1.8747E+13	1.2205E+13
2205037	1849328	1.967432	1.94281	1.860269	1.6826E+13	1.18353E+13
2180734	1878927	1.961221	1.951576	1.805556	1.5503E+13	1.15091E+13
2156492	1907689	1.954991	1.960026	1.753968	1.4307E+13	1.11959E+13
2134335	1937077	1.949265	1.968592	1.705247	1.3246E+13	1.09111E+13
2113654	1968151	1.943892	1.977575	1.659159	1.2298E+13	1.06633E+13
2090885	1998283	1.937946	1.986214	1.615497	1.141E+13	1.04214E+13
2071953	2030224	1.932978	1.995296	1.574074	1.0637E+13	1.02126E+13
2056008	2059728	1.928775	2.003615	1.534722	9.9566E+12	9.99262E+12
2040915	2088801	1.924782	2.011747	1.49729	9.3382E+12	9.78151E+12
2027140	2116149	1.921125	2.01934	1.46164	8.7791E+12	9.56695E+12
2012445	2141755	1.91721	2.026399	1.427649	8.2545E+12	9.34937E+12
1997303	2165495	1.913162	2.032899	1.395202	7.7654E+12	9.12827E+12
1982185	2187786	1.909105	2.038965	1.364198	7.3121E+12	8.90767E+12
1966040	2208398	1.904756	2.044543	1.334541	6.8841E+12	8.68597E+12
1950038	2227319	1.900428	2.049635	1.306147	6.4874E+12	8.46348E+12
1931384	2243447	1.895361	2.053955	1.278935	6.1015E+12	8.23244E+12
1915208	2261355	1.890949	2.05873	1.252834	5.7573E+12	8.02648E+12
1899292	2278645	1.88659	2.063319	1.227778	5.4378E+12	7.82695E+12
1878536	2291251	1.88088	2.066651	1.203704	5.113E+12	7.60649E+12
1863028	2306844	1.876594	2.070757	1.180556	4.8374E+12	7.41668E+12
1842928	2318062	1.871014	2.0737	1.158281	4.5566E+12	7.20905E+12
1818151	2326651	1.864097	2.075948	1.136831	4.2722E+12	6.99608E+12

Appendix D

λ	T_{14}	T_{16}	A_{14}	A_{16}	R_{14}	R_{16}	α_{14}	α_{16}
300	0.1851	0.29155	0.732594	0.535287	0.082306	0.173163	3312048	2337285
320	0.53539	0.53539	0.27133	0.27133	0.19328	0.19328	1226679	1184738
340	0.59045	0.6394	0.228817	0.194227	0.180733	0.166373	1034479	848077.2
360	0.6394	0.68227	0.194227	0.166044	0.166373	0.151686	878099.9	725015.7
380	0.61212	0.70917	0.213163	0.14925	0.174717	0.14158	963709.6	651685.8
400	0.61485	0.73346	0.211231	0.134624	0.173919	0.131916	954972.3	587822.3
420	0.61438	0.75262	0.211563	0.123424	0.174057	0.123956	956473.8	538921.4
440	0.614	0.76909	0.211832	0.114023	0.174168	0.116887	957688.5	497871
460	0.61345	0.78317	0.212221	0.106144	0.174329	0.110686	959448.1	463468.5
480	0.61211	0.79515	0.213171	0.099551	0.174719	0.105299	963741.7	434680.7
500	0.61012	0.80566	0.214585	0.093848	0.175295	0.100492	970135.3	409780.1
520	0.60776	0.81477	0.216268	0.088965	0.175972	0.096265	977744.8	388457.9
540	0.60555	0.82216	0.21785	0.085044	0.1766	0.092796	984897.5	371335.9
560	0.60349	0.82887	0.21933	0.081514	0.17718	0.089616	991588.2	355922.1
580	0.60124	0.83435	0.220952	0.078652	0.177808	0.086998	998922.2	343426.1
600	0.59972	0.83922	0.222051	0.076124	0.178229	0.084656	1003892	332389.7
620	0.59755	0.84323	0.223626	0.074054	0.178824	0.082716	1011010	323350.3
640	0.59596	0.84662	0.224783	0.072311	0.179257	0.081069	1016241	315741.9
660	0.59407	0.8495	0.226162	0.070837	0.179768	0.079663	1022478	309302
680	0.59302	0.85159	0.226931	0.069769	0.180049	0.078641	1025951	304642.3
700	0.59211	0.85353	0.227598	0.068781	0.180292	0.077689	1028966	300327.3
720	0.59142	0.85521	0.228104	0.067927	0.180476	0.076863	1031256	296598.4
740	0.59093	0.85657	0.228464	0.067237	0.180606	0.076193	1032883	293585.2
760	0.59033	0.85782	0.228905	0.066604	0.180765	0.075576	1034878	290819.9
780	0.59033	0.8587	0.228905	0.066159	0.180765	0.075141	1034878	288875.6
800	0.58974	0.85959	0.229339	0.065709	0.180921	0.074701	1036841	286911.2
820	0.58959	0.86041	0.22945	0.065295	0.18096	0.074295	1037341	285103.1
840	0.59855	0.86121	0.2229	0.064891	0.17855	0.073899	1007727	283340.7
860	0.58977	0.86206	0.229317	0.064463	0.180913	0.073477	1036741	281470
880	0.59009	0.86298	0.229082	0.063999	0.180828	0.073021	1035676	279447.3
900	0.5905	0.86383	0.22878	0.063572	0.18072	0.072598	1034312	277580.5
920	0.59106	0.86485	0.228368	0.063059	0.180572	0.072091	1032451	275342.7
940	0.59174	0.86594	0.227869	0.062512	0.180391	0.071548	1030194	272954.2
960	0.59247	0.86723	0.227334	0.061866	0.180196	0.070904	1027773	270131.3
980	0.59306	0.86829	0.226901	0.061335	0.180039	0.070375	1025819	267814.9
1000	0.59357	0.86929	0.226528	0.060835	0.179902	0.069875	1024131	265632.2
1020	0.59442	0.87068	0.225907	0.060141	0.179673	0.069179	1021321	262602.4
1040	0.59485	0.87175	0.225593	0.059608	0.179557	0.068642	1019901	260273.4
1060	0.59555	0.87321	0.225082	0.058881	0.179368	0.067909	1017592	257100.2
1080	0.59648	0.87489	0.224404	0.058047	0.179116	0.067063	1014529	253455.3

Appendix D

hv	$(\alpha h\nu)2(A_{14})$	$(\alpha h\nu)2(A_{16})$
4.14375	3.08E+15	1.53E+15
3.884766	3.26E+14	3.04E+14
3.65625	1.82E+14	1.22E+14
3.453125	1.04E+14	7.11E+13
3.271382	1.01E+14	4.63E+13
3.107813	8.1E+13	3.07E+13
2.959821	6.68E+13	2.12E+13
2.825284	5.56E+13	1.5E+13
2.702446	4.67E+13	1.09E+13
2.589844	3.98E+13	8.09E+12
2.48625	3.42E+13	6.11E+12
2.390625	2.97E+13	4.69E+12
2.302083	2.59E+13	3.69E+12
2.219866	2.27E+13	2.93E+12
2.143319	2E+13	2.37E+12
2.071875	1.77E+13	1.94E+12
2.00504	1.57E+13	1.61E+12
1.942383	1.4E+13	1.35E+12
1.883523	1.25E+13	1.15E+12
1.828125	1.12E+13	9.86E+11
1.775893	1E+13	8.54E+11
1.726563	8.99E+12	7.44E+11
1.679899	8.08E+12	6.53E+11
1.635691	7.29E+12	5.76E+11
1.59375	6.57E+12	5.12E+11
1.553906	5.96E+12	4.57E+11
1.516006	5.41E+12	4.09E+11
1.479911	4.63E+12	3.66E+11
1.445494	4.47E+12	3.29E+11
1.412642	4.06E+12	2.96E+11
1.38125	3.71E+12	2.67E+11
1.351223	3.38E+12	2.4E+11
1.322473	3.09E+12	2.17E+11
1.294922	2.83E+12	1.95E+11
1.268495	2.59E+12	1.77E+11
1.243125	2.38E+12	1.6E+11
1.21875	2.19E+12	1.45E+11
1.195313	2.02E+12	1.32E+11
1.172759	1.86E+12	1.19E+11
1.151042	1.72E+12	1.07E+11

Appendix E

01-075-1846 Dec 30, 2015 5:54 AM (XRD)

Status Primary **QM:** Star (S) **Pressure/Temperature:** Ambient **Chemical Formula:** Sn Pb2 O4
Empirical Formula: O4 Pb2 Sn **Weight %:** O10.72 Pb69.40 Sn19.88 **Atomic %:** O57.14 Pb28.57 Sn14.29
ANX: AB2X4 **Compound Name:** Tin Lead Oxide **Common Name:** tin(IV) dilead oxide

Radiation: CuKá1 : 1.5406Å **d-Spacing:** Calculated **Intensity:** Calculated **I/Ic:** 7.71

SYS: Orthorhombic **SPGR:** Pbam (55)
Author's Cell [AuthCell a: 8.7215(3)Å **AuthCell b:** 8.7090(3)Å **AuthCell c:** 6.2919(3)Å **AuthCell Vol:** 477.90Å³
AuthCell Z: 4.00 **AuthCell MolVol:** 119.47] **Author's Cell Axial Ratio [c/a:** 0.721 **a/b:** 1.001 **c/b:** 0.722]
Dcalc: 8.299g/cm³ **Dstruc:** 8.3g/cm³ **SS/FOM:** F(30) = 39.0(0.0133, 58)

Space Group: Pbam (55) **Molecular Weight:** 597.09
Crystal Data [XtlCell a: 8.709Å **XtlCell b:** 8.721Å **XtlCell c:** 6.292Å **XtlCell :** 90.00° **XtlCell :** 90.00°
XtlCell : 90.00° **XtlCell Vol:** 477.90Å³ **XtlCell Z:** 4.00]
Crystal Data Axial Ratio [c/a: 0.722 **a/b:** 0.999 **c/b:** 0.721]
Reduced Cell [RedCell a: 6.292Å **RedCell b:** 8.709Å **RedCell c:** 8.721Å **RedCell :** 90.00°
RedCell : 90.00° **RedCell :** 90.00° **RedCell Vol:** 477.90Å³]

Crystal (Symmetry Allowed): Centrosymmetric

Pearson: oP28.00 **Subfile(s):** ICSD Pattern, Inorganic, Primary Pattern **Entry Date:** 07/26/2010
Last Modification Date: 01/19/2012

References:

Type	Reference
Primary Reference	Calculated from ICSD using POWD-12++ (1997).
Additional Reference	Gavarri, J.R., Vigouroux, J.P., Calvarin, G., Hewat, A.W. Ark. Kemi, Mineral. Geo. 16, 14 (1943).
Additional Reference	Gavarri, J.R., Vigouroux, J.P., Calvarin, G., Hewat, A.W. J. Solid State Chem. 43, 12 (1982).
Structure	"Structure de Sn Pb2 O4 a quatre temperatures: relation entre dilatation et agitation thermiques". Gavarri, J.R., Vigouroux, J.P., Calvarin, G., Hewat, A.W. J. Solid State Chem. 36, 81 (1981).

Database Comments: ANX: AB2X4. Analysis: O4 Pb2 Sn1. Formula from original source: Sn Pb2 O4. ICSD Collection Code: 31482. Temperature of Data Collection: 300 K. Wyckoff Sequence: i h2 g2 f(PBAM). Unit Cell Data Source: Powder Diffraction.

d-Spacings (198) - 01-075-1846 (Fixed Slit Intensity) - Cu Kl 1.54056Å

2	d(Å)	I	h	k	l	*	2	d(Å)	I	h	k	l	*	2	d(Å)	I	h	k	l	*
14.3606	6.162610	9	1	1	0		44.0459	2.054200	m	3	3	0		58.1813	1.584310	m	3	2	3	
20.1526	4.402620	1	1	1	1		45.2435	2.002570	67m	1	4	1		58.6410	1.572980	46	0	0	4	
20.3777	4.354500	1m	0	2	0		45.2435	2.002570	m	4	1	1		58.8402	1.568130	82	5	2	1	
20.3777	4.354500	m	2	0	0		46.5432	1.949630	49m	2	4	0		58.9033	1.566600	83	2	5	1	
22.7869	3.899250	7m	1	2	0		46.5432	1.949630	m	4	2	0		59.9961	1.540650	35	4	4	0	
22.7869	3.899250	m	2	1	0		47.3819	1.917060	15m	2	3	2		60.7013	1.524430	3m	1	1	4	
24.8213	3.584060	17m	0	2	1		47.3819	1.917060	m	3	2	2		60.7013	1.524430	m	3	4	2	
24.8213	3.584090	m	2	0	1		48.1011	1.890060	3m	0	2	3		61.2748	1.511530	1m	0	4	3	
26.8774	**3.314390**	999m	1	2	1		48.1011	1.890060	m	2	0	3		61.2748	1.511530	m	4	0	3	
26.8774	**3.314390**	m	2	1	1		48.9063	1.860810	7m	2	4	1		61.6776	1.502620	14	5	1	2	
28.3457	3.145950	92	0	0	2		48.9063	1.860810	m	4	2	1		61.7474	1.501090	14	1	5	2	
28.9533	3.081300	66	2	2	0		49.3044	1.846710	170m	1	2	3		62.0193	1.495160	6m	3	5	0	
31.9129	**2.801970**	223	1	1	2		49.3044	1.846710	m	2	1	3		62.0193	1.495160	m	5	3	0	
32.4407	**2.757580**	278m	1	3	0		50.9668	1.790310	122m	0	4	2		62.3356	1.488330	25m	1	4	3	
32.4407	**2.757580**	m	3	1	0		50.9668	1.790310	m	4	0	2		62.3356	1.488330	m	4	1	3	
35.1452	2.551320	135m	0	2	2		52.0596	1.755270	6m	1	4	2		64.0000	1.453580	26m	3	5	1	
35.1452	2.551320	m	2	0	2		52.0596	1.755270	m	4	1	2		64.0000	1.453580	m	6	0	0	
35.5495	2.523230	4m	1	3	1		52.4409	1.743400	2m	3	4	0		64.1026	1.451500	21	0	6	0	
35.5495	2.523230	m	3	1	1		52.4409	1.743400	m	4	3	0		64.6911	1.439710	1m	2	5	2	
36.6737	2.448420	3m	1	2	2		53.2100	1.720000	181	3	3	2		64.6911	1.439710	m	5	2	2	
36.6737	2.448420	m	2	1	2		53.5348	1.710330	7	5	1	0		64.9931	1.433750	2	6	1	0	
37.1544	2.417840	17m	2	3	0		53.6112	1.708070	6	1	5	0		65.0920	1.431810	1	1	6	0	
37.1544	2.417840	m	3	2	0		54.5994	1.679470	10m	3	4	1		65.3237	1.427290	2m	2	4	3	
39.9115	2.256940	45m	2	3	1		54.5994	1.679470	m	4	3	1		65.3237	1.427290	m	4	2	3	
39.9115	2.256940	m	3	2	1		54.9836	1.668640	1m	1	3	3		65.8957	1.416280	2	6	0	1	
40.9647	2.201310	17	2	2	2		54.9836	1.668640	m	3	1	3		65.9971	1.414350	1	0	6	1	
41.3759	2.180380	29	4	0	0		55.3956	1.657200	2m	2	4	2		66.7087	1.400980	10	2	2	4	
41.4381	2.177250	28	0	4	0		55.3956	1.657200	m	4	2	2		66.8739	1.397920	12	6	1	1	
42.7144	2.115100	1m	1	4	0		55.6421	1.650440	4m	1	5	1		66.9720	1.396110	12	1	6	1	
42.7144	2.115100	m	4	1	0		55.6421	1.650440	m	5	1	1		67.6565	1.383640	5	4	4	2	
43.6403	2.072350	24m	1	3	2		56.8112	1.619220	1	5	2	0		67.9269	1.378790	1	6	2	0	
43.6403	2.072350	m	3	1	2		56.8756	1.617540	1	2	5	0		68.0155	1.377210	1	2	6	0	
44.0459	2.054200	28m	0	4	1		58.1813	1.584310	13m	2	3	3		68.6328	1.366320	57m	1	3	4	

Appendix E

01-075-1846 Dec 30, 2015 5:54 AM (XRD)

2	d(Å)	I	h	k	l	*	2	d(Å)	I	h	k	l	*	2	d(Å)	I	h	k	l	*
68.6328	1.366320	m	3	1	4		78.4984	1.217460	3m	3	5	3		89.0115	1.098860	9m	5	6	1	
68.9458	1.360880	2m	4	5	0		78.4984	1.217460	m	5	3	3		89.0115	1.098860	m	6	5	1	
68.9458	1.360880	m	5	4	0		79.2138	1.208250	3m	4	6	0		89.9107	1.090190	2m	0	4	5	
69.5575	1.350400	5m	3	5	2		79.2138	1.208250	m	6	4	0		89.9107	1.090190	m	8	0	0	
69.5575	1.350400	m	5	3	2		80.0629	1.197560	32m	2	1	5		90.0759	1.088620	2	0	8	0	
69.8559	1.345360	1	2	6	1		80.0629	1.197560	m	2	7	0		90.5980	1.083700	4m	3	5	4	
70.1547	1.340360	4m	3	4	3		80.9055	1.187200	4m	4	6	1		90.5980	1.083700	m	5	3	4	
70.1547	1.340360	m	4	3	3		80.9055	1.187200	m	6	4	1		90.8779	1.081090	8m	1	4	5	
70.7509	1.330520	25m	4	5	1		81.2022	1.183610	6	6	1	3		90.8779	1.081090	m	4	1	5	
70.7509	1.330520	m	5	4	1		81.2928	1.182520	6	1	6	3		91.4406	1.075900	6	7	3	2	
71.0611	1.325470	2m	1	5	3		81.7785	1.176720	2	7	2	1		91.5434	1.074960	6m	3	7	2	
71.0611	1.325470	m	5	1	3		81.8951	1.175340	3	2	7	1		91.5434	1.074960	m	8	0	1	
71.5269	1.317980	6m	0	6	2		82.5317	1.167880	1m	3	4	4		91.7928	1.072690	2m	0	8	1	
71.5269	1.317980	m	2	3	4		82.5317	1.167880	m	4	3	4		91.7928	1.072690	m	3	3	5	
72.3724	1.304650	2	6	1	2		83.4119	1.157780	3m	1	5	4		92.3635	1.067550	13	6	0	4	
72.4670	1.303180	2	1	6	2		83.4119	1.157780	m	5	1	4		92.4554	1.066730	16m	0	6	4	
72.7615	1.298630	1m	3	6	0		84.2595	1.148280	17m	5	5	2		92.4554	1.066730	m	8	1	1	
72.7615	1.298630	m	6	3	0		84.2595	1.148280	m	7	1	2		92.6882	1.064660	10m	1	8	1	
73.9379	1.280850	39m	2	5	3		84.3834	1.146910	17	1	7	2		92.6882	1.064660	m	4	7	1	
73.9379	1.280850	m	5	2	3		84.5632	1.144930	17m	1	3	5		93.2609	1.059620	1m	1	6	4	
74.2892	1.275660	9m	0	4	4		84.5632	1.144930	m	7	3	0		93.2609	1.059620	m	6	1	4	
74.2892	1.275660	m	4	0	4		84.6662	1.143800	17	3	7	0		93.4986	1.057550	1m	2	4	5	
75.1737	1.262830	11m	4	1	4		84.8436	1.141860	14m	4	5	3		93.4986	1.057550	m	8	2	0	
75.1737	1.262830	m	6	2	2		84.8436	1.141860	m	5	4	3		94.1666	1.051800	2m	5	6	2	
75.2583	1.261620	11m	1	4	4		86.1437	1.127930	26m	2	5	4		94.1666	1.051800	m	6	5	2	
75.2583	1.261620	m	2	6	2		86.1437	1.127930	m	4	6	2		94.5375	1.048650	2	0	0	6	
76.1623	1.248880	9m	3	3	4		86.9569	1.119460	4	7	2	2		94.6880	1.047380	2m	4	6	3	
76.1623	1.248880	m	4	5	2		87.0726	1.118270	3	2	7	2		94.6880	1.047380	m	6	4	3	
76.6860	1.241650	1	4	4	3		87.2825	1.116120	4m	2	3	5		95.2212	1.042920	1	8	2	1	
77.3590	1.232520	3m	1	7	0		87.2825	1.116120	m	5	6	0		95.3756	1.041640	1	2	8	1	
77.3590	1.232520	m	5	5	0		88.4772	1.104110	1m	3	6	3		95.5549	1.040160	2	7	2	3	
77.9831	1.224210	18m	2	4	4		88.4772	1.104110	m	6	3	3		95.6704	1.039210	2	2	7	3	
77.9831	1.224210	m	4	2	4		88.8275	1.100660	17	4	4	4		95.9588	1.036850	1	6	2	4	

Appendix F

01-073-1725 Dec 30, 2015 5:53 AM (XRD)

Status Primary **QM:** Indexed (I) **Pressure/Temperature:** Ambient **Chemical Formula:** Zn2 Sn O4
Empirical Formula: O4 Sn Zn2 **Weight %:** O20.42 Sn37.87 Zn41.72 **Atomic %:** O57.14 Sn14.29 Zn28.57
ANX: AB2X4 **Compound Name:** Zinc Tin Oxide **Common Name:** dizinc tin(IV) oxide

Radiation: CuKá1 : 1.5406Å **d-Spacing:** Calculated **Intensity:** Calculated **I/Ic:** 7.48

SYS: Cubic **SPGR:** Fd-3m (227)
Author's Cell [AuthCell a: 8.61(1)Å **AuthCell Vol:** 638.28Å³ **AuthCell Z:** 8.00 **AuthCell MolVol:** 79.78]
Dcalc: 6.524g/cm³ **Dstruc:** 6.52g/cm³ **SS/FOM:** F(30) = 999.9(0.0001, 30)

Space Group: Fd-3m (227) **Molecular Weight:** 313.45
Crystal Data [XtlCell a: 8.610Å **XtlCell b:** 8.610Å **XtlCell c:** 8.610Å **XtlCell :** 90.00° **XtlCell :** 90.00°
XtlCell : 90.00° **XtlCell Vol:** 638.28Å³ **XtlCell Z:** 8.00] **Crystal Data Axial Ratio [a/b:** 1.000 **c/b:** 1.000]
Reduced Cell [RedCell a: 6.088Å **RedCell b:** 6.088Å **RedCell c:** 6.088Å **RedCell :** 60.00°
RedCell : 60.00° **RedCell :** 60.00° **RedCell Vol:** 159.57Å³]

Crystal (Symmetry Allowed): Centrosymmetric

Pearson: cF56.00 **Subfile(s):** Primary Pattern, ICSD Pattern, Inorganic **Entry Date:** 07/26/2010
Last Modification Date: 01/18/2012

References:

Type	Reference
Primary Reference	Calculated from ICSD using POWD-12++ (1997).
Structure	"Spinel structures: with and without variate atom equipoints". Barth, T.F.W., Posnjak, E. Z. Kristallogr., Kristallgeom., Kristallphys., Kristallchem. 82, 325 (1932).

Database Comments: ANX: AB2X4. Analysis: O4 Sn1 Zn2. Formula from original source: Zn2 Sn O4. ICSD Collection Code: 24234. Minor Warning: No R factors reported/abstracted. Magnitude of e.s.d. on cell dimension is >1000 ppm. Wyckoff Sequence: e d a(FD3-MS). Unit Cell Data Source: Single Crystal.

d-Spacings (36) - 01-073-1725 (Fixed Slit Intensity) - Cu K1 1.54056Å

2	d(Å)	I	h	k	l	*	2	d(Å)	I	h	k	l	*	2	d(Å)	I	h	k	l	*
17.8284	4.970880	319	1	1	1		71.8396	1.313010	76	5	3	3		106.2956	0.962627	26	8	4	0	
29.3151	3.044090	205	2	2	0		72.8018	1.298010	80	6	2	2		109.1848	0.945070	9	9	1	1	
34.5210	2.596010	999	3	1	1		76.6058	1.242750	27	4	4	4		110.1587	0.939428	1	8	4	2	
36.1077	2.485490	236	2	2	2		79.4193	1.205640	17	7	1	1		114.1202	0.917829	2	6	6	4	
41.9369	2.152500	231	4	0	0		84.0543	1.150560	20	6	4	2		117.1727	0.902573	39	9	3	1	
45.9043	1.975270	23	3	3	1		86.8145	1.120930	100	7	3	1		122.4601	0.878754	63	8	4	4	
51.9883	1.757510	57	4	2	2		91.4024	1.076250	32	8	0	0		125.7840	0.865338	6	9	3	3	
55.4029	1.657000	317	5	1	1		94.1572	1.051880	1	7	3	3		131.6647	0.844280	8	10	2	0	
60.8062	1.522050	342	4	4	0		95.0770	1.044120	1	6	4	4		135.4626	0.832360	46	9	5	1	
63.9124	1.455360	36	5	3	1		98.7735	1.014700	9	8	2	2		136.7857	0.828498	27	10	2	2	
64.9295	1.435000	1	4	4	2		101.5695	0.994197	53	7	5	1		147.2300	0.802887	7	9	5	3	
68.9180	1.361360	17	6	2	0		102.5072	0.987635	28	6	6	2		148.9659	0.799418	1	8	6	4	

19.5 22.81
111 110

Appendix G

01-080-1466 Dec 30, 2015 5:51 AM (XRD)

Status Primary **QM:** Star (S) **Pressure/Temperature:** Ambient **Chemical Formula:** Cd2 (Sn O4)
Empirical Formula: Cd2 O4 Sn **Weight %:** Cd55.17 O15.70 Sn29.13 **Atomic %:** Cd28.57 O57.14 Sn14.29
ANX: AB2X4 **Compound Name:** Cadmium Tin Oxide **Common Name:** dicadmium stannate

Radiation: CuKá1 : 1.5406Å **d-Spacing:** Calculated **Intensity:** Calculated **I/Ic:** 6.09

SYS: Orthorhombic **SPGR:** Pbam (55)
Author's Cell [AuthCell a: 5.5686(2)Å **AuthCell b:** 9.8946(3)Å **AuthCell c:** 3.19370(12)Å
AuthCell Vol: 175.97Å³ **AuthCell Z:** 2.00 **AuthCell MolVol:** 87.98]
Author's Cell Axial Ratio [c/a: 0.574 **a/b:** 0.563 **c/b:** 0.323] **Dcalc:** 7.691g/cm³ **Dstruc:** 7.69g/cm³
SS/FOM: F(30) = 679.3(0.0012, 36)

Space Group: Pbam (55) **Molecular Weight:** 407.51
Crystal Data [XtlCell a: 5.569Å **XtlCell b:** 9.895Å **XtlCell c:** 3.194Å **XtlCell :** 90.00° **XtlCell :** 90.00°
XtlCell : 90.00° **XtlCell Vol:** 175.97Å³ **XtlCell Z:** 2.00]
Crystal Data Axial Ratio [c/a: 0.574 **a/b:** 0.563 **c/b:** 0.323]
Reduced Cell [RedCell a: 3.194Å **RedCell b:** 5.569Å **RedCell c:** 9.895Å **RedCell :** 90.00°
RedCell : 90.00° **RedCell :** 90.00° **RedCell Vol:** 175.97Å³]

Crystal (Symmetry Allowed): Centrosymmetric

Pearson: oP14.00 **Subfile(s):** Common Phase, Forensic, ICSD Pattern, Inorganic, Primary Pattern
Entry Date: 07/27/2010 **Last Modification Date:** 01/18/2012

References:

Type	Reference
Primary Reference	Calculated from ICSD using POWD-12++ (1997).
Structure	"Structures of orthorhombic and cubic dicadmium stannate by Rietveld refinement". Bowden, M.E., Cardile, C.M. Powder Diffr. 5, 36 (1990).

Database Comments: ANX: AB2X4. Analysis: Cd2 O4 Sn1. Formula from original source: Cd2 (Sn O4). ICSD Collection Code: 69296. Wyckoff Sequence: h2 g a(PBAM). Unit Cell Data Source: Powder Diffraction.

d-Spacings (185) - 01-080-1466 (Fixed Slit Intensity) - Cu K1 1.54056Å

2	d(Å)	I	h	k	l	*	2	d(Å)	I	h	k	l	*	2	d(Å)	I	h	k	l	*
17.9144	4.947300	7	0	2	0		65.7586	1.418900	70	2	6	0		85.5585	1.134140	15m	2	5	2	
18.2861	4.852850	54	1	1	0		67.2151	1.391650	179m	1	3	2		85.5585	1.134140	m	4	4	1	
24.0418	3.698500	93	1	2	0		67.2151	1.391650	m	4	0	0		86.0053	1.129390	1	1	8	1	
27.9133	3.193700	95	0	0	1		67.5701	1.385200	60	2	0	2		86.4642	1.124570	7m	1	6	2	
31.4994	**2.837800**	999	1	3	0		67.9392	1.378570	38	4	1	0		86.4642	1.124570	m	3	7	0	
32.1209	2.784300	303	2	0	0		68.3189	1.371830	23	2	1	2		88.2133	1.106730	9	5	1	0	
33.3660	**2.683190**	449m	0	2	1		68.4194	1.370060	12	1	7	0		90.2131	1.087320	24m	3	4	2	
33.3660	**2.683190**	m	2	1	0		69.3554	1.353840	1	3	5	0		90.2131	1.087320	m	5	2	0	
33.5640	**2.667610**	821	1	1	1		69.7988	1.346320	41	3	4	1		91.1490	1.078580	27	1	9	0	
36.2865	2.473650	23	0	4	0		70.1703	1.340100	17m	0	4	2		91.8137	1.072500	14	4	5	1	
37.1642	2.417220	13	1	2	1		70.1703	1.340100	m	4	2	0		92.5879	1.065550	43	2	8	1	
39.8434	2.260640	89	1	4	0		72.3962	1.304280	18	1	4	2		92.7876	1.063780	9	4	6	0	
42.5829	2.121340	96	1	3	1		72.8885	1.296680	1	2	6	1		93.1409	1.060670	57m	2	6	2	
43.0646	2.098710	3	2	0	1		73.8216	1.282580	2	4	3	0		93.1409	1.060670	m	3	7	1	
44.0721	2.053040	208	2	1	1		74.2545	1.276170	3m	2	3	2		93.7714	1.055190	2	5	3	0	
46.3916	1.955650	89	0	4	1		74.2545	1.276170	m	4	0	1		94.4536	1.049360	7	4	0	2	
46.9918	1.932060	389	2	2	1		74.9745	1.265690	42	4	1	1		94.8856	1.045720	6	5	1	1	
48.7981	1.864680	2	1	5	0		75.3446	1.260390	14	2	7	0		95.1515	1.043500	25	4	1	2	
49.2322	1.849250	14	2	4	0		75.4352	1.259100	21	1	7	1		95.5937	1.039840	36m	1	1	3	
49.3483	1.845170	35	1	4	1		76.3360	1.246470	37	3	5	1		95.5937	1.039840	m	1	7	2	
49.9490	1.824380	9	3	1	0		77.1216	1.235720	21m	0	8	0		96.4773	1.032650	1	3	5	2	
51.5743	1.770640	7	2	3	1		77.1216	1.235720	m	4	2	1		96.9801	1.028630	18m	3	8	0	
52.6196	1.737900	68	3	2	0		77.3359	1.232830	7	3	6	0		96.9801	1.028630	m	5	2	1	
55.6913	1.649100	102	0	6	0		78.8267	1.213210	8m	1	5	2		97.2466	1.026520	12	4	2	2	
56.8726	1.617620	95	3	3	0		78.8267	1.213210	m	4	4	0		97.7504	1.022570	2m	1	2	3	
57.1548	1.610300	278	1	5	1		79.1856	1.208610	5m	1	8	0		97.7504	1.022570	m	2	9	0	
57.5440	1.600330	105	2	4	1		79.1856	1.208610	m	2	4	2		97.8390	1.021880	2	1	9	1	
57.6812	1.596850	129	0	0	2		79.7412	1.201580	4	3	1	2		98.6631	1.015540	11	5	4	0	
58.1885	1.584130	81	3	1	1		80.6603	1.190190	2	4	3	1		99.4965	1.009260	5	4	6	1	
60.6094	1.526520	68	3	2	1		81.8520	1.175850	27	3	2	2		100.4932	1.001920	17	5	3	1	
61.0373	1.516840	4	1	1	2		82.1447	1.172400	26	2	7	1		100.7629	0.999965	2	4	3	2	
62.5061	1.484680	39	3	4	0		83.8038	1.153360	39	0	8	1		101.2120	0.996739	4	1	3	3	
63.3924	1.466040	13m	0	6	1		84.0838	1.150120	9	3	6	1		101.9001	0.991866	12	4	7	0	
63.3924	1.466040	m	1	2	2		84.3599	1.147170	47	0	6	2		102.2558	0.989379	23m	2	1	3	
64.5222	1.443070	6	3	3	1		85.1420	1.138620	11	4	5	0		102.2558	0.989379	m	2	7	2	
64.6866	1.439800	21	2	5	1		85.3469	1.136410	45	3	3	2		103.6792	0.979646	7	3	8	1	

Appendix G

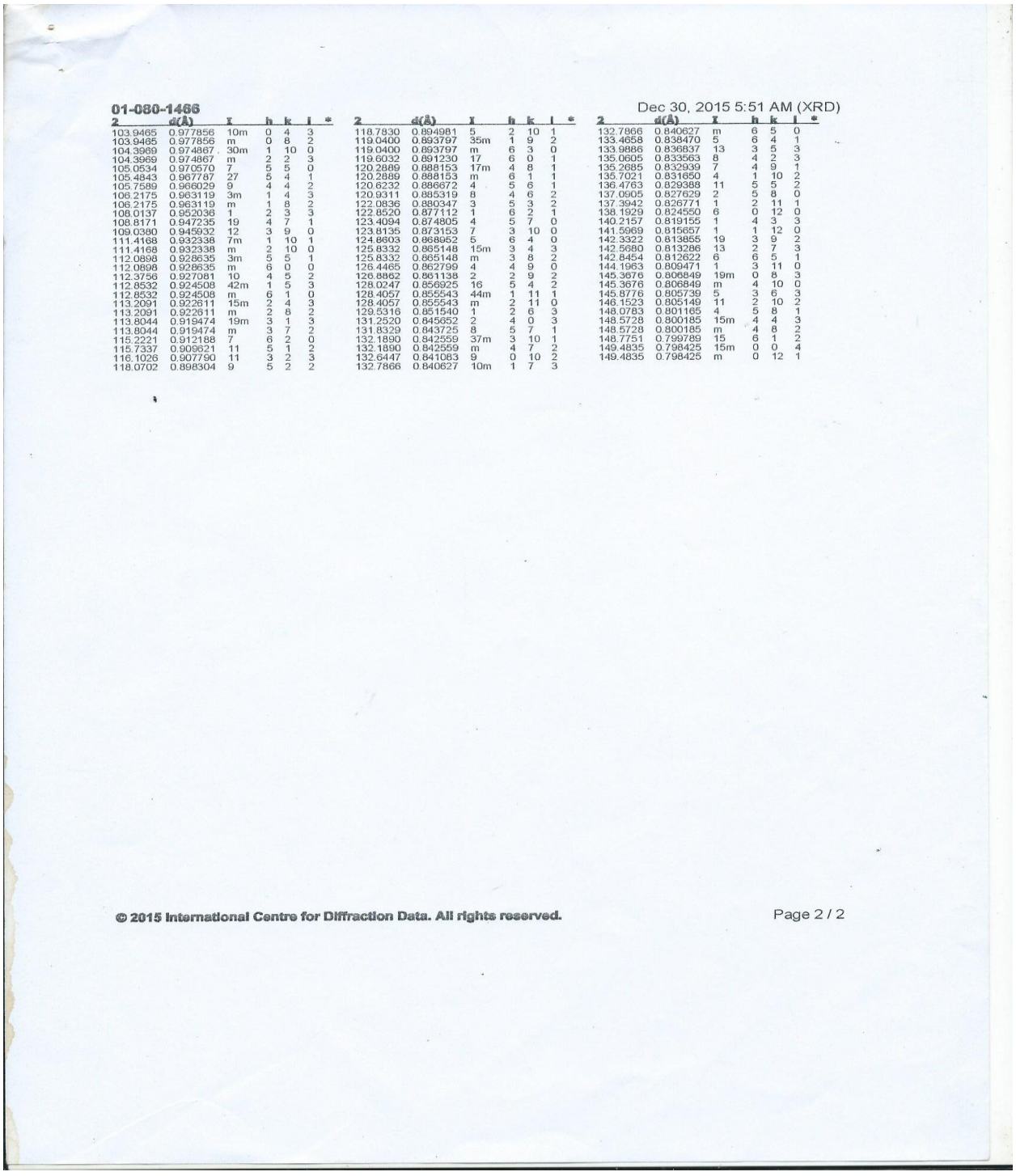

01-080-1466 Dec 30, 2015 5:51 AM (XRD)

2	d(Å)	I	h	k	l	*
103.9465	0.977856	10m	0	4	3	
103.9465	0.977856	m	0	8	2	
104.3969	0.974867	30m	1	10	0	
104.3969	0.974867	m	2	2	3	
105.0534	0.970570	7	5	5	0	
105.4843	0.967787	27	5	4	1	
105.7589	0.966029	9	4	4	2	
106.2175	0.963119	3m	1	4	3	
106.2175	0.963119	m	1	8	2	
108.0137	0.952036	1	2	3	3	
108.8171	0.947235	19	4	7	1	
109.0380	0.945932	12	3	9	0	
111.4168	0.932338	7m	1	10	1	
111.4168	0.932338	m	2	10	0	
112.0898	0.928635	3m	5	5	1	
112.0898	0.928635	m	6	0	0	
112.3756	0.927081	10	4	5	2	
112.8532	0.924508	42m	1	5	3	
112.8532	0.924508	m	6	1	0	
113.2091	0.922611	15m	2	4	3	
113.2091	0.922611	m	2	8	2	
113.8044	0.919474	19m	3	1	3	
113.8044	0.919474	m	3	7	2	
115.2221	0.912188	7	6	2	0	
115.7337	0.909621	11	5	1	2	
116.1026	0.907790	11	3	2	3	
118.0702	0.898304	9	5	2	2	
118.7830	0.894981	5	2	10	1	
119.0400	0.893797	35m	1	9	2	
119.0400	0.893797	m	6	3	0	
119.6032	0.891230	17	6	0	1	
120.2889	0.888153	17m	4	8	1	
120.2889	0.888153	m	6	1	1	
120.6232	0.886672	4	5	6	1	
120.9311	0.885319	8	4	6	2	
122.0836	0.880347	3	5	3	2	
122.8520	0.877112	1	6	2	1	
123.4094	0.874805	4	5	7	0	
123.8135	0.873153	7	3	10	0	
124.8803	0.868952	5	6	4	0	
125.8332	0.865148	15m	3	4	3	
125.8332	0.865148	m	3	8	2	
126.4465	0.862799	4	4	9	0	
126.8862	0.861138	2	2	9	2	
128.0247	0.856925	16	5	4	2	
128.4057	0.855543	44m	1	11	1	
128.4057	0.855543	m	2	11	0	
129.5316	0.851540	1	2	6	3	
131.2520	0.845652	2	4	0	3	
131.8329	0.843725	8	5	7	1	
132.1890	0.842559	37m	3	10	1	
132.1890	0.842559	m	4	7	2	
132.6447	0.841083	9	0	10	2	
132.7866	0.840627	10m	1	7	3	
132.7866	0.840627	m	6	5	0	
133.4658	0.838470	5	6	4	1	
133.9886	0.836837	13	3	5	3	
135.0605	0.833563	8	4	2	3	
135.2685	0.832939	7	4	9	1	
135.7021	0.831650	4	1	10	2	
136.4763	0.829388	11	5	5	2	
137.0905	0.827629	2	5	8	0	
137.3942	0.826771	1	2	11	1	
138.1929	0.824550	6	0	12	0	
140.2157	0.819155	1	4	3	3	
141.5969	0.815657	1	1	12	0	
142.3322	0.813855	19	3	9	2	
142.5680	0.813286	13	2	7	3	
142.8454	0.812622	6	6	5	1	
144.1963	0.809471	1	3	11	0	
145.3676	0.806849	19m	0	8	3	
145.3676	0.806849	m	4	10	0	
145.8776	0.805739	5	3	6	3	
146.1523	0.805149	11	2	10	2	
148.0783	0.801165	4	5	8	1	
148.5728	0.800185	15m	4	4	3	
148.5728	0.800185	m	4	8	2	
148.7751	0.799789	15	6	1	2	
149.4835	0.798425	15m	0	0	4	
149.4835	0.798425	m	0	12	1	